Chem Soc Rev

Chemical Society Reviews
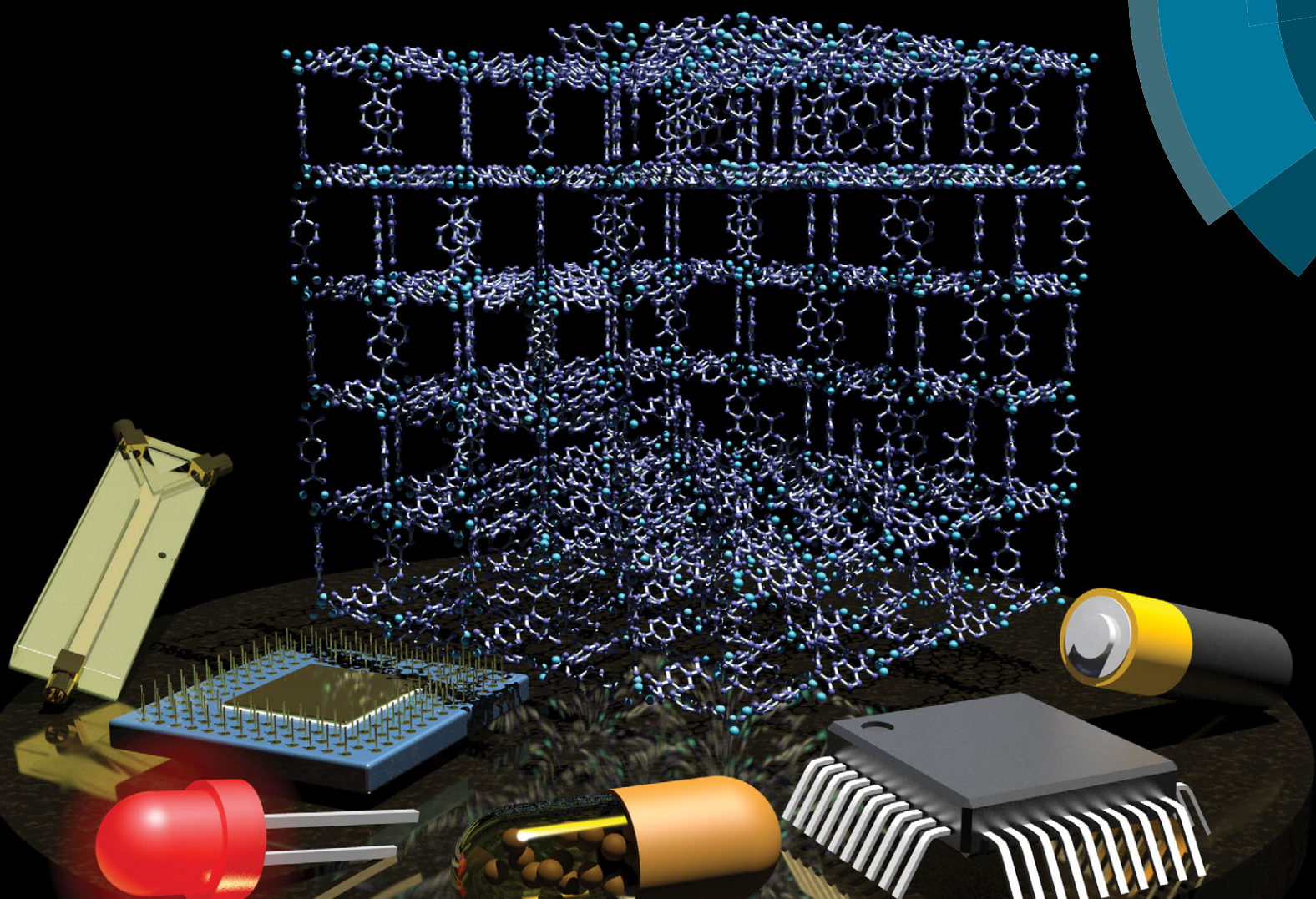
Themed issue: Metal–organic frameworks

ROYAL SOCIETY
OF CHEMISTRY

REVIEW ARTICLE
Paolo Falcaro *et al.*
MOF positioning technology and device fabrication

■·BASF
The Chemical Company

MOF positioning technology and device fabrication†

Paolo Falcaro,*[a] Raffaele Ricco,[a] Cara M. Doherty,[a] Kang Liang,[b] Anita J. Hill[b] and Mark J. Styles[b]

Metal organic frameworks (MOFs) offer the highest surface areas per gram of any known material. As such, they epitomise resource productivity in uses where specific surface area is critical, such as adsorption, storage, filtration and catalysis. However, the ability to control the position of MOFs is also crucial for their use in devices for applications such as sensing, delivery, sequestration, molecular transport, electronics, energy production, optics, bioreactors and catalysis. In this review we present the current technologies that enable the precise positioning of MOFs onto different platforms. Methods for permanent localisation, dynamic localisation, and spatial control of functional materials within MOF crystals are described. Finally, examples of devices in which the control of MOF position and functionalisation will play a major technological role are presented.

1. Introduction

The importance of a material is determined by the role it plays in our everyday life, as well as the impact it has on our future technological progress. In the case of many functional materials, our growing ability to confine their properties to a controlled location has allowed us to manufacture powerful and efficient devices for a wide variety of tasks, making functional materials important to our health, economy and environment. Microelectronics is an excellent example of a field where the ability to precisely control the position of a functional material with useful properties has had a substantial positive impact on society.[1] In this field, improved control over the size and location of the functional material (typically a semiconductor) has enabled the density of components on an integrated circuit to increase, improving the performance and lowering the cost of the final device.[2]

The crucial steps involved in controlling the location of functional materials are process optimization (making the desired functional material), engineering (control the geometry of the material and tune the properties for the desired application), and integration into a useful platform (connection with other materials and components). In this context, many opportunities for developing new, high-performance technologies originate from the ability to fabricate new types of microstructures or to recreate existing structures in down-sized versions.[3] This process can be identified as *miniaturisation*. Progress in device miniaturisation is strongly linked to functional materials and suitable protocols for controlling their location.[4]

The success of the microelectronics industry has provided a strong driving force for the development of new fabrication techniques at the micro- and nano-scale. These micro- and nano-fabrication techniques, combined with other kinds of advanced materials, have since shown that novel optical, chemical, magnetic, mechanical, medical and diagnostic devices can be fabricated with superior performance compared to their macro counterparts,[5] with applications ranging from sensing to microbiology. The technological and industrial advantages that can be achieved by device miniaturisation highlight the importance of combining improved fabrication techniques with materials with exceptional properties.

Despite the valuable attributes of porous materials,[6] methods for controlling the location of individual crystals and coatings with specifically designed pore sizes, arrangement and distribution are still in their infancy.[7] Although several studies have shown the potential of devices employing highly porous crystals, more research is required to fully understand the potential and the limitations of these materials, both for scientific reasons and for future technological applications. Among the different porous materials, metal organic frameworks (MOFs), also called Porous Coordination Polymers (PCPs), are a class of ultra-porous materials with exceptionally high accessible surface area due to the framework

[a] *CSIRO Materials Science and Engineering, Clayton, Victoria 3168, Australia. E-mail: Paolo.Falcaro@csiro.au; Tel: +61 3 9545 2968*

[b] *CSIRO Process Science and Engineering, Clayton, Victoria 3168, Australia*

† Electronic supplementary information (ESI) available: This material includes video animations to illustrate a variety of MOF patterning techniques, including: microcontact printing for self-assembled monolayers, liquid-phase epitaxy, layer-by-layer, gel-layer, electrochemical, precision milling, seeding, microcontact printing of MOF, micromolding in capillaries, pen-type, photolithography combined with conversion from ceramics, microcontact printing combined with conversion from ceramics, ink-jet printing, spray coating, photolithography with positive and negative resists, photolithography (deep X-ray lithography), photolithography (UV), photolithography combined with imprinting, and magnetic framework composite fabrication. See DOI: 10.1039/c4cs00089g

This journal is © The Royal Society of Chemistry 2014

Chem. Soc. Rev., 2014, 43, 5513–5560 | 5513

produced by the inorganic nodes coordinated by organic bridging ligands.[8,9] These surface areas can range from 1000 to 10 000 $m^2\ g^{-1}$, thus exceeding other porous materials such as mesoporous based oxides, zeolites and carbons.[10] As a result, MOFs have shown remarkable capabilities in application areas where the accessible surface area is a critical feature, such as in gas storage,[11,12] separation[13] and catalysis.[14] However, more recently, they have been shown to hold much promise for a variety of other applications including sensing,[15] microelectronics,[16,17] optics,[18–20] micro-motors,[21] molecular rotors,[22] pollutant sequestration,[23–25] energy production,[26,27] bioreactors,[24] diagnostics and controlled drug release.[28,29] Importantly, these are all fields that could benefit from advanced miniaturisation processes.

MOF crystals are produced by a process of self-assembly, which allows (under the proper conditions) for the spontaneous formation of ordered lattices. This bottom-up approach enables the growth of beautiful hybrid crystals with complex supramolecular architectures. However, achieving control over the spatial localisation of the self-assembly sites is a challenging task,[30] which remains a major scientific goal for the development of MOF-based technology.[7] To address this issue, a number of different approaches have been proposed to control the position of these ultra-porous crystals. These strategies range from the patient and carefully controlled growth of MOF lattices on chemically functionalised patterns by providing the framework components separately,[31] to the use of a magnetic field to quickly and easily manipulate the location of MOF crystals with embedded magnetic particles.[32] In this review, we critically present the different approaches for achieving spatial control over the location of MOF materials, which is a crucial step in enabling the fabrication of MOF-based devices.[7,33,34]

To highlight the significance of this field, we have analysed the publication trend regarding Metal Organic Frameworks in the 2003–2013 period.[35] As shown in Fig. 1, from 2003 to 2013, an increasing number of articles regarding MOFs have been published in peer-reviewed journals. In the same timeframe, the records related to *device fabrication* have followed a similar trend.

Here we present a classification based on the permanent localisation of MOFs by considering bottom-up and top-down approaches. We then discuss the dynamic localisation of MOF particles and the progress on positioning functional materials

From left to right: Mark J. Styles, Anita J. Hill, Kang Liang, Cara M. Doherty, Raffaele Ricco and Paolo Falcaro

Paolo Falcaro finished his PhD in material engineering jointly at Padova and Bologna universities in 2006. From 2005 to 2009 he worked in a research company helping industries to develop/optimize products. In 2009 he was fortunate to join Anita's group (CSIRO) applying his skills to MOFs. He is currently leading a small multidisciplinary research group of awesome young experts.

Raffaele Ricco received his PhD in molecular sciences at the University of Padova in 2008. From 2008 to 2012 he worked in a nanotechnology company developing dye loaded silica nanoparticles. From 2012 he is a Postdoctoral Fellow in Paolo's group at CSIRO; his main research interest is the application of magnetic framework composites.

Cara Doherty obtained her PhD in Physical Chemistry from the University of Melbourne in 2009 where she developed porous materials for use in high power lithium ion batteries. She is currently a research scientist at CSIRO and an ARC Discovery Early Career Research Fellow where she investigates porous materials in dynamic systems.

Kang Liang received his PhD degree from the University of Melbourne under the supervision of Prof. Frank Caruso, developing nanoengineered particles for biomedical applications. He is currently a Postdoctoral Fellow in Paolo's group at CSIRO, where he is utilizing his expertise in developing functional porous materials for bio-related applications.

Anita Hill obtained her PhD in Mechanical Engineering from Duke University. She is the Group Executive for Manufacturing, Materials and Minerals at CSIRO. She is a Fellow of the Australian Academy of Technological Sciences and Engineering and an Office of the Chief Executive Science Leader at CSIRO Materials Science and Engineering.

Mark Styles completed his PhD in mechanical engineering jointly at the University of Melbourne and CSIRO in 2012. He is currently a Postdoctoral Fellow at CSIRO, where he applies his skills in mechanical engineering and X-ray characterisation techniques to several projects, including investigating precipitation hardening processes in structural alloys and MOF growth and positioning technologies.
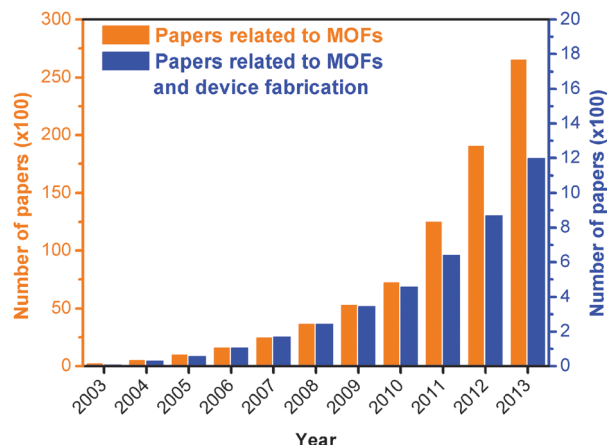
Fig. 1 Evolution of the cumulative number of papers related to metal organic frameworks (MOFs, orange columns and left Y-axis, ×100), and to MOFs and device fabrication (blue columns and right Y-axis, ×100), in the 2003–2013 period. Source: ISI Web of Science.[35]
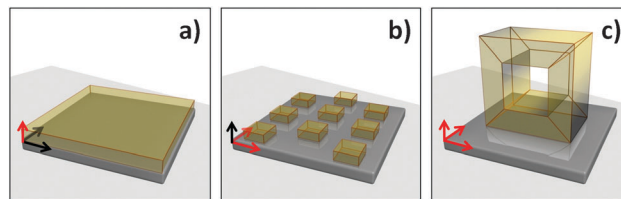

Fig. 2 Levels of control for MOF patterning. The red arrows are pointing towards the controlled direction of growth: (a) control perpendicular to the substrate (1D), (b) control in the plane of the substrate (2D), and (c) control in space (3D).

within MOFs. Finally we describe the progress in MOF-based device fabrication for the benefit of current and future applications.

2. Patterning and permanent localisation

Over the last decade, research scientists have been trying to control the growth of MOFs on different substrates with the intention of providing protocols suitable for MOF-based device fabrication.[36] Such protocols have focused in the first instance on controlling the location of specific MOFs on a substrate. When the MOF is grown or deposited on a support in order to confer new properties to the system (e.g. anchoring the MOF to the substrate), then it is termed *permanent localisation*. In this review we will briefly mention several methods for fabricating MOF films, as homogeneous MOF coatings are often the first step towards permanently localising MOFs for device fabrication, and hence are important to many patterning protocols.[24,31,37] If the reader wishes to gain a deeper understanding of the MOF thin film research field, a number of reviews have been published describing in detail the synthetic and technological aspects related to MOF films and coatings.[31,33,38,39] As previously mentioned, the aim of this review is to introduce the reader to the progress, advantages, and challenges of confining MOFs to specific locations, which extends the level of control from the direction perpendicular to the plane of the substrate (1D), up to a level of control in the plane (2D) or space (3D) that can be identified as *patterning* (Fig. 2).

2.1 MOF films

Research into the fabrication of MOF films focuses on the attempt to deposit or control the homogeneous growth of MOF crystals on a substrate. As reported in dedicated reviews,[31,33,38,39] the fabrication of films can be achieved in several different ways including surface functionalisation (e.g. self-assembled mono-layer, SAM) combined with Layer-by-Layer (LbL)[40] and *in situ*

crystallization (liquid phase epitaxy, LPE),[36] colloidal[24,41] and Langmuir–Blodgett (LB) depositions,[42] seeding,[43] electro-deposition,[44–47] microwave[48] and gel-layer deposition[49] techniques. The film thickness and homogeneity are the initial parameters primarily considered for film deposition. However, in order to fully control the MOF film properties, several additional important features need to be considered, including: lattice inter-penetration, film roughness, crystal alignment (in-plane and out-of plane orientations), density and size of crystals, crystal domain size, distribution and their cohesion, adhesion to the substrate, and mechanical properties. This promising research field has developed methodologies capable of addressing several of these aspects, and MOF thin films have successfully been used for the fabrication of a number of different devices, which will be discussed in this review. Each methodology has particular design features that are present in the resulting product. For example, with LbL assembly, the resulting MOF films are often ultra-thin, partially oriented and of adjustable thickness.[50] The microwave approach, and the electrochemical deposition approach generally require a conductive surface.[51] However, these approaches seem to be very versatile (able to produce a variety of MOFs). The seeding approach uses efficient seeds,[43] which can be either MOFs or other materials, to induce preferential growth of MOFs on a support rather than in solution.[52,53]

2.2 MOF patterns

When control of the MOF location is extended to planes (2D) or spaces (3D), it is appropriate to call the fabrication method *patterning*. As mentioned previously, microelectronics is the most successful example of the importance of micro fabrication protocols to economic prosperity; however, applications in other areas are rapidly emerging (e.g. solar cells, sensors, light emitters, microfluidic circuits, micro-vascular circuits, and lab-on-a-chip).[3,4] One of the most recent and fervent areas of investigation is micro- and nano-fabrication methods combined with MOFs. The use of MOFs and microfabrication may have the greatest impact and technological advantage in devices where a limited amount of porous material is needed, portability is required, and/or an integrated multifunctional system is desired. Recently, the synthetic procedures for preparing MOFs for functional applications have been improved to the point where ultraporous crystals have been used for sensing explosives[54] and solvents,[55] propulsion in specific directions,[21] transporting molecules,[22] electrons[16] and ions,[56] immobilizing enzymes[24] and

This journal is © The Royal Society of Chemistry 2014

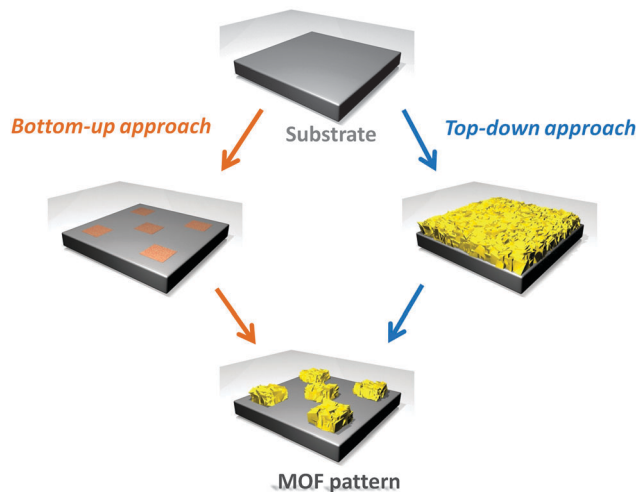*Chem. Soc. Rev.*, 2014, **43**, 5513–5560 | **5515**

Fig. 3 Schematic illustrating the bottom-up and top-down patterning approaches. Bottom-up patterning is defined here as any protocol which grows MOF crystals in pre-identified locations, whereas top-down patterning is defined as the transfer or removal of pre-existing MOF crystals.

growing cells.[57] Mastering the crystal growth (*e.g.* position, orientation and interpenetration) would allow full control over the crystal properties in miniaturised devices, enabling MOFs to be harnessed for their functional properties beyond the traditional gas uptake and separation.[11–13,58]

Although MOFs are always prepared by self-assembly, which is considered a bottom-up approach, we will refer to the patterning method used in order to classify a fabrication protocol as being either a bottom-up or a top-down protocol. In particular, we define *bottom-up* approaches as any protocol that achieves spatial control of MOFs *via* the growth of the porous crystals in pre-identified locations. Under ideal conditions the MOF would form only in controlled areas. Conversely, if the spatial control of MOFs is achieved by either removing or transferring pre-existing MOF crystals (*e.g.* powders or films), such that a smaller amount of MOF-based material is located in the final pattern, then we consider that protocol as being a *top-down* method (Fig. 3).

2.3 Bottom-up MOF patterning technologies

Self-assembly is a powerful route for the fabrication of complex materials.[59–61] However, the integration of such materials into miniaturised platforms remains an ongoing challenge, as it can be difficult to control the location of the self-assembly using bottom-up fabrication techniques.[62] This is particularly true for MOFs, and as a result, intensive ongoing research has been directed towards bottom-up protocols for patterning MOFs using a wide variety of strategies. These include: surface functionalisation, electrochemical deposition, nucleating agents, contact printing, microfluidics, conversion from ceramics, ink-jet coatings and spray coatings. Although the features and the potential of these protocols can be quickly identified, most are still being optimised. For this reason, the advantages and limitations of many of these approaches are not fully known or explored at present; however, based on the literature reported to date, basic parameters related to the feature dimensions in MOF patterns are summarised in Table 1.

2.3.1 Surface functionalisation

Technique development. One of the most efficient ways to pattern MOFs is to use a functionalised surface which promotes the nucleation and growth of MOFs on top of it. Early MOF positioning focused on forming films and 2D patterns by functionalising the substrate prior to film growth. Several extensive reviews have been published covering the formation mechanisms of MOF films;[31,38,39] however, we focus here on the position and patterning of MOFs and how the resulting MOF surfaces can be utilised in various applications. Initially, organic SAMs of 16-mercaptohexadecanoic acid and 1*H*,1*H*,2*H*,2*H*-perfluorododecane thiol were anchored to a gold substrate and then immersed in a supersaturated solution of the MOF-5 ($Zn_4O(BDC)_3$, H_2BDC = terephthalic acid) precursor.[36] Using microcontact printing (μCP), the functionalisation of substrates can be precisely controlled; a schematic illustrating the process is given in Fig. 4. Fischer's group initiated the crystal formation with fully protonated carboxylate groups on the SAM surface, which allows the bond between the terephthalate bridge and surface-bound Zn^{2+} cation units to form and progress to the growth of a MOF-5 film.[36] This technique has been referred to as liquid-phase epitaxy (LPE); a schematic illustrating the process is given in Fig. 5a–j.

Fischer's group also developed various MOF films of HKUST-1 ($Cu_3(BTC)_2$, H_3BTC = 1,3,5-benzenetricarboxylic acid) and $Zn_2(BDC)_2$(dabco) [dabco = 1,4-diazabicyclo[2.2.2]octane] on different SAM functionalised substrates (alumina and silica) and were able to observe preferential orientation of crystal growth.[52,63,64] Bein's group simultaneously was able to tune the crystal orientation of the MOF growth by changing the functionality of the SAM layer.[65–67] They found that the MOF films grown on the –COOH functionalised SAM were oriented in the [100] direction, whereas the MOFs grown on the –OH SAM were aligned along the [111] direction. Thin films grown on the methyl functionalised SAM were also found to be much less oriented.[65]

Additional control over MOF crystal growth orientation was achieved through the development of the LbL technique, in which the SAM functionalised substrate was alternately placed in the metal precursor and organic linker solutions with washing steps in between.[40,68–71] Cobo and Molnár *et al.*, simultaneously developed a multilayer sequential assembly to form 3D coordination polymers [Fe-(pyrazine){M(CN)$_4$}] (M = Ni, Pd, or Pt) that feature spin crossover, making them ideal materials for memory storage devices at room temperature.[68,69] The LbL technique produces ultrathin MOF films (termed SURMOF for surface anchored MOFs)[72–74] where the MOF crystals were preferentially oriented in the out-of-plane direction. The films are nanometres thick and, due to the precision afforded by the step-wise building process (Fig. 5k–t), the thickness of each film can be tailored by adjusting the number of layers prepared.[38] The resulting LbL films feature very smooth surfaces with roughness in the order of only a few molecules.[38]

Patterning. The ability to pattern MOF films on functionalised surfaces allows their potential use in commercial devices for industrial applications. The key to pattern these MOFs is to

5516 | *Chem. Soc. Rev.,* 2014, **43**, 5513–5560

This journal is © The Royal Society of Chemistry 2014

Table 1 Permanent localisation of MOFs: patterns

Classification	Patterning approach	MOF	Pattern thickness[a]	Pattern resolution/ gap size[a]	Preferential orientation	Year	Ref.
Bottom-up							
Surface functionalisation	LPE	ZIF-8	∼700 nm	∼2 μm	[001]	2012	77
	AFM	HKUST-1	∼60 nm	∼15 μm	[111]	2013	78
	Gel-layer	NH_2-MIL-88B(Fe)	40–550 nm	N/A	[001]	2010	49
	LPE	ZIF-9	N/A	mm range	N/A	2013	79
	LPE	$Cu_2(ndc)_2(dabco)$	N/A	μm range	[001]	2011	84
Electrochemical deposition	Anodic deposition	HKUST-1	1 to 20 μm	∼100 μm	N/A	2009	44
	Precision milling and anodic deposition	HKUST-1	5 to 15 μm	mm range	N/A	2013	100
	Galvanic displacement	HKUST-1	N/A	∼20 μm	N/A	2010	101
Nucleating agents	Heterogeneous seeding with lithography	MOF-5	N/A	∼5 μm	N/A	2011	125
Contact printing	EISA combined with μCP	HKUST-1 MOF-5	N/A	μm range	$[111]_{HKUST-1}$	2010	102
	MIMIC	Zn-[4,4′-di(4-pyridyl)cyanostilbene]	2 μm	μm range	N/A	2010	136
	Pen-type lithography	HKUST-1	N/A	μm range	[111]	2011	137
	Pen-type lithography	HKUST-1	<1 μm	μm range	N/A	2011	139
	Pen-type lithography	HKUST-1, $Cd_3[Co(CN)_6]_2$, $Zn_3[Co(CN)_6]_2$, $Mn_3[Co(CN)_6]_2$, and $Ag_3[Co(CN)_6]$	N/A	μm range	N/A	2013	140
	μCP (click printing)	MOF-5	∼40 nm	μm range	N/A	2011	141
Microfluidics	Microfluidics	HKUST-1	N/A	μm range	[111]	2012	144
	Microfluidics with LbL	HKUST-1	∼550 nm	μm range	N/A	2013	145
	Microfluidics	HKUST-1 spheres	Diameter ∼1–2 μm	∼ 400 μm	N/A	2011	152
Conversion from ceramics	Pseudomorphic replication mechanism	$[Al(OH)(ndc)]_n$	0.2–1 μm[b]	200 nm	N/A	2012	170
	Combined mechanisms	HKUST-1	N/A	10 μm	N/A	2014	172
	N/A	ZIF-8	∼1–5 μm	15 μm	N/A	2013	173
Ink-jet printing and spray coating	Ink-jet printing	HKUST-1	∼6 μm	μm range	[111]	2013	184
	LbL spray coating	HKUST-1	∼1 μm	μm range	[111]	2011	185
Top-down							
Photolithography	Deep X-ray lithography	ZIF-9	5 μm	25 μm	N/A	2012	189
	UV lithography	ZIF-8	200 nm	μm range	[100]	2012	37
	UV lithography & imprinting	NH_2-MIL-53(Al), ZIF-67$(Co(Im)_2)$, and ZIF-8	N/A	5 μm	N/A	2013	24

[a] If not explicitly written in the paper, the dimensions of the MOF crystals and/or the pattern resolution, if possible, are deducted from the images in the original manuscripts and it should be considered as an indication only. [b] Several microns can be achieved in porous systems such as inverse opals.

prepare the SAM layer *via* well established techniques. For example, 2D MOF patterns can be produced by combining μCP of the functionalised SAM layer with LPE methods.[75–77] Terfort *et al.* prepared a patterned SAM layer of 1-hexadecanethiol (HDT) on a Au substrate using μCP. The LbL growth technique was then employed to form a well defined square patterned Cu–ADA MOF film from Cu–carboxylate dimer secondary building units (SBUs) and 4,4-azobenzene dicarboxylic acid (H$_2$ADA) ligands.[76] Li *et al.* patterned Zeolitic Imidazolate Framework ZIF-8 (Zn(mIm)$_2$, HmIm = 2-methylimidazole) dot arrays on a Au substrate by using μCP to first pattern the SAM with 1-octadecanethiol (ODT) and passivate the unfunctionalised surface with 16-mercaptohexadecanoic acid (MHA).[77] The patterned substrate was then immersed in an aqueous solution of HmIm with the gradual addition of zinc acetate. The ZIF-8 crystals preferentially grew on the SAM non-polar regions due to their high surface energy (see Fig. 6). The growth conditions

were varied to produce single crystal patterns of oriented ZIF-8 by reducing the size of the patterned SAM layer to 500 nm and diluting the MOF precursor solution.[77]

An alternative method of patterning the SAM layer is *via* nanografting or nanoshaving, which is a lithographic protocol that uses scanning probe microscopy techniques such as atomic force microscopy (AFM) to laterally pattern with resolutions of several nanometers.[78] Nanografting of the SAM layer involves cleaving the bond between the Au substrate and the thiolate species using the AFM tip. This is typically performed in an organothiol containing solution. Ladnorg *et al.* were able to selectively grow the SURMOF HKUST-1 *via* the LbL technique on nanografted thiol-based SAM surfaces.[78]

A number of alternative methods for preparing thin MOF films and patterns on functionalised surfaces have emerged in the last few years. Bein's group developed a novel approach employing a gel layer over the functionalised SAM which
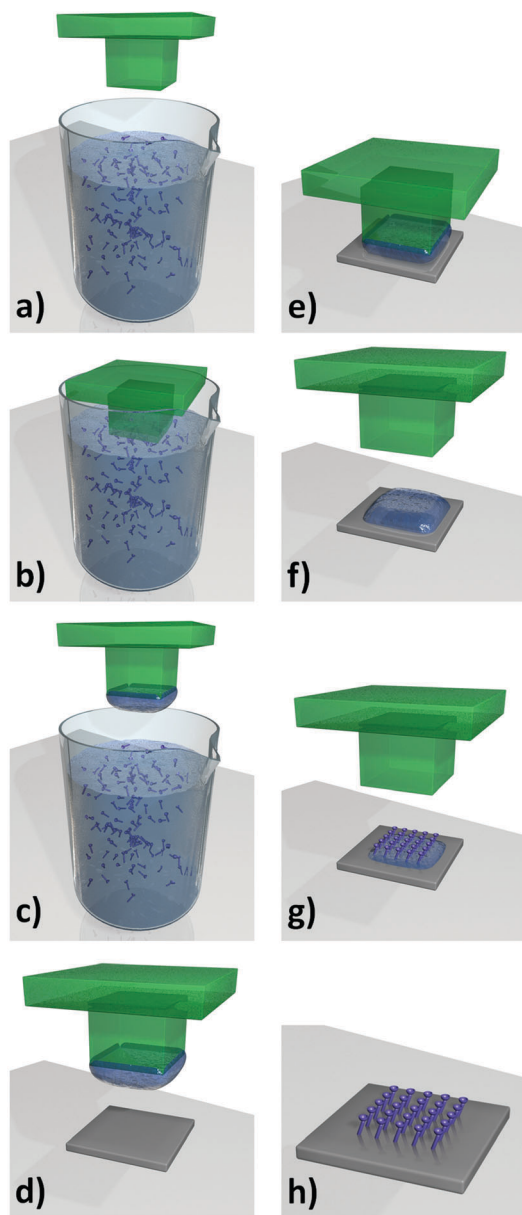
Fig. 4 Surface functionalisation by microcontact printing (μCP). (a–c) A lithographed stamp is inked with solution containing the functional units. (d–f) The solution is then transferred to the substrate by placing the stamp in contact with the substrate. (g and h) The solvent is then allowed to evaporate, producing the self-assembled monolayer (SAM). Video animation provided as ESI.†

contains the metal salt precursor (Fig. 7).[49] This is then covered by a concentrated linker solution which diffuses through the gel, forming a highly oriented MOF film on the –COOH-functionalised SAM. The method allows for concentrated reactants to be used, and produces homogeneous films of NH$_2$-MIL-88B(Fe) (Fe$_3$OCl(aBDC)$_3$, H$_2$aBDC = 2-aminoterephthalic acid) MOFs with excellent crystal orientation. The thickness was readily controlled by altering the concentration of the Fe precursor in the gel layer.

Alternative methods of functionalising surfaces have also been employed to form MOF films on different substrates.

Dimitrakakis *et al.*, demonstrated the patterning ability of a ZIF-9 (Co(bIm)$_2$, HbIm = benzimidazole) film using a plasma polymer coating technique which selectively alters the surface chemistry of a PTFE substrate.[79] Different polymers will either promote MOF growth (DGpp = diglyme-based plasma polymer), or inhibit MOF growth (AApp = allylamine-based plasma polymer) *via* a standard solvothermal mechanism. The highly oxygenated DGpp polymer allows the metal cations to coordinate with the hydroxyl and carbonyl groups, whereas the amino groups in the AApp polymer prevent the metal cations from coordinating to the surface. Another alternative to SAM functionalisation is the protocol proposed by Kida *et al.*[80] These authors formed ZIF-8 films in an aqueous system using 3-(2-imidazolin-1-yl)propyl-triethoxysilane to functionalise the glass substrate surface to which the MOF films were grown using the general solvothermal growth technique.[80]

Advantages and limitations. As well as the fine control over the film thickness, crystal orientation and morphology, there are several key advantages to producing films and patterns by the LbL technique. The ability to prepare MOF films with architectures that are not available *via* the conventional solvo-thermal methods is a major benefit. Shekhah *et al.* used the LbL technique to prepare a non-interpenetrated version of MOF-508 (Zn$_2$(BDC)$_2$(bpy), bpy = 4,4'-bispyridyl).[72,81] Previously, the known polymorph MOF-508a featured two interpenetrating, pillared, paddle-wheel-type networks, where sublattices occupy the same space, hence reducing the pore volume within the MOF lattice. The SAM formed from 4,4-pyridyl-benzene-methanethiol on an Au substrate was alternately immersed into two solutions of zinc acetate and the organic ligands (H$_2$BDC and bpy). The resulting SURMOF (Fig. 8) was a non-interpenetrated, solvent-free analogue of MOF-508a and had a surface area of 1010 m^2 g^{-1} compared to 660 m^2 g^{-1} for the original interpenetrated MOF.[72]

The same group was also able to demonstrate the use of LbL to form isoreticular MOFs (IRMOFs) with 3 × 3 nm channels[82] and layered MOF-2 (Zn$_2$(BDC)$_2$(H$_2$O)$_2$) and its copper analogue Cu$_2$(BDC)$_2$(H$_2$O)$_2$ with *P*4 symmetry which had not been obtained *via* solvothermal methods, as other monoclinic unit cells were preferentially formed due to interlayer interactions of the solvent molecules.[83] The perpendicular orientation of the 2D metal-bdc planes from the surface was achieved due to the anchoring of the paddle wheel units to the COOH-terminated 16-mercaptohexadecanoic acid SAM layer.

LbL films also provide more control over the selective functionalisation or modification of MOFs than the conventional solvothermal synthesis.[84–86] Due to the step-wise process of LbL, the selective modification of the external surface of the MOF films can be performed. Liu *et al.* were able to function-alise an amino monolayer onto Cu$_2$(ndc)$_2$(dabco) [H$_2$ndc = 1,4-naphthalenedicarboxylic acid] MOF using a pyridine-terminated SAM on an Au substrate.[84] The amino functionalisa-tion was confirmed *via* the labelling of fluorescein isothiocyanate (FITC) as it reacts covalently with the amine and can be readily detected from its fluorescent properties. Bein's group was able to
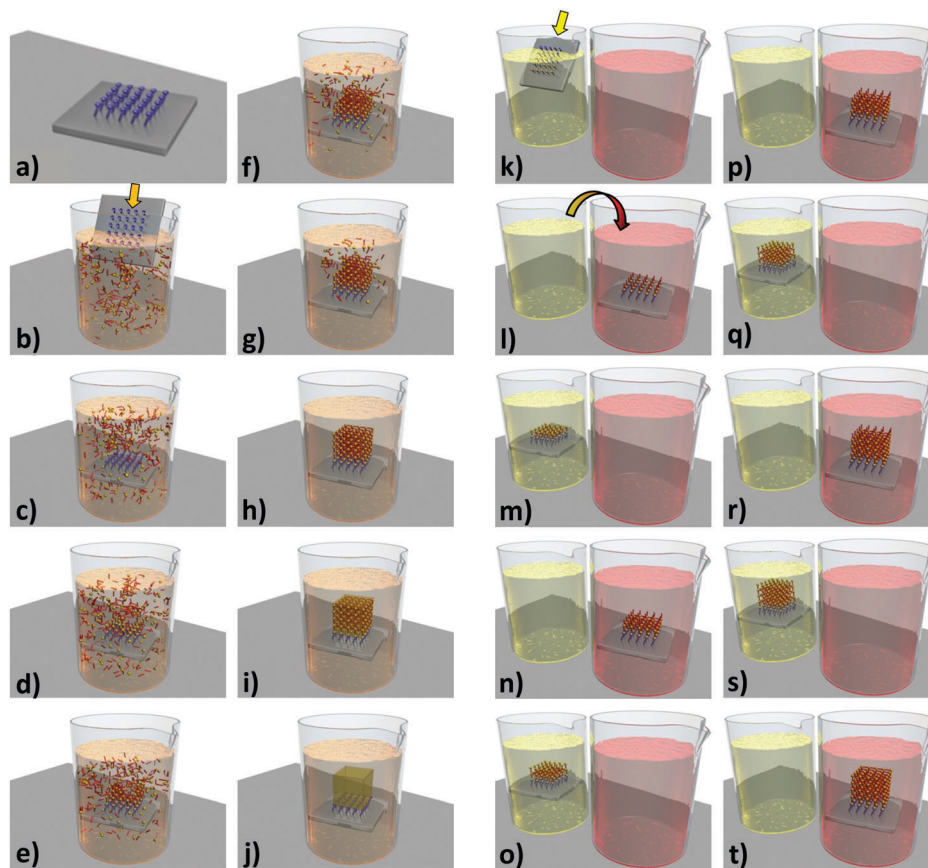
Fig. 5 (a–j) Schematic of the growth of MOFs on a patterned SAM surface *via* the LPE process. The patterned SAM substrate is placed in a solution containing both metal precursor and organic linker, resulting in the controlled formation of MOF crystals on the SAM pattern. (k–t) Schematic of LbL growth of MOFs on patterned SAM surface. In this case, the SAM functionalised substrate is alternately placed in the metal precursor and organic linker solutions, with washing steps in between. Video animations provided as ESI.†
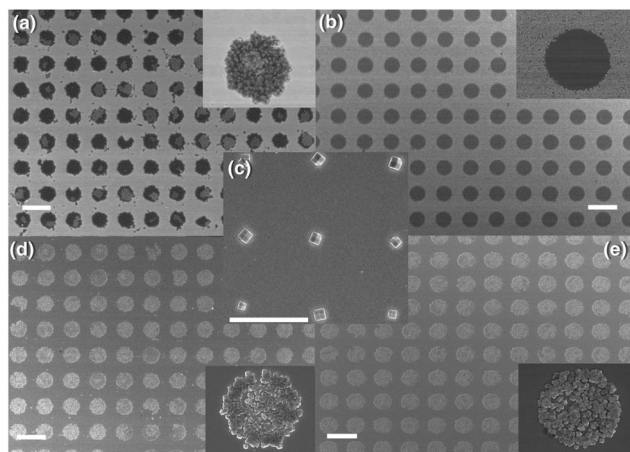

Fig. 6 SEM images of ZIF-8 crystals grown by LPE on gold substrates patterned with SAM. (a) ZIF-8 dots grown on ODT and MHA background. (b) ZIF-8 grown in methanolic solution to form a negative pattern. (c) Single ZIF-8 crystals grown on ODT dots and MHA background. (d) ZIF-8 grown on MHA dots and 4-methylbenzenthiol background. (e) ZIF-8 grown on MHA dots with ODT background using a platinum substrate. Insets show magnified images of the dots. Scale bars are 10 µm for a, b, d, e and 4 µm for c.[77]
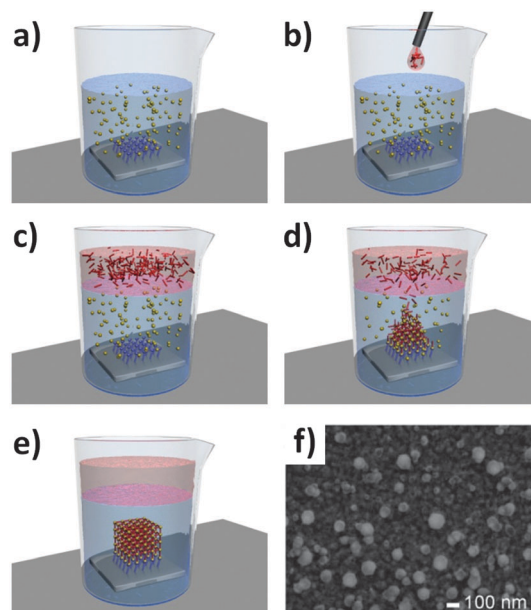

Fig. 7 Schematic of the gel-layer approach where a SAM-functionalised gold substrate is coated with the metal salt gel precursor (a) and then covered in a solution of the organic MOF linker (b). Over time the linker precursor diffuses through the gel to form an oriented MOF crystal (c–e). SEM of NH_2-MIL-88B(Fe) MOF film formed from the gel layer (f).[49] Video animation provided as ESI.†
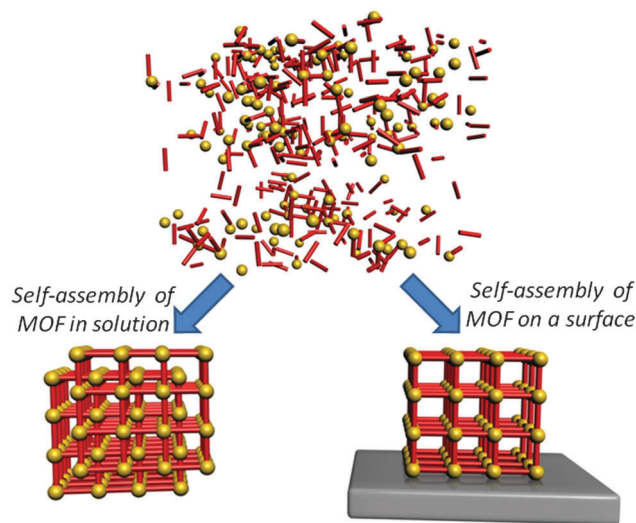
Fig. 8 Schematic demonstrating the advantage of the LbL technique to form MOF films that are not interpenetrated (right), unlike the conventional solvothermal bulk synthesis (left).[72]

confirm that the amino functionalisation within their LPE formed NH$_2$-MIL-88B(Fe), featuring a flexible framework structure, had a significantly higher ethanol uptake than the unfunctionalised MOFs, using a quartz crystal microbalance (QCM) and *in situ* XRD analysis.[85] This example highlights the influence of the surface functionalisation technique on controlling selective host–guest interactions for chemical sensing applications.

Some limitations are evident with MOF films prepared using SAMs. The long synthesis time is a significant consideration due to the number of steps required to build up the desired film thickness. The SAM layers also carry their own limitations as they are inherently thermally and chemically sensitive, and therefore may not be compatible with the MOF formation requirements including pH levels, temperatures, solvents or atmospheres.[7] No ideal synthesis technique has been established which can be employed to make all MOF thin films and patterns.[87] Each specific MOF has its own unique chemistry and consequent synthesis conditions, resulting in continued research in the field of MOF film fabrication.

Anchoring the MOF films and patterns to a substrate using the SAM can also restrict the flexibility of some MOFs. Bein's group demonstrated that the flexible NH$_2$-MIL-88B(Fe) MOF when grown *via* LPE only showed structural changes in the [001] direction upon sorption of water, whereas the bulk crystals showed structural changes in all directions.[85] This should be considered when using MOF films, as the restricted flexibility may prevent access to the MOF's porous structure.

One limitation to the LPE MOF formation method is the lack of control in the crystal orientation along the direction parallel to the substrate (in-plane). Interesting results are achieved in direction normal to the substrate (out-of-plane) with LPE and LbL; however, the Langmuir–Blodgett (LB) method to prepare 2D MOF arrays is required.[42,88–91] The combination of LB with LbL shows promising results for formation of MOF films with controlled crystal orientation.

2.3.2 Electrochemical deposition

Technique development. Electrochemical methods for generating MOF films and coatings are particularly attractive for some applications, such as separation membranes, where mild synthesis conditions are desirable.[92] Electrochemical approaches for synthesising MOF coatings include anodic and cathodic deposition. Anodic deposition was first reported for the well-known MOF material HKUST-1[93] by Mueller and co-workers from BASF,[94] using metallic Cu anodes immersed in a solution of H$_3$BTC in methanol. When voltage is applied to the electrochemical cell the Cu anode begins to dissolve, releasing Cu ions into solution where they react with the ligand to produce the Cu-based MOF. As the metal ions are concentrated near the anode, MOF crystals preferentially nucleate and grow on the surface, producing a uniform coating with crystal sizes between 0.5 and 5 μm. Subsequent studies have shown that anodic deposition can also be used to synthesise Zn and Al based MOF coatings,[95] as well as HKUST-1 coatings on Cu mesh anodes.[95,96] Furthermore, Van de Voorde *et al.*, using the same electrochemical growth technique, have shown the influence of the process parameters over the mechanical properties.[97] Interestingly, good adhesion and hardness were achieved, as measured by nano-indentation and scratch tests.

Conversely, in cathodic deposition, the substrate to be coated acts as the cathode of the cell and is suspended in a solution that already contains both the metal ions and bridging ligands. Li and Dincă[45] first reported how the reduction of Zn^{2+} ions and the deprotonation of H$_2$BDC induced by the formation of a localised concentration of OH$^−$ ions near the cathode of such a cell, could be used to synthesise MOF-5[98] coatings on fluorine-doped tin oxide (FTO) electrodes. In a recent study, the same authors have demonstrated how mixed, as well as bilayer, coatings of MOF-5 and (Et$_3$NH)$_2$Zn$_3$(BDC)$_4$[99] can also be synthesised using cathodic deposition.[46] This shows the potential of cathodic deposition for the fabrication of multi-MOF-based systems.

Patterning. The first high quality MOF patterns to be achieved using an electrochemical approach were reported by Ameloot *et al.*[44] The authors demonstrated that the anodic deposition method could be used to efficiently grow MOF crystals in precise locations on a lithographed metallic substrate. In the approach proposed, a copper microelectrode is immersed in a solution containing the ligand (H$_3$BTC) for the preparation of the HKUST-1 and an electrolyte (methyltributylammonium methyl sulphate). HKUST-1 crystal coatings with a controlled thickness between 1 to 20 μm were obtained by applying a voltage in the range 2.5 to 25 V. The deposition process, which takes advantage of the fact that free metal ions are concentrated near bare regions of the electrode surface to produce a highly uniform coating of MOF crystals, is depicted in Fig. 9a–f. The surface roughness appears to scale with the thickness of the coating, with variations of 4–5 μm observed for 20 μm thick films. The authors used this straightforward technique to generate a patterned MOF coating on top of a Cu plated QCM.[44] The proposed MOF-based microsystem was used as a humidity sensor,
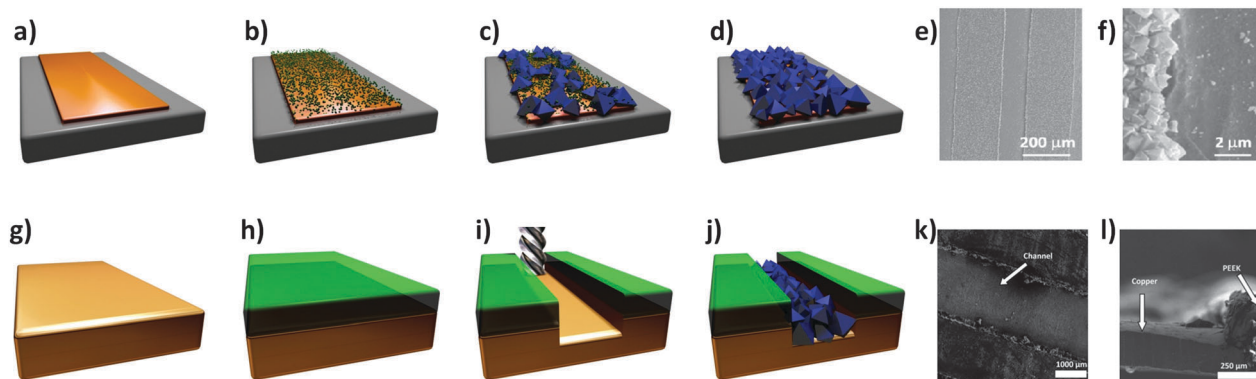
Fig. 9 (a–d) Schematic of the electrochemical method proposed by Ameloot et al.[44] for depositing HKUST-1 on copper substrates. (a) A copper pattern (orange) is produced using standard lithographic techniques, and connected as the anode in an electrochemical cell. (b) Voltage is then applied, releasing Cu cations into solution. (c) The ligand (H_3BTC) in solution reacts with the metal cations concentrated near the anode surface, growing the MOF crystals (blue). (d) The concentration of the metal precursor remains higher over the uncoated regions of the anode, promoting MOF growth on these areas, resulting in a dense coating. (e) SEM measurements performed on the patterned regions and (f) detail showing the preferential growth of HKUST-1 on metal. Images have been reprinted with permission from Ameloot et al.[44] (g–j) Schematic of MOF patterns produced using precision milling combined with electrochemical deposition. (g) A copper substrate is coated with (h) a PEEK layer, and (i) a meandering channel is cut via a precision milling process. (j) Electrochemical synthesis is then used to deposit HKUST-1 crystals in the channels. SEM images showing the (k) top and (l) side view of MOF-coated microchannels. SEM images reproduced from Van Assche and Denayer.[100] Video animations provided as ESI.†

providing evidence that an electrochemical method can be combined with standard lithographic techniques for fabricating miniaturised electrodes.

Van Assche et al.[100] recently described the fabrication of a microseparator device that is also based on anodic deposition of HKUST-1 crystals. In this case, thin (300 μm) copper plates were coated with an adhesive layer (100 μm) of polyether ether ketone (PEEK), through which a meandering channel ~ 200 μm deep was cut via a precision milling process (Fig. 9g–l). After a temporary plastic cover was applied to the reverse side, the copper plates were submersed as the anode in an electrochemical cell employing an ethanolic solution containing 35 wt% water, 16 g L^{-1} H_3BTC, and 10 g L^{-1} of electrolyte (methyl-tributyl-ammonium methyl sulphate). A HKUST-1 film approximately 5 to 15 μm thick was then grown within the channels by applying a voltage of 2.0 V to the plate for 20 minutes. Multiple plates were prepared using this approach, and subsequently stacked within an aluminium housing to form a microseparator, with the PEEK layers acting as gaskets between each plate. The authors used this device to separate n-hexane from a stream containing methanol.

In 2010 Ameloot and co-workers made further progress,[101] combining controlled evaporative conditions[102] with another anodic deposition process known as galvanic displacement. In this experiment, a glass slide was coated with trimethylsilane groups to create a hydrophobic substrate. Afterwards, an array of Cu micropatches (50 × 50 μm in size) was vapour deposited on top of the hydrophobic substrate using a shadow mask. A solution containing the H_3BTC ligand and silver nitrate dissolved in dimethylsulfoxide (DMSO) was then spin-coated on top of the patterned substrate. The exposed methyl functionalised areas caused the solution to preferentially wet the regions covered by Cu, allowing the electrochemical reaction to be confined to the 50 × 50 μm areas. Upon heating to 80 °C

the Ag ions in solution oxidised the Cu substrate, releasing Cu ions into solution. Interestingly, the deposition of metallic silver occurring during this electrochemical process helped to anchor the 100–200 nm HKUST-1 crystals to the micropatches due to its roughness.[101] This work demonstrates that anodic deposition can be used to grow MOFs on isolated metallic patterns without needing to apply an external electric field.

Advantages and limitations. The advantages of electrochemical deposition techniques include that (i) they can be performed in a relatively short amount of time (compared to other procedures such as LbL), (ii) they only require a small amount of reactants (high efficiency), (iii) a high density of crystals can be obtained on the metallic surfaces, and (iv) the crystal growth has been shown to be confined to the regions of metal exposed to solution. Although the only MOF patterns to be grown by electrochemical methods reported to date are based on HKUST-1,[44,100,101] it should be straightforward to extend the film deposition techniques discussed here to a variety of MOFs using suitably lithographed metal patterns. Furthermore, lithographic methods for the fabrication of complex metallic micro- and nano-structures are widely available. Importantly, once the metal patterns have been fabricated, conversion into high quality MOF patterns can be achieved in a single-step electrochemical process. This fabrication method can be considered reasonably inexpensive, due to the limited amount of chemicals used (although the power supply or noble metals required may influence the production costs), and versatile, and is therefore very promising for industrial applications.

2.3.3 Nucleating agents

Technique development. An efficient and versatile method of controlling MOF growth and patterning is via the process of seeding, in which MOF nucleation is induced on specific substrates or particles. The 'seeds' for MOF nucleation can be

either *homogeneous* where the seed has the same MOF chemistry as the subsequent grown MOF, or *heterogeneous* where the seed is a different material that also promotes the formation of MOF.

Homogeneous nucleation. Many of the initial investigations into seeded growth focused on using the preformed nano- or micro-MOF particles, coating them onto a porous substrate for the secondary growth of MOF films for use as membranes for gas separation.[103] Caro's group pioneered this field of research in both MOF and ZIF membranes.[104–108] Their first attempt to grow MOFs on a porous alumina and graphitic support was similar to the techniques established for preparing zeolite membranes.[104] However, regardless of the surface activation and basic treatment the MOF density was poor. They also trialled a seeding approach where ground $Mn(HCO_2)_2$ MOFs were rubbed into the support membranes. This method improved the MOF films; however, the crystal orientation prevented the MOFs from being useful as a separation membrane as the pores ran parallel to the support.[104] Caro *et al.* increased the MOF density and controlled the crystal orientation of the ZIF-7 $(Zn(bIm)_2)$ and ZIF-8 membranes by the preparation of a viscous seeding solution containing polyethyleneimine (PEI) to improve the adhesion of the homogeneous seeds to the membrane support, and by the use of microwaves to grow the secondary ZIF membrane film.[105–108]

A variety of MOF type membranes have since been developed using the homogeneous seeding and secondary growth method with improved orientation for the use in gas separation including; MMOF $[Cu(hfipbb)(H_2hfipbb)_{0.5}][(H_2hfipbb)4,4'-(hexafluoroiso-propylidene)-bis(benzoic acid)]$,[103] ZIF-8,[109,110] HKUST-1,[111] ZIF-69[112] $(Zn(nIm)_2, H2nIm = 2-nitroimidazole)$, MOF-5,[113] MIL-101(Cr)[114] $(Cr_3OF(BDC)_3)$, MIL-53(Al)[115] $(Al(OH)(BDC))$, MIL-96(Al)[116] $(Al_{12}O(OH)_{18}(Al_2(OH)_4)(BTC)_6)$ and NH_2-MIL-53(Al) $(Al(OH)-(aBDC))$.[117] Yusenko *et al.* used the LbL deposition technique to seed the membrane support with $[Cu_2(ndc)_2(dabco)]$ MOF particles on non-functionalised substrates $(Al_2O_3, SiO_2, Ta_2O_5$ and $Si_3N_4)$.[87] The seeded supports were then placed in the $Cu_2(ndc)_2(dabco)$ mother solution for the secondary growth to form a thick MOF layer. Nan *et al.* used a similar LbL technique to form HKUST-1 membranes on α-alumina supports.[118] The HKUST-1 seeds were grown from the initial reaction of the H_3BTC carboxyl groups and the hydroxyl groups of the alumina substrate. The substrate was then immersed in a copper acetate solution to form the MOFs. After several cycles, the HKUST seeds were formed and then used in a secondary mother solution to form a full membrane.[118]

Heterogeneous nucleation. Gascon *et al.*[43] were one of the first groups to develop a heterogeneous seeding approach for the growth of MOF membranes.[119,120] Using coordination polymers, they were able to prepare dense coatings of HKUST-1 MOFs on α-alumina supports. Homogeneous seeds were found to grow MOF crystals that were too large, forming cracks in the membrane, whereas the use of heterogeneous seeds produced a thin, uniform HKUST-1 membrane. In this case the heterogeneous seeds were a 1D isomorph of the 3D HKUST-1 MOF structure.

The phase of the MOF changed from 1D to 3D during the secondary growth.[43]

Yoo *et al.* have used microwave synthesis to directly nucleate the MOF seeds onto a graphitic membrane support.[121,122] The heterogeneous nucleation and growth on the graphite supports required no additional surface modification. The microwave-assisted heating at the interface of the support and the MOF precursor solution induces heterogeneous nucleation as this growth method is not favourable under regular solvothermal conditions.

The same authors used the microwave seeding technique to prepare the heteroepitaxial growth of framework structures in which MOF-5 was used as a seed to grow IRMOF-3 $(Zn_4O(aBDC)_3)$ on a porous alumina support.[123] IRMOFs have identical crystal structures and similar unit cell parameters; however, they have different chemical functionalities, making them ideal materials for heterogeneous seeding and for building core–shell type hybrid structures.[123,124]

Koh *et al.* simultaneously prepared core–shell IRMOF-3/MOF-5 particles using this seeding method. They extended the method further by making multiple alternate layers by growing a third layer (Fig. 10).[124]

Patterning. Falcaro *et al.* developed a seeding method using a number of different heterogeneous seeds to spatially control the position as well as the growth rate of MOFs.[125–127] Using poly-hydrate phosphate (α-hopeite) microparticles as nucleation seeds allowed the MOFs to be grown both in solution and on solid surfaces. The addition of a surfactant, Pluronic F-127, into the MOF-5 precursor solution, promoted the formation of these ceramic microparticles (denoted Desert Rose Microparticles, DRMs, due to their flower-like appearance). These particles then become seeds for the nucleation and growth of MOF-5 and their presence in the MOF-5 solution increases the rate of MOF growth by a factor of 3.[125] The ability to spatially locate the MOF growth was demonstrated by positioning isolated DRMs into litho-graphed patterned wells and then nucleating and growing MOF particles and films from the wells (Fig. 11). Another advantage to this method is that the DRMs can be further functionalised with quantum dots (QDs). These luminescent MOFs were placed in a solution of two different thiols, demonstrating that only thiols
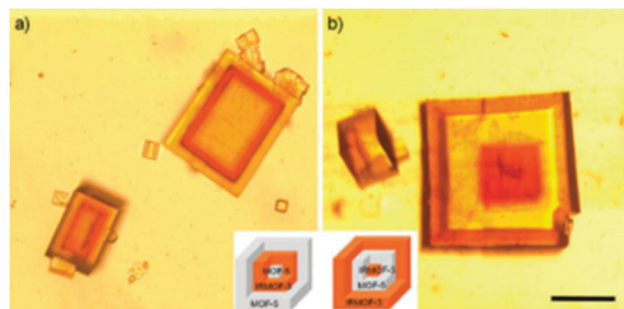

Fig. 10 Microscope images of the core–shell MOFs grown by heterogeneous nucleation. (a) MOF-5 core, IRMOF-3 middle layer and MOF-5 outer layer. (b) IRMOF-3 core, MOF-5 middle layer and IRMOF-3 outer layer. Scale bar is 200 μm.[124]

5522 | *Chem. Soc. Rev.*, 2014, **43**, 5513–5560

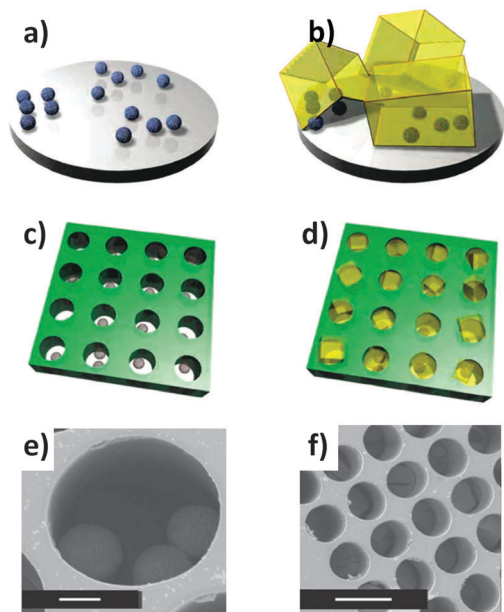This journal is © The Royal Society of Chemistry 2014

Fig. 11 (a and b) Schematics of ceramic particles used for the nucleation of MOF–5 particles. (c) A ceramic particle suspension was positioned on the patterned substrate. (d) A standard MOF–5 growing medium is introduced for the MOF formation within the membrane holes. SEM images of (e) ceramic particles located in a hole of the substrate (scale bar, 10 μm), and (f) MOF–5 crystals growing within each one of the lithographed holes (scale bar, 50 μm).[125] Video animation provided as ESI.†

that are small enough to penetrate the MOF porous lattice could reach the functional DRMs and quench the QD luminescence.[125]

Falcaro et al. extended this technique to other heterogeneous seeds in order to demonstrate the versatility of the approach.[126,127] Carboxy- and amino-functionalised silica nanoparticles were used for the fast nucleation of mono-dispersed MOF-5 crystals. Using these seeds, the nucleation and growth of MOF-5 is up to 10 times faster than the regular solvothermal methods used. By seeding a silicon substrate with the silica nanoparticles, MOF-5 films were successfully grown without any surface modification of the substrate.[126,127] Recently, Liu et al. reported a seeding technique using microsized zeolite crystals (MOR, Y and ZSM-5) as nucleating seeds for the synthesis of MIL-101(Cr), MIL-100(Cr) $(Cr_3OF(BTC)_2)$, and MIL-53(Fe) $(Fe(OH)(BDC))$. As with Falcaro's technique, the presence of the zeolites shortened the crystallisation time by up to 75%.[128]

Advantages and limitations. Although the use of heterogeneous seeds often requires an extra step in preparing the MOF materials, there are many advantages to using seeds for the spatial localisation and the fast production of MOFs. The heterogeneous seeds are more chemically stable than homogeneous MOF seeds and are potentially easier to form and store. Heterogeneous MOFs can be combined with lithographic techniques for the spatial localisation of the grown MOFs and can also be functionalised for further applications. The seeding technique speeds up the growth of MOFs, making this a promising method for the industrial synthesis of MOFs. One limitation is that the seed remains in the final MOF, and can

therefore reduce the overall porosity and surface area of the final material. The nanoparticles can induce defects into the lattice structure, and this could interfere with the final properties in instances where single crystals are required. If the seeds constitute a problem, customised washing steps may be required to remove any unreacted seeds from the final product material.

2.3.4 Contact printing (evaporation induced growth)

Technique development. The solvent used to synthesise MOF precursor solutions has been found to play a critical role in the kinetics of MOF formation. For example, the standard precursor solutions used for MOF-5 (zinc nitrate and H_2BDC acid in dimethylformamide (DMF)[98] or diethylformamide (DEF)[129]), are stable at ambient temperature for prolonged periods. In the case of other MOF precursor solutions, such as those commonly used to make HKUST-1 (copper nitrate and H_3BTC in an ethanol–water mixture[93]) and ZIF-8 (zinc nitrate and HmIm in methanol[130]), nucleation of the MOF is observed at room temperature. The premature crystallisation of MOF particles within their respective precursor solutions can be problematic for device fabrication, as it becomes difficult to anchor the particles securely to the substrate.

Ameloot et al.[102] demonstrated that the precursor solution for HKUST-1 could be stabilised at room temperature by replacing the ethanol–water solvent with DMSO. Compared to water or ethanol, DMSO has a strong affinity towards the metal ions in solution and also allows for the formation of hydrogen bonded solvate structures with the H_3BTC ligand. These solute–solvent interactions stabilise the solution, preventing nucleation of the MOF crystals at room temperature. The authors went on to demonstrate that the stabilizing effect is reversible, and that well-formed HKUST-1 crystals could be produced by prolonged heating of the solution, and more interestingly from a patterning perspective, by evaporating the solvent under controlled conditions.

Patterning. In their report,[102] Ameloot et al. describe how evaporation induced growth (also known as Evaporation Induced Self Assembly (EISA)[131]) combined with μCP[132–134] can be used to directly produce high quality patterns of HKUST-1 crystals. In this process, a microlithographed polydimethylsiloxane (PDMS) stamp is wet with the MOF precursor solution, and subsequently placed in contact with the substrate (Fig. 12a and b). Due to capillary forces, the MOF precursor solution is confined underneath the stamp protrusions (a process known as lithographically controlled wetting[135]), limiting the growth of the MOF crystals to specific areas. Upon heating the substrate to 100 °C, the solvent begins to evaporate, causing MOF crystals to nucleate and grow in an ordered fashion (Fig. 12c–e). The authors observed that the HKUST-1 crystals produced by this process were all of a very similar height (due to the confined synthesis volume) and preferentially orientated along the [111] direction. This result was irrespective of the substrate surface chemistry, as the same crystal orientation was observed for silanol, vinyl or carboxylic acid functionalised substrates. In addition, the authors demonstrated that evaporation is the main driving force for MOF nucleation in this process, by showing that no nucleation occurs within a
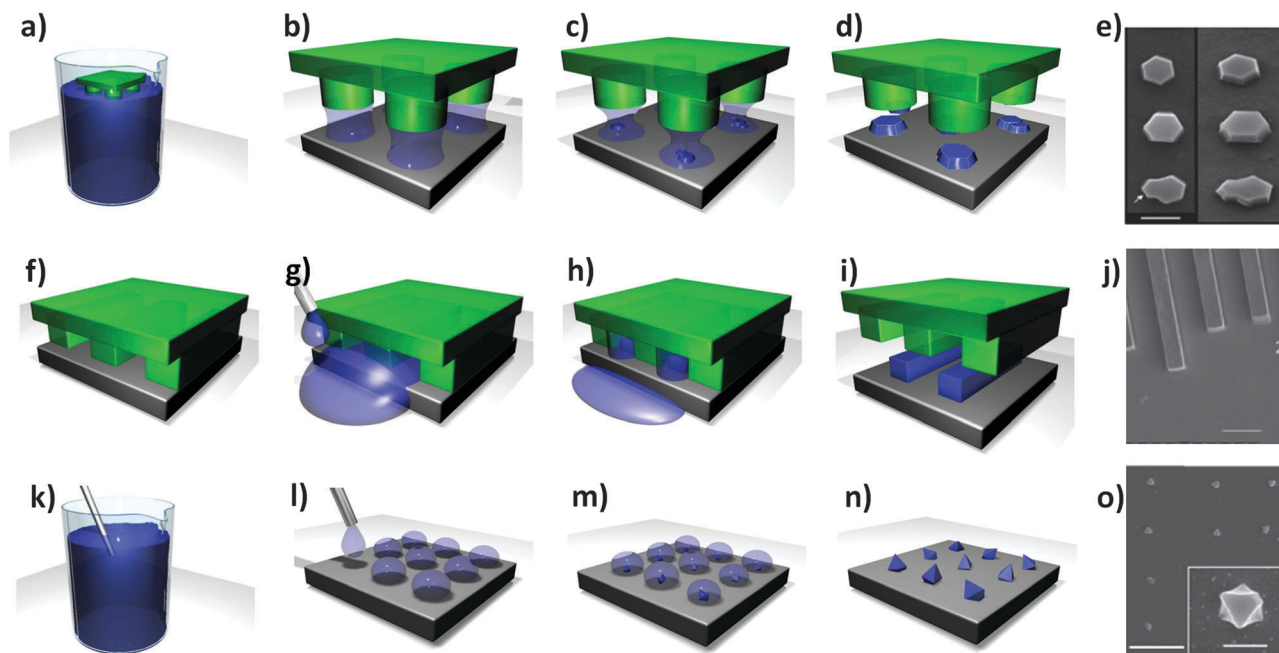
This journal is © The Royal Society of Chemistry 2014

Chem. Soc. Rev., 2014, 43, 5513–5560 | 5523

Fig. 12 (a–d) Schematic showing the formation of HKUST-1 crystals within confined volumes, using µCP combined with controlled solvent evaporation. (a and b) A lithographed stamp is wet with a stable precursor solution and placed in contact with the substrate. (c and d) The stamp is left in contact with the substrate while the solvent evaporates, producing well-defined MOF crystals. (e) SEM image of the HKUST-1 crystal patterns obtained (scale bar 1 mm). Reproduced with permission from Ameloot et al.[102] (f–i) Schematic showing the coordination polymer line patterns obtained using the MIMIC process. (f) A dry stamp is placed in contact with the substrate. (g and h) a droplet of solution is dispensed at the edge of the stamp, filling the channels by capillary forces. (i) The solvent is allowed to evaporate, leaving a pattern which follows the contours of the stamp. (j) FESEM image of coordination polymer line patterns (scale bar 10 µm). Reproduced with permission from You et al.[136] (k–o) Schematic of the pen-type lithography method for fabricating single crystal MOF arrays. (l) Droplets are dispensed by bringing a microfluidic pen into contact with a substrate. (m and n) MOF crystals are then grown by controlled evaporation of the solvent. (h) FESEM image of an array of HKUST-1 single crystals formed on a gold substrate prepared with CH₃-terminated functional groups. Scale bar 5 µm and inset 500 nm. Reproduced with permission from Carbonell et al.[137] Video animations provided as ESI.†

sealed vessel (*i.e.* evaporation blocked) heated to the same temperature for an equivalent time. An ordered array of MOF-5 crystals was also produced by the authors using the same method.

An interesting feature of coordination polymers is that they can be reversibly de-polymerised by dissolving them in a strong coordination solvent, and then re-polymerised back into their initial macrostructure by controlled removal of the solvent. You *et al.*[136] showed that this reversible de-polymerisation behaviour of coordination polymers could be combined with a standard lithographic method known as micromolding in capillaries (MIMIC[138]) to produce well-defined patterns. In this process, a dry PDMS stamp featuring lithographed micro-channels is pressed against the substrate to be patterned (Fig. 12f). The precursor solution, in this case zinc coordinated 4,4′-di(4-pyridyl)cyanostilbene dissolved in an excess of pyridine, is then deposited at the edge of the stamp, causing the solution to be sucked into the micro-channels by capillary forces (Fig. 12g and h). The solvent is then removed, either by evaporation or by absorption into the stamp, depositing the desired material onto the substrate (Fig. 12i). Finally, once the crystallisation process is completed, the stamp can be removed from the substrate to reveal the pattern (Fig. 12j). The authors demonstrated that bi-dimensional micro-arrangements of highly luminescent reticular superstructures could be fabricated on a silica substrate using this approach. The authors observed that the polymer microstructures reproduced the

geometry of the micro-channels with high precision and that shrinkage of the pattern was minimal.

When the process of evaporation induced growth is combined with other free-form methods for depositing individual droplets on substrates, such as pen-type nanolithography, highly accurate and customisable MOF patterns can be achieved.[137,139,140] This approach provides control over the volume of precursor solution to be deposited at a specified location, which allows the conditions necessary for producing single MOF crystals of a particular size to be quickly investigated and selected for use in specific applications. Although precise droplet deposition can be achieved by functionalising the tip of a conventional atomic force microscope (AFM),[139] dedicated commercial instruments are now available that allow control over both the dispensing and mixing of nano to femtolitre droplets.[137,140] Once the droplets of the MOF precursor solution are located on the surface of the substrate, controlled evaporation of the solvent can then be used to synthesise the MOF crystals (Fig. 12k–o).

Carbonell *et al.*[137] first reported the use of pen-type nanolithography for patterning MOF crystals, using a stable precursor solution for HKUST-1 employing DMSO as the solvent. The authors found that the contact angle of the droplets is a critical factor in obtaining controlled precipitation of a single MOF crystal per droplet under ambient conditions. If the surface is coated with hydrophobic functional groups such as

5524 | *Chem. Soc. Rev.*, 2014, **43**, 5513–5560

This journal is © The Royal Society of Chemistry 2014

–CF$_3$ or –CH$_3$, the contact angle is increased and single crystals are obtained. However, if the surface is made hydrophilic by using functional groups, such as –NH$_3$, –COOH or –OH, the solution wets the substrate and multiple small crystals are formed. By controlling the size of the droplets deposited and their contact angle, single HKUST-1 crystals were obtained in the 0.5 to 1.2 μm range. The authors noted that the HKUST-1 crystals grown on the –CH$_3$ and –CF$_3$ functionalised surfaces tended to preferentially orientate along their [111] directions.

Recently Carbonell et al.[140] reported further progress in the use of pen-type nanolithography, demonstrating that mixing of femtolitre volumes could be accurately and reproducibly achieved. The authors showed that a microfluidic pen, located in an controlled atmosphere to limit evaporation, could be used to compartmentalize the crystallization of HKUST-1, by introducing a femtolitre droplet of H$_3$BTC in DMSO to another femtolitre droplet of Cu(NO$_3$)$_2$·2.5(H$_2$O) in DMSO that had already been deposited on a SiO$_2$ surface. Crystallization of HKUST-1 was then induced by removing the substrate from the instrument and allowing the DMSO to evaporate under ambient conditions (Fig. 13a–c). The authors also described how this approach could be extended to produce multiplexed arrays of crystalline materials, using four microfluidic pens to deposit and mix precursor solutions for four different Prussian blue analogues (PBAs): Cd$_3$[Co(CN)$_6$]$_2$, Zn$_3$[Co(CN)$_6$]$_2$, Mn$_3$[Co(CN)$_6$]$_2$, and Ag$_3$[Co(CN)$_6$]) (Fig. 13d–i). The problem of cross-contamination from the microfluidic pen during mixing was solved by introducing a cleaning step, which involved depositing several droplets of solution outside the working area between each mixing operation.

Finally, Gassensmith et al.[141] have proposed a novel approach based on μCP that can be used to pattern substrates as well as the surfaces of larger crystals. The authors first prepared an azide-terminated SAM on a silicon substrate. This monolayer was then patterned by μCP, using a PDMS stamp loaded with a solution of copper sulphate, ascorbic acid and pentynoic acid, to form repeating rows of carboxylic acid groups exploiting the azide–alkyne Huisgen reaction, which is part of the click chemistry methodology.[142] When immersed in a MOF-5 precursor solution (zinc nitrate, H$_2$BDC and DMF), the pentynoic acid pattern provides a nucleation site for MOF growth. Thin films of MOF-5 approximately 40 nm high were shown to grow preferentially on top of the pentynoic acid pattern by leaving the substrate in the solution at 85 °C for 48 h, while negligible MOF growth was observed on the azide coated surfaces. However, much larger crystals (>0.5 mm) could also be grown on the substrate by continued immersion in the precursor solution. Interestingly, when these crystals were gently removed from the substrate, the surface which had been in contact with the pentynoic acid was shown to be embossed with a replica of the printed pattern. This work demonstrates the possibility of using μCP SAMs as a form of stamp for patterning the surfaces of crystals with nano-scale features.

Advantages and limitations. The contact printing methods presented here each have its own set of advantages and limitations. μCP followed by evaporation induced growth has the advantage of being low cost and relatively straightforward, the stamps are reusable (important for mass production), and the crystal growth is controlled. MIMIC is also low cost, straightforward, allows reusable stamps, and can produce well-defined geometries. Pen-type lithography is very flexible, provides mixing capabilities, and can precisely control crystal size and shape. However, none of these contact printing methods is particularly compatible with 3D substrates, and these methods can be considered slow compared to competing protocols such as electrochemical deposition.

2.3.5 Microfluidics

Technique development. Microfluidic devices are increasingly being used to study crystallisation reactions, due to the fine control they provide over the way precursor solutions are brought into contact with one another and/or manipulated. The unique conditions offered by microfluidic devices, such as turbulence-free environments, reduced gravity effects, large surface to volume ratios, precise manipulation of small liquid volumes and excellent control over mass and heat transport, as well as their compatibility with in situ characterisation techniques, makes them very attractive for both research and end-user applications.[143] There are a number of different ways in which microfluidic technologies can be used to synthesise, pattern and employ MOF materials and coatings. Broadly speaking, these technologies can be divided into three different application areas, including: (1) methods for printing MOF patterns on removable substrates, (2) devices that employ localised MOFs as functional components directly, and (3) methods for synthesising MOF particles with highly consistent properties and morphologies.

Fig. 13 (a–c) FESEM images of an HKUST-1 crystal array (feature distance = 25 μm), produced using pen-type lithography. (d and e) FESEM images of a multiplexed 4 × 4 array of crystalline PBAs with general formula M$_3$[Co(CN)$_6$]$_2$, where M is Cd(II), Zn(II) and Mn(II), and Ag$_3$[Co(CN)$_6$] (feature distance = 25 μm), illustrating the mixing capabilities of this technique. (f–i) FESEM images of individual deposits of (f) Cd(II)-PBA, (g) Zn(II)-PBA, (h) Mn(II)-PBA, and (i) Ag(I)-PBA nanocrystals (scale bars, 2 μm). Reproduced from Carbonell et al.[140]

Patterning. Digital microfluidics is a rapidly emerging technology that is particularly well suited to printing MOF patterns on a range of substrates (i.e. application area 1). This technique enables small droplets of solution (<1 μL) to be independently
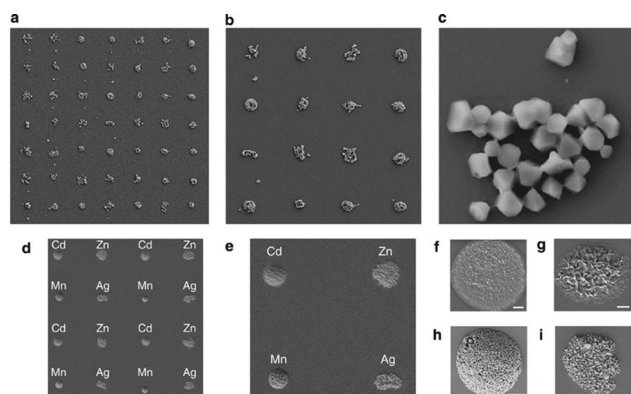
This journal is © The Royal Society of Chemistry 2014

Chem. Soc. Rev., 2014, 43, 5513–5560 | 5525

manipulated on the surface of a hydrophobic substrate using software controlled electronic signals. The major advantage of digital microfluidics is that only selected areas of the substrate come into contact with the solution, meaning that contact with other features of the substrate, such as electrical connections which may be sensitive to corrosion, can be avoided. The droplet actuation technology is relatively inexpensive and allows all fluidic elementary operations (droplet dispensing, splitting, merging, transport, and mixing) to be performed on-chip using reconfigurable pathways.

Witters *et al.*[144] have described an implementation of digital microfluidics which enables large arrays of MOF crystals to be rapidly and accurately printed. Their methodology consists of a modular two-plate digital microfluidic device in which the bottom plate of the assembly, containing the electronics, is dedicated to the transport of micro- to nanolitre-sized 'mother droplets'. Droplet actuation is achieved by the electrowetting-on-dielectric principle, in which an imbalance in the interfacial tension between a liquid droplet and an electrode coated with a dielectric layer is used to propel the droplet. The hydrophilic substrate onto which the MOF crystals are to be printed is coated with a patterned hydrophobic layer (*e.g.* Teflon AF), forming hydrophilic-in-hydrophobic micropatches, and constitutes the top plate of the device. Mother droplets are generated on-chip from a fluid reservoir, and then transported over these micropatches, dispensing femtolitre droplets into the hydrophilic micropatches in the process, as shown in Fig. 14.

By removing the top plate after printing and controlling the evaporation rate of the solution contained in the micropatches, large grids of single MOF crystals can be grown with high spatial control, high monodispersity and high crystal orientation ([111] direction) (Fig. 14e–g). Furthermore, the size of the MOF crystals was shown to be controlled by the size of the micropatches in which the MOFs are grown.

Witters *et al.*[145] have also demonstrated that this digital microfluidic methodology can be used to deposit thin, dense,
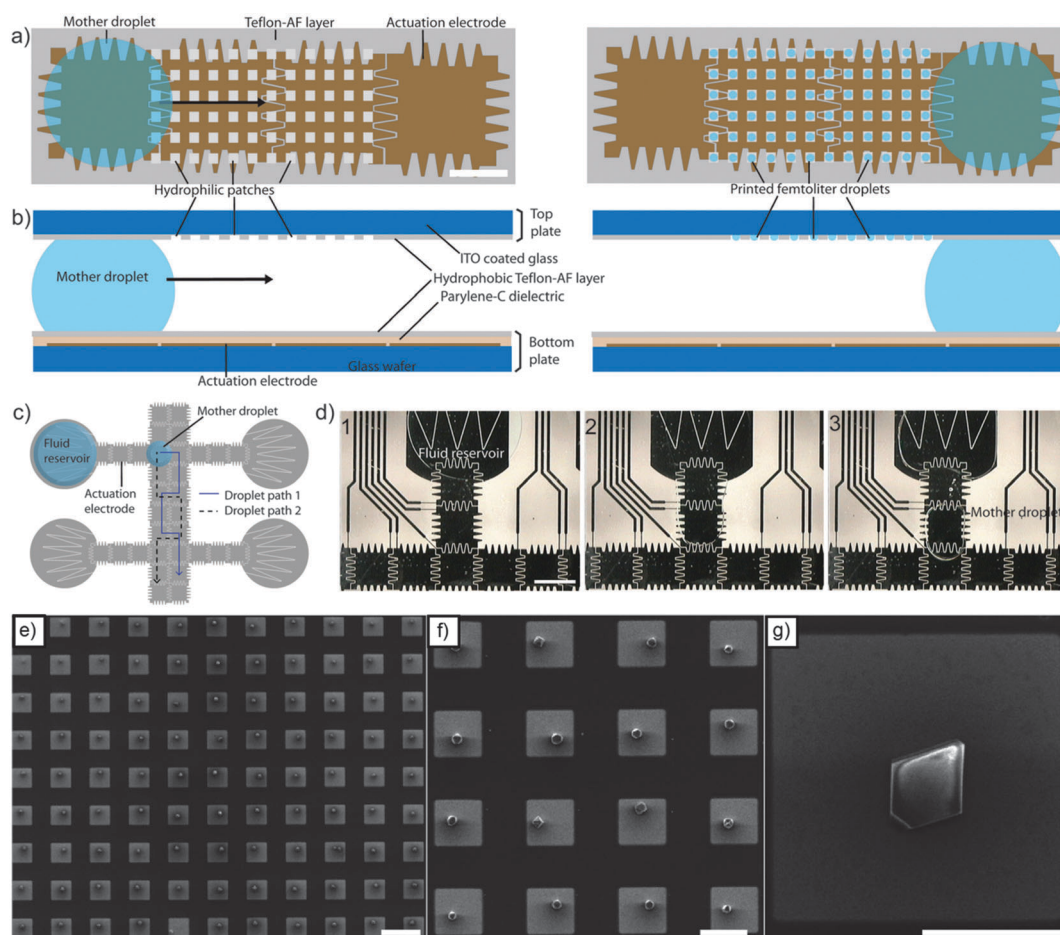

Fig. 14 (a and b) Schematic of the digital microfluidic chip implemented by Witters *et al.*[144] for printing of MOF crystals (scale = 700 μm). Mother droplets are transported over arrays of hydrophilic-in-hydrophobic micropatches, dispensing femtolitre droplets of solution in the process. (c) Schematic illustrating two different paths that could be taken by a mother droplet by applying different actuation sequences to the electrodes. (d) Sequence of images from a movie showing how a mother droplet is dispensed from a fluid reservoir onto a path made from actuation electrodes (scale = 1.4 mm). (e–g) SEM images of single HKUST-1 crystal arrays produced by controlled evaporation. The square-shaped micropatches (20 μm × 20 μm) are ITO in a hydrophobic Teflon-AF matrix, over which a mother droplet has passed. Highly monodisperse single crystals can be observed after controlled evaporation of the solution. Scale bars represent 40 μm (e), 20 μm (f), and 10 μm (g). Reproduced with permission from Witters *et al.*[144]

5526 | *Chem. Soc. Rev.*, 2014, 43, 5513–5560

This journal is © The Royal Society of Chemistry 2014

polycrystalline films within the micropatches using the LbL technique. In that work, droplets of a metal salt solution, an organic ligand solution, and clean rinsing solvent are repeatedly dispensed from on-chip fluid reservoirs and transported over the micropatches in the top plate by the actuation electrodes in the bottom plate. Using this approach, micropatches with thicknesses of around 550 nm can be grown after an equivalent of 40 LbL cycles.

Using the same methodology Witters et al.[146] have recently shown that digital microfluidics can also be used to seed micro arrays with magnetic particles. This was achieved by repeatedly passing a droplet loaded with micron-sized particles over a patterned micro array, using a permanent magnet to attract and trap the particles in the individual wells. When combined with magnetic MOF composites, such as those described by Falcaro et al.,[147] this technology could easily be extended to seeding micro arrays with MOF particles.

Microfluidic technology is not restricted to material synthesis; it can also employ localised functional materials directly in order to achieve certain functionality within a miniaturised device (i.e. application area 2). For example, Puigmartí-Luis et al.[148] have recently described a continuous flow microfluidic device containing pneumatically actuated clamps that can be used to trap material on top of sensing electrodes. These authors have shown that bundles of silver-tetracyanoquinodimethane (Ag(I)TCNQ) coordination polymer nanowires, produced by interfacial reaction between two laminar flows of precursor solution and trapped using the pneumatic clamps, can be used as an organic memory element in this device. Microfluidic devices employing pneumatically actuated barriers have also been used by authors from the same group to confine and mix sub-nanolitre volumes of solution over sensing electrodes.[149] The parallelism of this approach lends itself to screening platforms and multifunctional array fabrication.

Modern continuous flow and droplet-based microfluidic devices offer a very high level of control over fluid dispensing and mixing operations, and hence are well suited to the final application area. For example, these devices can be used to mix and subsequently confine MOF precursor solutions within individual droplets that are suspended in an immiscible fluid (Fig. 15). Solvothermal MOF crystallisation can then be precisely controlled by passing the droplets through a heating stage with a prescribed dwell time.[150,151] The advantages of this approach over conventional solvothermal processes include significantly increased reaction kinetics, continuous production, narrow particle size distribution and high efficiency. Novel heterostructures, such as core–shell particles, can also be produced using this technique by merging droplets at different stages of the process.[150]

The morphology of the MOF particles produced using continuous flow microfluidic devices can also be controlled by taking advantage of the interface between different fluids. This is highlighted very well in the article by Ameloot et al.,[152] which describes the synthesis of hollow MOF spheres. If the organic and inorganic precursors are dissolved in two different immiscible solvents, the precursors can be made to encounter each other from opposite sides of a liquid–liquid interface, enabling the
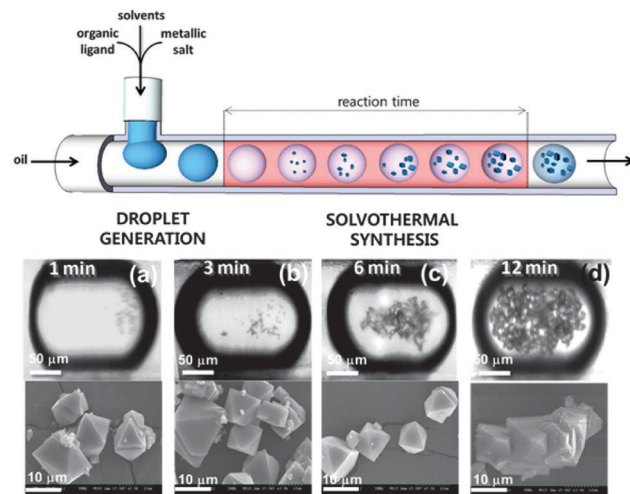

Fig. 15 Schematic representation of a continuous flow microfluidic device for producing high quality MOF crystals (top). Optical and SEM micrographs of HKUST-1 crystals obtained via the microfluidic approach after (a) 1, (b) 3, (c) 6, and (d) 12 min of synthesis. Reproduced from Faustini et al.[150]

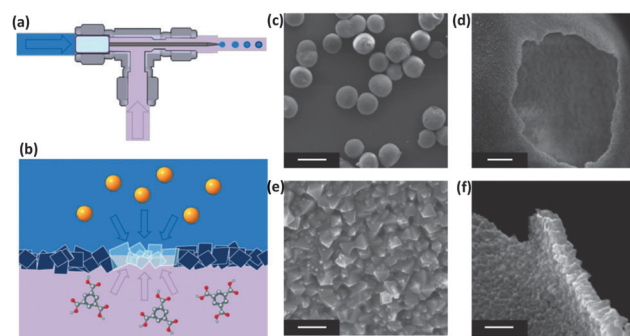

Fig. 16 (a) Schematic showing the T-junction used by Ameloot et al. to synthesise hollow MOF spheres. Individual droplets of an aqueous metal-ion-containing solution (blue) are suspended within a flowing organic ligand solution (purple) using a tapered capillary positioned within the T-junction. (b) The metal cations encounter the organic linkers at the surface of the droplet, resulting in the localised formation of MOF crystals. (c–f) SEM of the hollow HKUST-1 spheres. (c) The capsules retain their spherical shape upon drying and are highly monodisperse in size (scale bar 500 μm). (d) The hollow interior of the sphere is revealed by creating a hole with a needle (scale bar 25 μm). (e) Detail of the defect-free capsule wall. The gaps between larger crystals are sealed by smaller crystals (scale bar 2 μm). (f) Cross-sectional view of the capsule wall, showing its thin and uniform thickness (scale bar 2 μm).[152]

self-completing interfacial formation of a MOF layer (Fig. 16). Using a simple T-junction, the authors have shown how the surface of droplet can act as a template for growing hollow MOF structures that are interesting candidates for applications such as microreactors.[152] Importantly, the precursor solutions do not necessarily have to be immiscible in order to achieve interfacial control. Puigmartí-Luis et al.[153] have demonstrated that coordination polymer nanowires can be produced by an interfacial reaction between two precursor solutions using a laminar-flow microfluidic device. This approach is promising for the synthesis of novel 1D MOF structures.[154]

Advantages and limitations. Microfluidic methods offer a number of advantages for the fabrication of MOF-based devices, including fine control over the composition and morphology of the MOF, rapid crystallisation, efficient use of precursor solutions, and accurate positioning of the MOF onto various substrates. Microfluidics can also be used to directly synthesise and employ MOFs within multifunctional platforms. However, depending on the synthetic approach used to prepare the MOF, a compatible microfluidic chip may need to be fabricated, and this can be an expensive option. If a large quantity of material needs to be prepared, a large number of microfluidic systems need to be used in parallel, which can increase the cost of the process.

2.3.6 Conversion from ceramics

Technique development. Very recently, a new research trend in MOF technology has shown how ceramics can be used as feedstock materials for MOF synthesis. This emerging field is now presenting tremendous potential for MOF-based device fabrication, taking advantage of the different technologies used for the production of ceramic films and patterns with finely tuned chemical compositions (*e.g.* sol–gel,[155,156] physical and chemical vapour methods,[157–160] spray deposition,[161–165] chemical processing of metals[166–168]).

The first breakthrough was proposed by Zou and co-workers, who used a zinc slice activated with H_2O_2 to induce the formation of zinc hydroxide.[169] The coating was immersed in an aqueous solution of H_3BTC. Further treatment in an autoclave at 140 °C for 6 h showed a change in the surface roughness and the formation of needle shape crystals. The film was investigated using XRD revealing a pattern corresponding to that of $Zn_3(BTC)_2$. Interestingly, such a film was found to be highly sensitive to, and selective for dimethylamine. Under excitation, this film demonstrated variations in emission spectra depending on the amount of dimethylamine and the solvent used (*e.g.* water, acetonitrile, ethanol).

Hu and co-workers proposed a reactive seeding approach for the synthesis of MIL-53(Al) framework by direct reaction of the metal precursor with the ceramic support.[115] A ceramic α-Al_2O_3 support was used as the aluminium precursor (instead of $Al(NO_3)_3\cdot 9H_2O$), which reacted with H_2BDC under mild hydrothermal conditions to grow a homogeneous MIL-53(Al) MOF film that was subsequently used as a seeding layer. A secondary growth process was carried out using $Al(NO_3)_3\cdot 9H_2O$ and H_2BDC to form the MIL-53(Al) membrane under hydrothermal conditions at 220 °C for 12 hours. X-ray diffraction (XRD) studies showed that the MOF crystal structure, which was synthesised using a porous alumina membrane as the source of Al, is consistent with the MIL-53(Al) pattern reported in the literature. Later, these authors studied the mechanisms of reactive seeding in detail by employing MIL-96(Al) as a model. A two-step reaction mechanism was proposed. The α-Al_2O_3 support was shown to firstly react with H_2O to produce γ-AlO(OH) under hydrothermal conditions, and then the γ-AlO(OH) interacted with the ligand to form the MIL-96(Al) seed crystals.[116]

Patterning. An important discovery in this field was proposed by Reboul *et al.* in 2012.[170] The authors discovered a versatile synthetic strategy for 3D mesoscopic MOF architectures using

pseudomorphic replication, the morphologic replacement of a shaped sacrificial metal oxide, used as both a metal source and an "architecture-directing agent", by an analogous MOF architecture. An ordered array of 1 μm polystyrene beads was used as a template for the synthesis of two-dimensional honeycomb patterns or three-dimensional inverse opal structures.[171] The ordered array was then infiltrated with a sol–gel solution containing aluminium tri-*sec*-butoxide subsequently calcined at 580 °C for 7 h. The subsequent reaction of the pattern for 10 min at 180 °C in an aqueous solution of H_2ndc under microwave conditions induced the formation of an aluminium naphthalene dicarboxylate framework $[Al(OH)(ndc)]_n$ based on one-dimensional inorganic chains of $[Al(OH)(COO)_2]_n$.[170] The major advantage of this method was the simultaneous spatio-temporal synchronization of the metal oxide template dissolution and the MOF crystallization, allowing the preservation of very fine morphological details of the parent metal oxide architectures. Using structurally diverse alumina with 2D honeycomb, 3D inverse-opal, and 3D randomly structured aerogels as the sacrificial template, aluminum-based frameworks $[Al(OH)(ndc)]_n$ with parental alumina architectures were fabricated. In particular, the 3D randomly structured MOF aerogels possessing hierarchical porosities (hydrophobic micropores of the MOF and the mesopores/macropores inherited from the alumina aerogels) synergistically enhanced the material's flux and selectivity for water–ethanol separation. Since the fabrication of 3D architectures based on ceramics is widely realized, this emerging method of MOF processing into 3D architectures allows the processing of MOF materials in almost any desired shape including patterns with different architectures (Fig. 17a–e).[53]

Majano and co-workers discovered that a commercial slurry of $Cu(OH)_2$ could be easily and quickly transformed into HKUST-1 at room temperature.[174] The addition of the slurry into an alcoholic solution of H_3BTC induced MOF formation, with a few seconds being enough to visibly detect the change from light blue to deep turquoise. The Brunauer–Emmett–Teller (BET) surface area was approximately 1500 m^2 g^{-1}, and most importantly, DMF was not needed for the preparation of these Cu-based MOFs. Although this work presented a synthesis for powder HKUST-1-, the discovery was adopted for use in the patterning of MOFs by Okada and coworkers.[172] The authors used a well established protocol for the conversion of copper metal substrate into $Cu(OH)_2$ nanotubes based on the immersion of the metal into an aqueous solution of sodium hydroxide and ammonium persulphate.[9] The formation of $Cu(OH)_2$ nanotubes was detected within 30 min of reaction.[172] The nanotubes were subsequently transformed into HKUST-1 using the previously discovered DMF-free alcoholic solution with H_3BTC. This method has illustrated an alternative to the autoclave and electrochemical methods used to grow HKUST-1 from copper metal.[44,176] With this new conversion method, a mesh was decorated with a film of MOFs and the catalytic activity was tested using the Friedländer reaction test to evaluate the MOF catalytic properties.[177–179] In this study, established technology for patterning copper for microelectronics applications was translated to the MOF field. Photolithography was used for
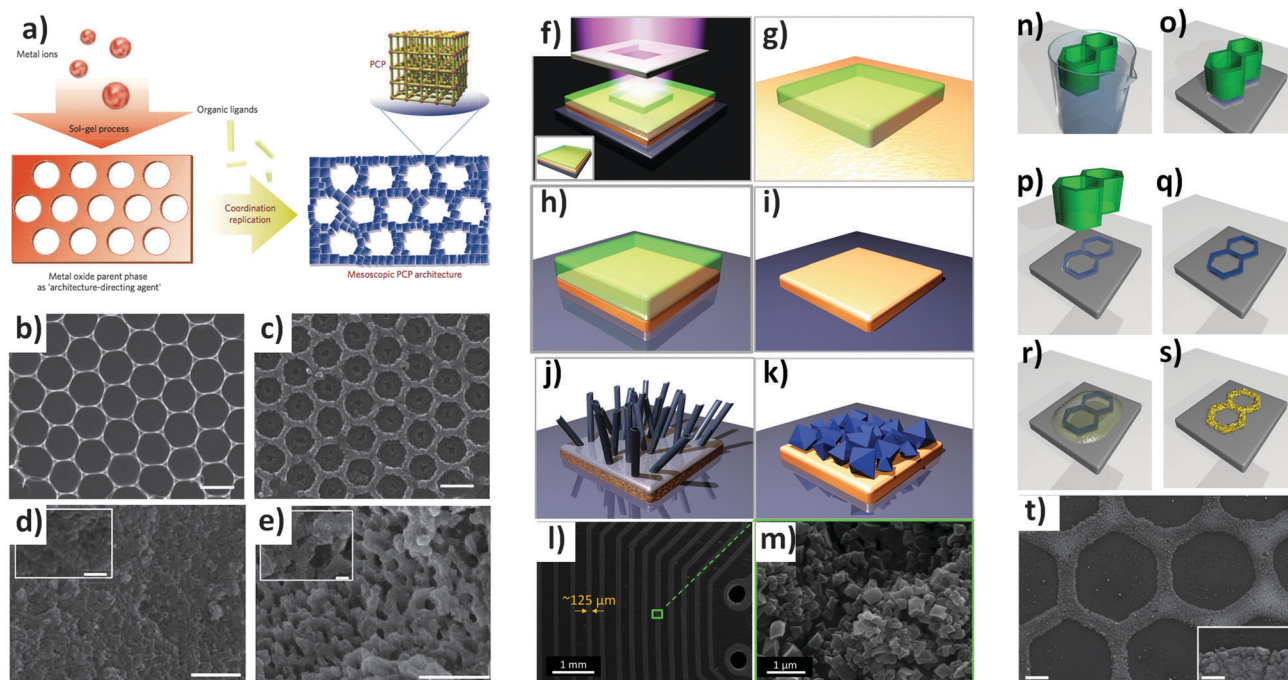
Fig. 17 (a) Schematic illustration of the coordination replication method. (b) Top-view FESEM images of the alumina hexagonal pattern. (c) Top-view FESEM images of the $[Al(OH)(ndc)]_n$ replica obtained from (b) after microwave treatment. (d) FESEM images of meso-$[Al(OH)(ndc)]_n$ replica obtained from mesoporous aerogel. (e) FESEM images of macro-$[Al(OH)(ndc)]_n$ replica obtained from macroporous aerogel. (b and c) scale bars are 1 μm. (d and e) scale bars are 10 μm (1 μm for the inset).[170] (f–k) Schematic illustration of the formation of HKUST-1 crystals from patterned copper substrates. (f) The copper substrate is coated by a commercial resist, which is exposed to UV radiation through a photomask with a Cr pattern. (g–i) After washing the remaining photoresist with ethanol, the patterned Cu board is formed. (j) $Cu(OH)_2$ nanotubes are then formed via a treatment with NaOH and $(NH_4)_2S_2O_8$ in water. (k) MOF formation can be obtained by exposing the $Cu(OH)_2$ to the H_3BTC ligand. (l and m) SEM images showing the conversion from a Cu pattern into HKUST-1 achieved on a printed electronic circuit board (PCB).[172] The light gray parallel lines are made on copper decorated by MOF. The MOF growth occurs only on top of the copper. (n–t) Schematic showing ZIF-8 patterns produced by direct conversion from zinc oxide precursor films. (n–p) A hexagonal ZnO pattern was fabricated using μCP of a sol–gel solution, followed by (q) thermal treatment. (r and s) Finely ground HmIm powder is deposited on top of the ZnO film and heated to melt the ligand, leading to a ZIF-8 formation. SEM of ZIF-8 pattern (scale bars 20 μm, and 1 μm inset).[173] Video animations provided as ESI.†

the fabrication of copper patterns. This photolithographic approach is widely used in electronics for the fabrication of printed circuit board (PCB). The authors showed how HKUST-1 crystals were selectively grown and homogeneously covered the conductive copper strips on a PCB, while the dielectric area on the naked support does not show the presence of any MOF crystals (Fig. 17f–m).

Recently, Majano et al. applied the HKUST-1 conversion process to the $Fe_3(BTC)_2$ MOF which crystallised within 5 min at room temperature.[180] A mixed Fe^{2+}–Fe^{3+} layered double hydroxide called "green rust" (GR = $Fe^{2+}_4Fe^{3+}_2(OH)_{12}\cdot SO_4\cdot 2H_2O$), was synthesized by mixing NaOH, $FeCl_2\cdot 4H_2O$, and Na_2SO_4. Fe-BTC crystals were formed instantly after the addition of H_3BTC ligand into the GR solution; this reaction was detected by the colour change from dark green to yellowish brown. However, neither pure $Fe(OH)_3$ nor $Fe(OH)_2$ resulted in the final porous material, indicating a flexible layered structure in the mixed iron hydroxide precursor is necessary for the MOF crystal formation. The obtained $Fe_3(BTC)_2$ demonstrated a higher crystallinity and a higher content of accessible Lewis-acid sites compared to the commercial counterpart (Basolite F300), which in turn resulted in a higher catalytic activity for Knoevenagel condensation.

Ameloot and co-workers reported in 2013 a solvent-free approach for synthesizing ZIF-8 thin films and micropatterns by direct conversion from zinc oxide precursor films.[173] ZnO films in the 500–1000 nm thickness range were deposited by physical vapour deposition (Radio Frequency magnetron sputtering in vacuum). A hexagonal pattern was fabricated using μCP combined with a sol–gel solution based on zinc acetate, monoethanolamine and 2-propanol. The stamp was inked in the sol–gel solution, the excess solution was removed, and finally the stamp was placed in contact with a preheated substrate. The pattern was thermally treated to induce the formation of ZnO. To induce the MOF formation, finely ground HmIm powder was deposited on top of the ZnO film and heated to melt the ligand. During this process the excess liquid HmIm quickly wetted the complete surface, leading to a homogeneous reaction with the precursor ceramic pattern. Using SEM, well-intergrown crystals up to 2 μm in size were detected after a 5 minute reaction, showing that the approach is fast and effective for the preparation of ZIF-8 films, patterns, and flake-like structures (Fig. 17n–t).

Advantages and limitations. Although researchers are currently pioneering the fabrication of MOFs from ceramics, important discoveries have already shown how this field is potentially very

important for the progress of MOF technology. A major advantage of this approach would be the use of established protocols for patterning ceramics thanks to the different technologies already available. Also, the low residual content of metallic ions in the solution after the conversion into MOFs would help to decrease the environmental impact of MOF fabrication.[181]

2.3.7 Ink-jet and spray coatings. While the preceding sections of this review have highlighted and discussed a number of different methods for producing MOF patterns suitable for miniaturised device applications, one can imagine that the ability to produce large MOF patterns over areas in the range 10 cm^2 to 1 m^2 may lead to other novel applications. For example, the ability to pattern fabrics with MOFs may lead to MOFs being utilised in smart textiles for sequestration and controlled release of small molecules. Patterning methods which make highly efficient use of the expensive precursor materials and solutions will be required to economically achieve this goal. Progress in this area is presented in this section.

Patterning. Ink-jet printing technology has been widely investigated for producing large patterns of functional materials, for applications such as "printed electronics",[182,183] due to its ability to accurately, rapidly and efficiently deposit droplets onto a variety of substrates. Zhuang *et al.*[184] have recently demonstrated for the first time that a standard office ink-jet printer can be used to print large patterns of the MOF HKUST-1 onto flexible substrates including plastic, paper and textiles. As the viscosity and surface tension of the "ink" plays a crucial role in the ink-jet process, the authors have adapted a commonly used HKUST-1 precursor solution[102] (Cu(NO$_3$)$_2$·3H$_2$O and H$_3$BTC dissolved in DMSO) for use in an ink-jet printer by including ethanol and ethylene glycol in the solvent. Ethylene glycol has several beneficial effects, including controlling the viscosity of the solution, stabilising the solution against the addition of ethanol so that it can be stored for a long time, and producing a desirable porous mesostructure in the final MOF coating (when combined with the wet development step).

After printing, the pattern can be dried in an oven, allowing thicker layers to be deposited by repeated printing-drying cycles. For example, 8 printing-drying cycles were shown to produce coatings 6 µm thick. The final conversion of the printed material into a MOF coating is achieved by a solvent development step which involves immersing the printed MOF pattern in methanol for 30 minutes to remove the less volatile solvents, namely ethylene glycol. This process produced densely grown, non-orientated crystals that could hardly be distinguished from one another. However, if the solvent development is done slowly with methanol vapour in a desiccator, the nucleation rate is slowed, and well defined crystals can be obtained. The scale and complexity of the MOF patterns and gradients that can be achieved using this process are shown in Fig. 18.

Zhuang *et al.*[184] have also demonstrated the utility of the ink-jet printing method for producing inexpensive and practical
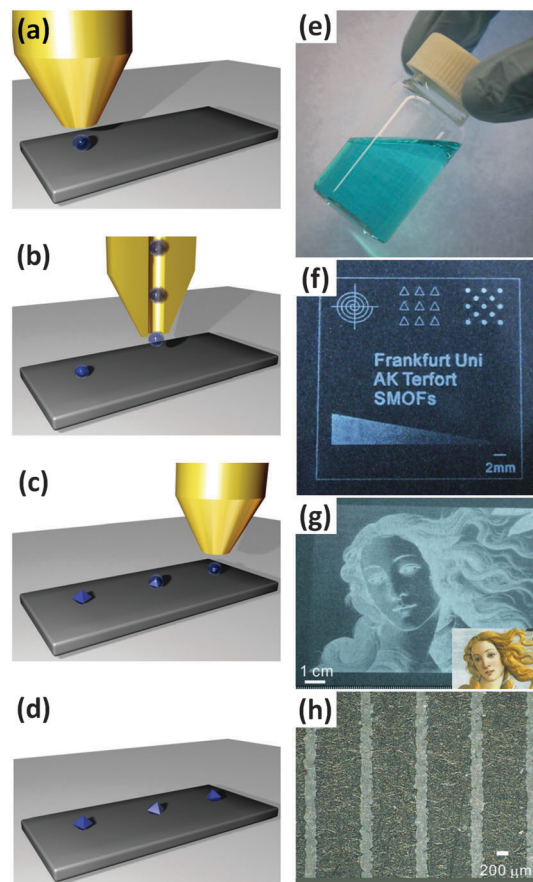

Fig. 18 (a–d) Schematic showing the ink-jet printing process for depositing MOF precursor solutions onto various substrates. (e) HKUST-1 ink solution containing ethylene glycol (f) patterns, letters, and a gradient wedge printed onto PET foil (g) Botticelli's "Venus" (original shown inset) was printed in HKUST-1, demonstrating the ability of this approach to pattern large areas. (h) The resolution of this method was tested by printing an array of lines 200 µm wide. To enhance the contrast, pictures (f), (g), and (h) were taken with black paper as background. Images reproduced from Zhuang *et al.*[184] Video animation provided as ESI.†

gas sensors on textiles. The printed HKUST-1 pattern was shown to rapidly change colour from turquoise to dark blue, yellow, and brown after exposure to NH$_3$, HCl, and H$_2$S vapour respectively, visibly indicating the presence of these noxious molecules, as well as their capture. Applications for such a material include protective textiles for first responders.

Another process that can be used to produce large patterns with a minimum amount of precursor solution is spray coating. Arslan *et al.*[185] first reported the use of a spray coating methodology to automate the LbL[40,70] or LPE process for producing highly uniform and orientated MOF films and patterns. In their implementation, the authors initially patterned Au substrates with a SAM of 16-mercaptohexadecanoic acid by µCP. These substrates were then alternately sprayed with a solution containing Cu$_2$(CH$_3$COO)$_4$·H$_2$O (for 10 seconds) and a solution containing H$_3$BTC (for 20 seconds) in order to grow a well orientated HKUST-1 film. Between each step the substrate was rinsed with a spray of ethanol to remove any excess precursor solution. The time taken to deposit a film with 20 full spray
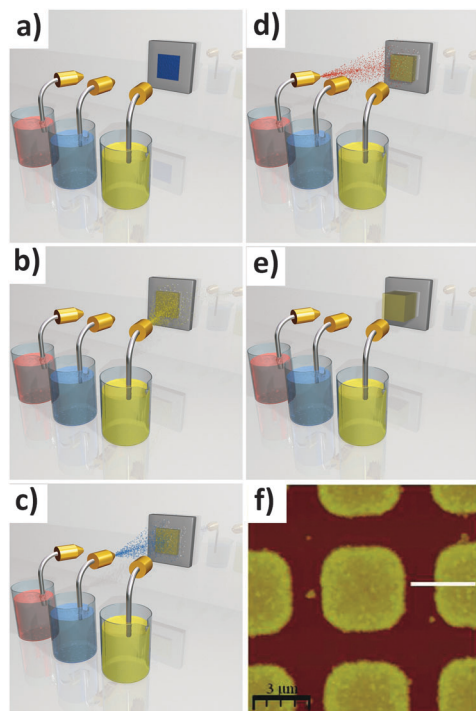
Fig. 19 Schematic showing spray coating of HKUST-1 films. A SAM surface patterned by μCP (a) is alternately sprayed (b–d) with a solution containing Cu$_2$(CH$_3$COO)$_4$·H$_2$O (yellow) and a solution containing H$_3$BTC (pink), with a rinsing step in between (blue). This effectively automates the LbL process for producing well orientated HKUST-1 films and patterns (e). (f) AFM image showing the spray coated HKUST-1 pattern. AFM image reproduced from Arslan et al.[185] Video animation provided as ESI.†

cycles was only 30 minutes, compared to the 48 hours required to produce an equivalent film using the conventional LbL process.[40] The resulting MOF micropatches are well orientated, uniform and retain the geometry of the microcontact printed SAM. Since the initial publication, the spray method has been used to produce a range of MOF coatings with different crystal structures based on Cu and Zn (Fig. 19).[78,82,185,186]

An obvious patterning approach which has so far received relatively little attention for MOFs is physical vapour deposition (PVD) and other forms of gas-phase deposition. The advantages of this approach in other material systems are the very high purity and high level of control over thickness that can be achieved, and the ease with which patterns can be obtained using simple masks. However, in the case of MOFs and coordination polymers, the properties of the organic ligands, namely their low vapour pressure and limited thermal stability, make them unsuitable for processes like thermal evaporation. Nonetheless, Fischer et al.[187] have recently demonstrated that an advanced form of PVD known as pulsed-laser deposition (PLD) can be used to produce coatings of MOFs which feature relatively high thermal stability. These authors synthesised the dense MOF europium(II) imidazolate[188] ($^3_\infty$[EuIm$_2$], HIm = imidazole) in powder form, which was then pressed into a pellet target for the PLD system. By tuning the parameters of the pulsed laser beam (wavelength, laser power, pulse duration, and repetition rate), the europium imidazolate was evaporated

from the pellet and deposited onto a sapphire substrate where it recrystallised with the crystal structure of the original MOF. The MOF coating was shown to retain its distinctive photoluminescent properties, allowing the film to be transparent under visible light and opaque under UV light. The gas phase in the PLD chamber was investigated by matrix-assisted laser desorption/ionization time-of-flight (MALDI-TOF) mass spectrometry, revealing that the ablation mechanism is likely to consist of fragments containing both Eu atoms and imidazolate ligands. Although no patterns were reported in this work, the ability to deposit MOF coatings by a PVD-based process represents significant progress.

Advantages and limitations. Ink-jet printing has a number of advantages including simplicity and efficient use of precursor solution. Importantly, ink-jet printing technology is well established and widely available, making this approach very attractive for a number of MOF applications and devices. However, the spatial control and resolution (minimum feature dimensions) of this technique are limited compared to other lithographic techniques, and achieving fine control over the crystallisation process may prove problematic, particularly for absorbent substrates. Spray coating is also an efficient process, and can be used to achieve the high quality films normally associated with the LbL process relatively quickly. A current limitation of this technique is needed for a SAM layer in order to anchor the crystals to the substrate. PVD processes such PLD offer the opportunity to create high-purity, solvent-free films and patterns. However this approach is currently limited to MOFs with high thermal stability.

2.4 Top-down MOF patterning technologies

In contrast to bottom-up patterning methods, top-down approaches can take advantage of the wide range of protocols available for synthesising thin films and powders, as the patterning step is applied after the MOF material has been produced. These techniques can be particularly powerful in situations where a MOF that can only be produced using harsh synthesis conditions needs to be incorporated within a delicate device. Top-down approaches for permanently localising MOF are only just beginning to emerge, and are currently based on photolithographic methods. Although only a few methods have been reported to date, the pattern features are summarised in Table 1.

2.4.1 Photolithography and imprinting

Technique development. Photolithography is one of the most widely used micro- and nano-fabrication techniques for device fabrication involving the top-down approach. This lithographic process uses photons with different energies, from the visible spectrum right up to hard X-rays, to induce the formation of a pattern in a light sensitive material.[1,5] Generally speaking, the photolithographic process uses a radiation source and a mask with a pattern defined by transparent and opaque regions. Depending on the type of photoresist used in the patterning process, the photoresist will be chemically transformed from exposure to photons (Fig. 20a–c). A negative photoresist cross-links under exposure to photon radiation, becoming insoluble
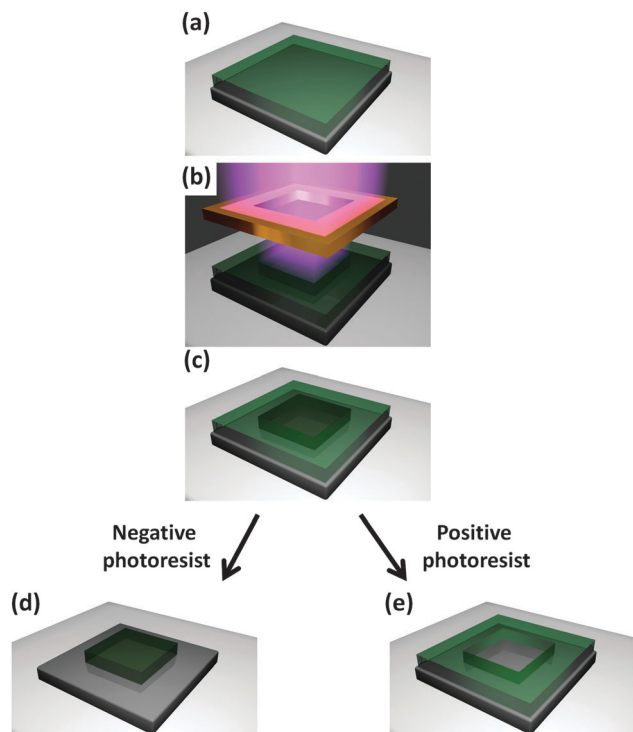
Fig. 20 Schematic of the photolithography technique. A photoresist (a) is exposed to photons through a shadow mask (b), altering the chemistry of the photoresist (c). In a negative photoresist the exposed region is insoluble in developing solutions (d), while in a positive the masked region is insoluble (e). Video animation provided as ESI.†

within developing solutions. Consequently, upon contact with a developing solution, only the parts not exposed to light (masked regions) will be removed (Fig. 20d). On the other hand, a positive photoresist becomes more soluble in a developing solution. As a result, in the exposed regions, the photoresist can be removed by a proper developing solution (Fig. 20e). Recently, this patterning technique has been used for the fabrication of MOF patterns, and both strategies involving negative and positive photoresists have been successfully used.

Patterning. The first example of such a top-down approach to pattern MOFs in order to control the ultraporous crystal location was provided by Dimitrakakis and co-workers.[189] Deep X-ray Lithography (DXRL)[190] was used to selectively crosslink a phenyltriethoxysilane (PhTES) sol–gel matrix[191] loaded with ZIF-9 crystals. In this work, a pre-hydrolyzed PhTES based solution was drop-cast on silicon wafers (Fig. 21a). The film was heated to promote solvent evaporation (Fig. 21b). Once the film was dried, the sample was removed from the hotplate. Pre-synthesized ZIF-9 nanocrystalline powder was spread on the hybrid sol–gel film and a homogenous coverage was obtained (Fig. 21c). A subsequent heating process was used to anchor the ZIF-9 particles to the substrate (Fig. 21d). The sample was covered with a mask containing a gold pattern and then exposed to synchrotron X-rays; the mask allows for controlled regions of the substrate to be exposed to the high-energy photons (Fig. 21e). In the exposed regions, the PhTES-based

sol–gel film crosslinks, while in the unexposed regions the sol–gel film remains almost unchanged. Using ethanol, the sol–gel film from the mask region was etched away, leaving a well-defined pattern with a superficial layer of MOFs (Fig. 21f and g). In the present case, the high penetration depth of hard X-rays is not affected by the potential scattering induced by the MOF crystal powder and high-quality patterns (*e.g.* high aspect ratio and smooth walls) were quickly prepared.[189] This study highlights an interesting property of ZIF-9; while a variety of materials (*e.g.* self-assembled materials, surfaces, porous ceramic films, hybrid materials, thick porous polymers)[155,192–195] have shown drastic chemical changes under hard X-ray exposure, ZIF-9 exhibits good chemical and structural stability under such high energy radiation. The reason is not yet fully understood and further experiments are needed to find a scientific explanation for this behaviour.

Lu *et al.*[37] prepared a thin ZIF-8 film that can be grown without the need for chemical functionalisation of the surface. A substrate (*e.g.* silicon) was immersed in an alcoholic solution of the Zn precursor and the ligand at room temperature ($Zn(NO_3)_2$ and HmIm respectively). Repeating the procedure several times with fresh precursor solution produced a smooth 200 nm thick film. The ZIF-8 film was then spin-coated with a positive photoresist (AZ1815), covered with a chromium mask and exposed to UV-light. The subsequent immersion in a basic solution revealed the pattern exposing the MOF film in controlled locations (*i.e.* areas exposed to the UV-light). A further etching process with an acid solution removed the exposed ZIF-8. The final step requires the use of a solvent to remove the remaining photoresist covering the MOF pattern. Arrays of patterned squares (11 µm edge) were obtained, confirming that the pattern reproduces the photomask design very closely. A resolution of 500 nm was estimated by SEM observations of the edge of the patterns (Fig. 21n); this feature seems to be related to the etching conditions used. Interestingly, the methodology takes advantage of both the ability to grow a smooth film and the excellent chemical stability of ZIF-8 in aqueous base.[196] As a proof of concept, the MOF coatings were used to sense the presence of different vapors and gases including H_2, using an optical detection method.

To address the problem of the compatibility of MOFs with the radiation or the patterning process, and to make the process faster, Doherty and co-workers proposed an approach that enables the patterning of almost any type of MOFs.[24] In accordance with the focus on improving existing micro-fabrication techniques,[155] the proposed protocol makes the patterning process easier, faster and more versatile, thereby potentially enabling rapid progress in the fabrication of MOF-based devices.[24] The proposed procedure involves a commercial epoxy-based photoresist (SU-8, negative photoresist) that is treated using a normal photolithography procedure (UV-lamp and a photomask) to fabricate a SU-8 pattern. On a different flat substrate (*e.g.* silicon or SiO_2 microscope slide) loose MOF crystals are evenly dispersed making a continuous coating of separate porous crystals. The patterned SU-8 film is pressed onto the MOF film and heated up to a temperature slightly higher than the glass
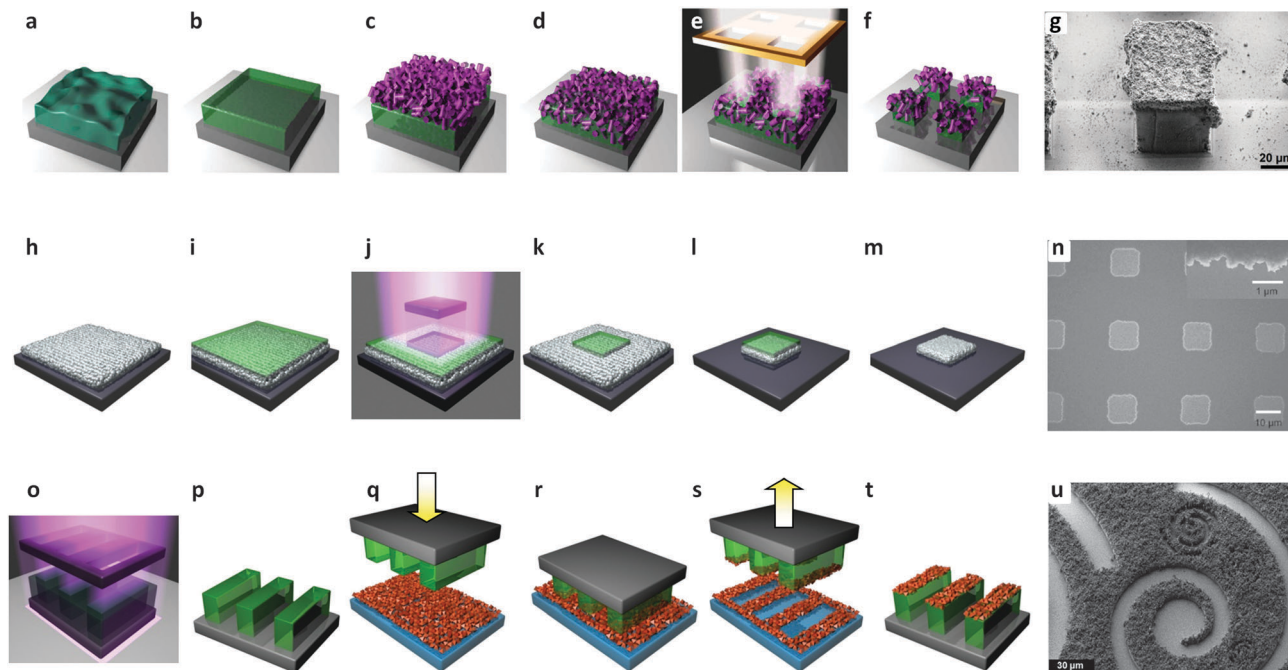
5532 | *Chem. Soc. Rev.*, 2014, **43**, 5513–5560

This journal is © The Royal Society of Chemistry 2014

Fig. 21 Schematic illustration of the photolithography and imprinting techniques for the formation of MOF patterns. (a) A pre-hydrolyzed PhTES based solution is drop-cast on silicon wafers, and dried (b). (c) Pre-synthesized MOF powder is spread on the film. (d) The film is heated to soften out, thereby anchoring the MOF particles to the substrate. (e–g) A photo mask positioned on top of the film is exposed to synchrotron X-rays. The unexposed region is etched off, leaving a well-defined pattern with a superficial layer of MOFs.[189] (h) A substrate is immersed in MOF precursor solution, forming a MOF film. (i) A photoresist was then spin-coated on top of the MOF film, and (j–k) covered with a shadow mask and exposed to UV-light. (l) The subsequent immersion in a base solution reveals the pattern exposing the MOF film in controlled locations (areas exposed to the UV-light). (m and n) A further etching process removes the exposed MOF film.[37] (o and p) A UV lithographed film of photoresist is prepared and pressed (q) onto a pre-prepared MOF film. (r and s) The two films are separated, (t and u) resulting a patterned MOF surface.[24] Video animations provided as ESI.†

transition (T_g) of the resist ($\sim 95\ ^\circ$C). Thanks to this imprinting step, the loose MOF crystals are transferred and partially embedded into the SU-8 pattern. Once the SU-8 cools back to room temperature, the MOF crystals are anchored onto the resist, resulting in a well defined patterned surface (Fig. 21o–u). To test the versatility of this protocol for positioning different types of MOFs, NH$_2$-MIL-53(Al), ZIF-67(Co(Im)$_2$), and ZIF-8 were used. Interestingly, the procedure combining UV-lithography and imprinting requires just a few minutes and the properties of the MOFs on the substrate are very similar to the properties of the equivalent MOFs as a powder. Examples were reported for the uptake of 1,2-benzanthracene and Pd cations confirming for patterned MOF films the sequestration capabilities for polycyclic aromatic hydrocarbons (PAHs) and metal ions. After the patterning process, the NH$_2$ functionality was retained as proven by the bioconjugation with β-glucosidase enzyme. The bio-processing efficiency was measured, confirming that the enzyme was active in the MOF films, as well as in the transferred MOF patterns.

Advantages and limitations. Although the suitability of top-down approaches is currently being investigated for MOF-based device production, they do present some advantages over the bottom-up protocols. In particular, this technology is compatible with an industrial lithographic technique commonly used for micro-fabrication, namely photolithography. The good versatility

(compatible with several different MOFs) and potentially high production rates of photolithography and imprinting make these approaches very attractive for device fabrication. Although this particular research stream is promising, the type of research required to progress the field involves the combination of multidisciplinary expertise not readily available in most research teams. This requirement may slow the rate of progress.

3. Dynamic localisation

Dynamic localisation refers to the positioning of free, pre-formed species with the aid of an external control. Different studies have proposed the use of temperature,[197] light,[198] electricity,[199] mechanical interactions,[200] chemical reactions,[201] and magnetism[202] for the controlled movement of interesting nano and micromachines. MOFs can be spatially arranged in order to integrate them into functional nanosystems, dynamically responding to external stimuli. For applications where control over the position is required and subsequent relocation is needed, MOFs functionalised with magnetic nanoparticles are one of the most studied classes of materials. The magnetic functionality of the nanoparticles can be retained in these MOF composites without significantly affecting the unit cell of the original framework lattice. Compared to the pure MOF, only a minor decrease in the surface area of the magnetic MOF composites has been

Table 2 Dynamic localisation

Magnetic framework composite	Particle size	MOF thickness	Precision of positioning with a magnet	Preferential orientation	Year	Ref.
$(Fe_3O_4@SiO_2)@HKUST-1$	$Fe_3O_4@SiO_2$: 30–100 nm	Layer: 20–25 nm	N/A	N/A	2013	218
Co@MOF-5	< 50 nm	Cubic: 100 μm	mm range	N/A	2011	203
$Co@Zn_4O(BDC)_{2.25}(NH_2BDC)_{0.75}$	< 50 nm	Cubic: 50 μm	μm range	N/A	2013	147
$CoFe_2O_4$ or $NiFe_2O_4@MOF-5$	> 5 μm (fiber length)	Cubic: 100 μm	mm range	N/A	2012	23
$Fe_2O_3@DUT-4$: Al(OH)(ndc)	Fe_2O_3: 10–20 nm	N/A	mm range	N/A	2011	204
$Fe_3O_4@Cu(bpdc)$ and Cu(bpy)	200 nm (with NH_2)[215,221] 1–4 μm (with COOH)[221]	N/A	None (used in reaction mixture)	N/A	2012	217 and 223
$Fe_3O_4@HKUST-1$	Fe_3O_4 nanorods: 15 nm (d) × 75 nm (l)	Irregular particles: 50–150 nm	mm range	N/A	2011	210
$Fe_3O_4@HKUST-1$	N/D	Hollow capsules: 1.7 μm	mm range	N/A	2013	211
$Fe_3O_4@ZIF-8$	Fe_3O_4: 600 nm	Layer: 100 nm	Centimeter in capillary reactor	N/A	2013	216
$Fe_3O_4@Zn(bix)(NO_3)$	Fe_3O_4: 10	Spheres: 600 nm	mm range	N/A	2009	214

measured in optimised systems.[203,204] The main advantage of this approach lies in the simplicity with which magnetic nanoparticles can be prepared and combined with MOFs.[32,53,205] As a result, magnetic nanosystems can be easily produced through large scale synthesis, customizing the physical properties, the size distribution and the surface chemical functionalisation.[206,207] In addition, a wide range of magnetic nanoparticles are already commercially available. For the purpose of fabricating repositionable MOF-based systems, there is no special need to design and synthesize new intrinsically magnetic frameworks. However, intrinsically magnetic MOFs may offer advantages in applications where external stimuli are used to tune the physical and chemical properties of the functional material,[208] such as in Magnetic Resonance Imaging (MRI).[209]

The combination of MOFs with magnetic nanoparticles leads to a new class of materials called magnetic framework composites (MFCs).[32] This is already considered a promising new field in MOF technology; however, the precision that can be achieved with dynamic localisation of MOFs is currently lower than can be achieved with permanent localisation methods. A rough comparison is presented in Table 2. The application of these materials in sensing, drug delivery, pollution control, and catalysis has been recently reviewed.[32] An updated list of applications is presented in Table 3. In this section, a survey of the synthetic routes for the production of MFCs is presented, including the preparation of MFCs using a microfluidic approach. The application of MFCs in the fabrication of devices is also reviewed.

3.1 Synthetic techniques for the production of magnetic framework composites

Different methodologies for the synthesis of MFCs have been explored and reported in the literature. Depending on the protocol used, it is possible to obtain MFCs by heat-driven growth using conventional routes,[23,126,147,203,204,210] or by exploiting techniques such as spray drying,[211,212] microfluidics,[150] or mixing.[25]

Heat-driven growth is a widely used approach in MOF synthesis, and is the general procedure used for the preparation of MFCs, as presented in Fig. 22. In the MOF precursor solutions (metal salt, organic ligand and proper solvent), magnetic nanoparticles are added (Fig. 22a). Either solvothermal or

hydrothermal processes[213] can then be used to induce the MOF growth (Fig. 22b). After MOF formation, the mixture usually contains unreacted magnetic particles, pure MOFs and MFCs; the former usually have a lower sedimentation rate and it is therefore possible to extract them without affecting the frameworks. Furthermore, an external magnetic field allows the pure MOFs to be efficiently separated from the MFCs and hence extracted from the growth solution, leaving behind a powder of the porous magnetic composite material (Fig. 22c–f).

Among the different approaches for the fabrication of MFCs,[32] the main strategies to combine magnetic nanosystems into the framework are *embedding* or *encapsulation*. The difference depends on the use of naked magnetic particles or magnetic nanosystems with a buffer coating, respectively. In 2009, Imaz *et al.*[214] pioneered the embedding technique using iron oxide nanoparticles into a zinc based framework, where the ligand was bix: 1,4-bis(1-imidazolyl)benzene. The $Fe_3O_4@Zn(bix)(NO_3)$ composite (Fig. 23a) was obtained in the form of 600 nm spheres, and the authors were also able to prepare multifunctional magnetic/luminescent MOFs.

An important example of embedding synthesis was reported in the work of Ke *et al.*,[210] where iron oxide nanorods were used to produce a HKUST-1 based MFCs (Fig. 23b), using a conventional heating route in water as the solvent (hydrothermal route), obtaining mainly irregular MFC nanoparticles in the range 50–150 nm. The nanocomposite was loaded with nimesulide and an *in vitro* test illustrating the delivery capacity for anti-inflammatory drugs was proposed. Almost at the same time, a similar protocol was proposed by Lohe and co-workers.[204] In this study superparamagnetic Fe_3O_4 nanoparticles were embedded into HKUST-1 and two different aluminium-based MOFs, DUT-4 Al(OH)(NDC) [H_2NDC = 2,6-naphthalenedicarboxylic acid] and DUT-5 Al(OH)(bpdc) [H_2bpdc = biphenyl-4,4′-carboxylic acid], using a solvothermal reaction in DMF in a Teflon lined stainless steel autoclave at 180 °C (Fig. 23c). In this case, the versatility of MFCs was demonstrated, providing evidence for both the catalytic performance of the composite made with DUT-4, and the possibility of applying an alternating magnetic field for the temperature-triggered release of ibuprofen with a magnetic HKUST-1 composite (Table 4).

The encapsulation route exploits a buffer interface between the magnetic nanoparticles and the porous framework, provided by a

Table 3 Applications and devices reported in literature based on metal organic frameworks

Technique	Material, compound, or device	Application proposed or device outcome	Year	Ref.
MOF films				
	Cu(TCPP)	Proton conductivity	2013	322
	DA-MOF: Zn(Por)(TCPB)	Light harvesting	2013	50
	HKUST-1: $Cu_3(BTC)_2$	VOCs detection	2011	263
		QCM-electrodes	2008	278
		Inductive sensing	2009	280
		Capacitive humidity sensing	2011	266
		Piezo-resistive gas sensor	2008	264
		Electrical insulator (low-k)	2013	299
		Electrical conductor	2014	16
		Photovoltaic	2013	307
	Ln(BTC)(H$_2$O) [Ln = Dy^{3+}, Eu^{3+}, Tb^{3+}]	Luminescence	2010	313
	MOF-5: $Zn_4O(BDC)_3$, MOF-177: $Zn_3(BTB)_2$	Photoconductivity	2012	323
	NU-901: $Zr_6O_4(OH)_4(Por)_3$	Electrochromism	2013	272
	ZIF-8 on Si and glass	Gas optical sensor	2010	274
	ZIF-8 on Si	Electrical insulator (low-k)	2013	298
	$Zn_3(BTC)_2$	Photocatalysis	2013	48
	ZnPO-MOF: $[Zn_2(TCPB)(ZnPor)]_n$	Catalysis	2009	320
Bottom-up patterning for MOFs				
Surface functionalisation	CAU-1: $Al_4(OH)_2(CH_3O)_4((NH_2)BDC)_3$@SAM on Au surface	Ethanol sorption *via* QCM-electrode	2010	67
	Cu(ADA) bulk and on Au surface	Thin film, patterning and orientation growth	2011	76
	$Cu_2(L_2)$(dabco) [L = see ref.] membrane on TiO$_2$ and Al$_2$O$_3$ support	CO$_2$ separation	2012	283
	Fe(pyrazine){M(CN)$_4$} [M = Ni, Pd, Pt] on Au surfaces	Room temperature spin crossover	2006	68
	HKUST-1 on Ag nanoparticles	Localised SPR gas sensor	2010	268
	HKUST-1 on microcantilever	Piezoresistive sensor for VOCs	2013	265
	HKUST-1 on quartz	Surface acoustic wave sensor for gases	2012	267
	HKUST-1@SAM on Au surface	High-throughput spray coating	2011	185
	MIL-53(Fe): Fe(OH)(BDC) and MIL-88B(Fe): Fe$_3$O(BDC)$_3$@SAM on Au surfaces	Solvent vapour sorption	2008	66
	MOF-5 in GC fused silica capillary	Gas chromatographic separation	2011	270
	MOF-5@SAM on SiO$_2$/Si surface	Air exposure effect	2008	64
	MOF-74(Ni): Ni$_3$O$_3$(dhBDC)$_{1.5}$ on Al$_2$O$_3$	CO$_2$ separation	2012	284
	ZIF-8 on ITO surface	Photoluminescence	2013	297
Electrochemical deposition	HKUST-1 on QCM	Humidity sensor	2009	44
	HKUST-1 on Cu sheet	Microseparator device	2013	100
	HKUST-1 on patterned Cu on glass	Patterning and wettability	2010	101
Nucleating agents	DRM/QD@MOF-5	Thiol sensing	2011	125
Pen lithography	HKUST-1 on Si/SiO$_2$ substrates	Combinatorial screening	2013	140
Microfluidics	HKUST-1 on chip	Droplet routing	2012	144
	Fe$_3$O$_4$@ZIF-8	Catalysis in microfluidics	2013	150
	HKUST-1 hollow capsules	Sieving	2011	152
Conversion from ceramics	$Zn_3(BTC)_2$	VOCs detection	2009	169
	MIL-53(Al) on Al$_2$O$_3$	Gas permeability	2010	115
	Al(OH)(ndc) from Al$_2$O$_3$ architecture	Water–ethanol separation	2012	170
	HKUST-1 from Cu(OH)$_2$ nanotubes	Catalysis	2013	172
	Fe$_3$(BTC)$_2$ from iron hydroxide	Catalysis	2013	180
Spray and plasma coating	Spray-coated HKUST-1 on paper, plastics and textile	Colourimetric gas sensor	2013	184
	Eu(Im)$_2$ and Eu(Im)$_2$/C on sapphire *via* PLD	Switchable transparency, luminescence	2014	187
Top-down patterning technologies for MOFs				
Photolithography and imprinting	ZIF-9 on sol–gel patterns *via* DXRL	N$_2$/CO$_2$ selectivity	2012	189
	ZIF-8: Zn(mIm)$_2$ on patterned photoresist	Chemical vapour optical sensor	2012	37
	MIL-53(Al): Al(OH)(BDC) on patterned SU-8	Polycyclic aromatic hydrocarbon sequestration and enzymatic activity evaluation	2013	24
Dynamic localisation of MOFs				
	(Fe$_3$O$_4$@SiO$_2$)@HKUST-1	HPLC separation	2013	218
	Co@MOF-5	Positioning/sensing	2011	203
	Co@Zn$_4$O(BDC)$_{2.25}$(NH$_2$BDC)$_{0.75}$	Positioning/sensing	2013	147
	CoFe$_2$O$_4$ or NiFe$_2$O$_4$@MOF-5	PAH sequestration	2012	23
	Fe$_3$O$_4$@DUT-4: Al(OH)(ndc), DUT-5: Al(OH)(bpdc), and HKUST-1	Thermal therapy and catalysis	2011	204
	Fe$_3$O$_4$@Cu(bpdc) and Cu(bpy)	Catalysis	2012	217 and 223
	Fe$_3$O$_4$@HKUST-1	Drug delivery	2011	210
	Fe$_3$O$_4$@HKUST-1	Fuel decontamination	2013	211
	Fe$_3$O$_4$@ZIF-8	Catalysis	2013	216
	Fe$_3$O$_4$@Zn(bix)(NO$_3$)	Fluorescence probe	2009	214

This journal is © The Royal Society of Chemistry 2014

Chem. Soc. Rev., 2014, 43, 5513–5560 | 5535

Table 3 (continued)

| Technique	Material, compound, or device	Application proposed or device outcome	Year	Ref.
Positioning functional materials within MOFs				
	Ag, Au@Ni(cyclam)$_2$(bptc)	Ag and Au NP synthesis	2006	245
	Ag@Ni(cyclam)(bpydc)	Ag NP redox synthesis	2005	244
	Au, Ag@Rb-CD-MOF and Cs-CD-MOF	Ag and Au NP redox synthesis	2011	247
	Au@MIL-100(Fe): Fe$_3$O(OH)(BTC)$_2$	Catalysis	2013	241
	Au@MOF-5	SERS detection	2013	240
	Eu^{3+}@SMOF-1: In$_3$(BTB)$_2$	White light emitter	2012	234
	Eu$_x$Tb$_{1-x}$(dmBDC)$_3$	Thermometry	2012	233
	Hemicyanine dye@bio-MOF-1: Zn$_8$O(Ad)$_4$(bpdc)$_6$	Two photon lasing	2013	238
	Ir, Re, Ru WOCs@UiO-67: Zr$_6$O$_4$(OH)$_4$(bpdc)$_6$	Water oxidation, CO$_2$ reduction, organic photocatalysis	2011	232
	Mg@SNU-90: Zn$_4$O(atb)$_2$	Gas uptake	2012	252
	Pd, Cu, Cu/ZnO, Au@MOF-5	Catalysis	2005	250
	Pd, Pd + Cu and Cu@MIL-101(Cr): Cr$_3$OF(BDC)$_3$	CO catalytic oxidation	2009	243
	Pd@MIL-100(Al): Al$_3$O(OH)(BTC)$_2$	Hydrogen storage	2010	248
	Pd@Zn$_3$(ntb)$_2$	Hydrogen storage	2009	246
	Pt@MIL-101(Cr)	H$_2$ generation and CO oxidation	2012	249
	Pt@Zr$_6$O$_4$(OH)$_4$(L)$_6$ (R: Ir based complex, see ref.)	Photocatalysis	2012	242
	QD@MOF-5	Thiol sieve with luminescence detection	2012	239
	R-MOF-5: Zn$_4$O(R-BDC)$_3$ (R: see ref.)	Various properties with ligand tuning (i.e.: CO$_2$/CO selectivity)	2010	236
	Ru@MOF-5	Catalysis	2008	251
	Au@Al(OH)(ndc)	NIR induced molecular release	2013	253
	Pd, Pt, Au@ZIF-8 shells	Size selective catalysis	2012	255
	Dyes@MOF-5 and Rb-CD-MOF	Light responsive micropatterning	2011	261
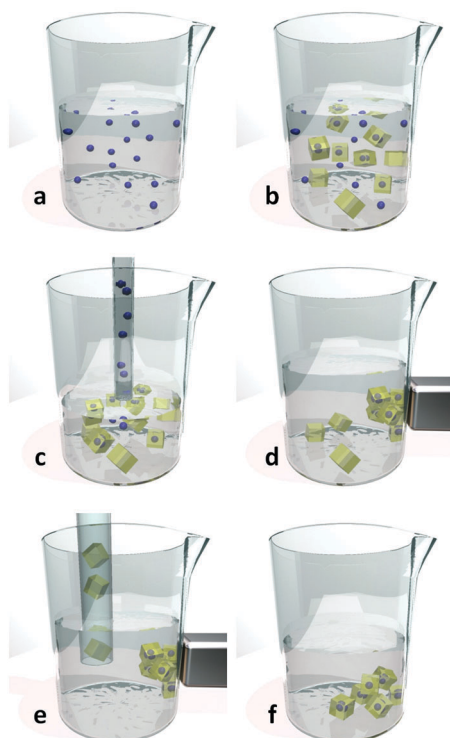
Fig. 22 General synthetic route for MFCs[32] (a) dispersion of magnetic particles in the precursors mix; (b) reaction mixture after solvothermal or hydrothermal reaction; (c) extraction of unreacted magnetic particles after sedimentation of MOFs and MFCs; (d) collection of MFC with an external magnet; (e) separation of MOFs from MFCs; (f) magnetic responsive MFC isolated and purified. Video animation provided as ESI.†

coating that enhances the compatibility with the MOF (e.g. polymer or a carbonaceous coating).[32] In the extensive report by Lu and co-workers on the precise encapsulation of nanoparticles in MOFs,[215] 8 nm iron oxide nanospheres were stabilized with amphiphilic polyvinylpyrrolidone (PVP) before being integrated into ZIF-8 (Fig. 23d). The non-ionic polymer is commonly regarded as a suitable stabilizing and capping agent for a wide range of nanoparticles in polar solvents like methanol or DMF.[219] A similar approach was reported by Zhang et al.,[216] in which Fe$_3$O$_4$ nanoparticles, prepared from the corresponding iron(III) chloride using a solvothermal approach, were coated with sodium polystyrene sulfonate (PSS). This anionic polymer altered the surface charge of the nanoparticles in order to enhance the absorption of zinc(II) ions, and improve the subsequent preparation of the composite, based on ZIF-8 (Fig. 23e).

In the work of Falcaro et al.,[203] ferromagnetic carbon-coated cobalt nanoparticles were encapsulated into the archetypal MOF-5 using the block copolymer Pluronic F-127. The carbon coating was compatible with the organic ligand used in this synthesis,[220–222] and the copolymer was used to prevent the premature sedimentation of the particles (Fig. 23f). In a similar procedure reported by Doherty et al.,[23] cobalt ferrite and nickel ferrite nanofibres were inserted into MOF-5 using the same block copolymer. The obtained system (Fig. 23g) was used as a proof-of-concept for the time resolved monitoring and sequestration of PAH 1,2-benzanthracene.

The exploitation of a reacting group to enhance the grafting of the frameworks was brought to light by Arai and co-workers,[217,223] where commercially available magnetic beads with carboxylic acid or amino groups on the surface form the basis for the preparation of composite MOFs with bpy (Fig. 23h) or H$_2$bpdc ligands. These materials were used as recoverable catalysts for different reactions with >50% yields.
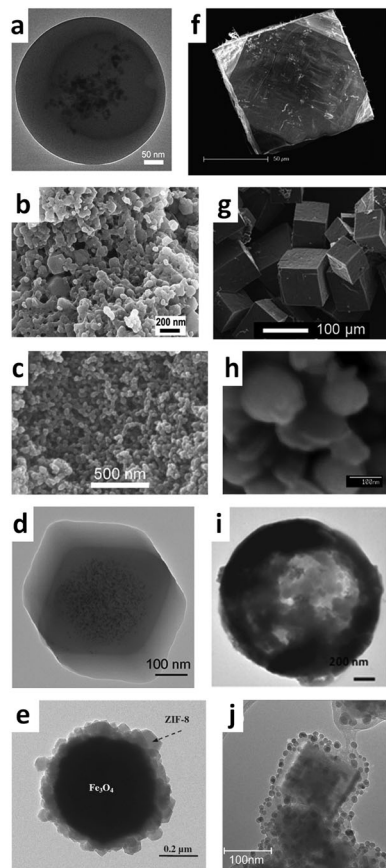
5536 | Chem. Soc. Rev., 2014, 43, 5513–5560

This journal is © The Royal Society of Chemistry 2014

Fig. 23 Electron microscopy images of different MFCs obtained in literature. (a) Fe_3O_4@Zn(bix)(NO$_3$) from Imaz et al.;[214] (b) Fe_3O_4@HKUST-1 from Ke et al.;[210] (c) Fe_3O_4@HKUST-1 from Lohe et al.;[204] (d) Fe_3O_4@ZIF-8 from Lu et al.;[215] (e) Fe_3O_4@ZIF-8 from Zhang et al.;[216] (f) Co@MOF-5 from Falcaro et al.;[203] (g) NiFe$_2$O$_4$@MOF-5 from Doherty et al.;[23] (h) Fe_3O_4@Cu(bpy) from Arai et al.;[217] (i) Fe_3O_4@ZIF-8 from Carné-Sanchez et al.;[211] (j) (Fe_3O_4@SiO$_2$)@HKUST-1 from Silvestre et al.[218]

Using conventional batch synthetic approaches, the production of suitable quantities of MOFs and related MFCs can take several hours. For example, MOF-5 synthesis can take up to 24 hours to obtain a few milligrams of block crystals,[126] while the standard protocol for the synthesis of aluminium based MIL-53(Al) takes 72 hours in an autoclave reaction.[224] Although the addition of ceramic nano- and micro-particles can be used as crystallization facilitators,[125,126] no evidence that magnetic nanoparticles can shorten the reaction time for the MOF synthesis has been reported to date.

An innovative synthetic method involving spray-drying has been developed in order to speed up the MFC synthesis. In the article from Carné-Sanchez and co-workers,[211] micrometer sized hollow capsules of HKUST-1 were prepared using a commercial Mini Spray Dryer, opening the way to a low cost and scalable method for mass production of MOF particles. HKUST-1 was also prepared along with magnetic Fe_3O_4, providing a MFC superstructure in which the iron oxide nanoparticles were enclosed inside the cavity of the MOF capsules. The Fe_3O_4@hollow HKUST-1 (Fig. 23i) was investigated as a sequestering agent for the fuel contaminant dibenzothiophene (DBT),

demonstrating the efficient extraction of 200 g of DBT for every kg of MFC used.

In the recent work of Park et al.,[225] hierarchically functionalised colloid nanoparticles were prepared using an electrohydrodynamic co-jetting process, resulting in the growth of HKUST-1 MOF on the surface of compositionally anisotropic particles. The authors prepared two rationally designed copolymers with different butyl groups (linear and tertiary), both containing cross-linkable vinyl groups. Two syringes were filled with the linear butyl copolymer and a green dye, and a mixture of both copolymer and a blue dye, respectively. Subsequently, they co-jetted the two solutions in a laminar flow junction, producing a biphasic Taylor cone[226] that was electrically deposited on an aluminium substrate in the form of patchy Janus particles.[227] To induce the final spherical shape, the authors applied a short sonication treatment. To demonstrate the bicompartmental characteristics of their particles, a confocal microscope analysis showed two distinguished areas for every sphere, where the different colours were located. Using a selective deprotection of *tert* butyl groups with trifluoroacetic acid, only the blue coloured portion contained exposed carboxylic groups; a spatially controlled LbL growth of HKUST-1 was therefore possible only on this side. To demonstrate the possibility of obtaining a multifunctional composite, iron oxide nanoparticles were added in the green coloured copolymer solution. In this way, it was possible to further localise the magnetic particles in one portion of the final system, whereas the other part was surface grafted with the HKUST-1 MOF, obtaining a new kind of hierarchically functionalised organic inorganic hybrid with magnetically positionable porous MOF crystals. Given the magnetic property and the controllable porosity of this MFC, this system may find applications as a switchable catalyst, smart delivery vehicle, or smart adsorbent.

3.2 Localisation of magnetic framework composites under dynamic control

In the report by Falcaro and co-workers,[203] the dynamic spatial control of a luminescent Co@MOF-5 composite was investigated. The material was prepared as described before, using ferromagnetic carbon coated cobalt nanoparticles encapsulated into the MOF-5 crystals (Fig. 23f and 24a). The magnetic properties were retained, enabling fast collection with a commercial magnet. The material was positioned in a controlled fashion using a magnetic finger made with two magnetic bars inserted into a 1 mm glass capillary, permitting the localisation of the MFCs where the field lines were most dense (Fig. 24b). After secondary growth of MOF-5, the composite was impregnated with FITC, resulting in a miniaturised probe with sensing capabilities toward aromatic amines (Fig. 24c), which was then inserted into a solution containing 1,4-phenylendiamine. The MOF-5 pore size was sufficient to permit the diffusion of the analyte into the framework, and its reaction with the reactive groups of FITC. The fluorescence emission was quenched and real time monitoring of this effect could be easily performed with a spectrofluorometer.

Further work on the precise control of MFCs in a defined space was reported in a subsequent article by Falcaro et al.[147] A mixed component MOF[99] was prepared with a 3 : 1 mixture of

This journal is © The Royal Society of Chemistry 2014

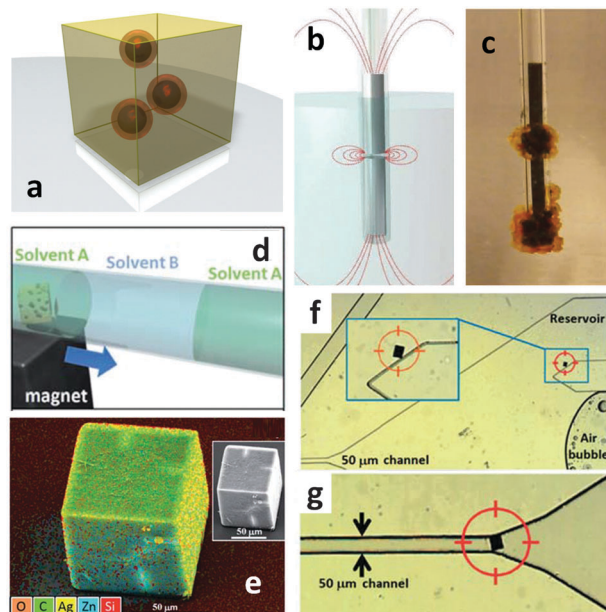Chem. Soc. Rev., 2014, 43, 5513–5560 | 5537

Fig. 24 (a) Design of Co@MOF-5 composite produced with the encapsulation approach; (b) representation of the magnetic finger force field and the obtained device (c). From Falcaro et al.[203] (d) Three-zone experiment for the uptake of silver ions or silica nanoparticles under precise positioning of Co@Zn$_4$O(BDC)$_{2.25}$(aBDC)$_{0.75}$ thanks to an external magnetic field; (e) EDX and SEM (inset) image of composite after sequestration of Ag$^+$ ions. (f) Single Co@MOF-5 particle in a microfluidic device, moved from a reservoir to the 50 μm channel (g). From Falcaro et al.[147]

H$_2$BDC acid and H$_2$aBDC ligands, along with the encapsulation of cobalt nanoparticles, to obtain the composite with a nominal composition of Co@Zn$_4$O(BDC)$_{2.25}$(aBDC)$_{0.75}$ (i.e. 25% amino-functionalised MOF-5). In this case, a single crystal X-ray diffraction study on the crystallinity of the cubic blocks highlighted the presence of different misaligned domains in a single particle; this effect was attributed to the presence of magnetic nanoparticles interfering with the continuity of the MOF lattice.

The ability to carefully govern the position of this MFC was demonstrated in a prototype device composed of a three-zone 1 mm glass capillary, containing two dodecane sections divided by a central, methanol filled, portion (Fig. 24d). In two separate experiments, this middle zone contained silver nitrate or epoxy functionalised silica particles. A single MFC particle was moved from the first section to the central one using an external magnet, allowing the MFC to sequester Ag$^+$ ions, or react with the epoxy groups of SiO$_2$ nanoparticles, then moved again to the final dodecane zone collecting the metal cations and the nanoparticles, respectively. The SEM/EDX analysis showed the presence of silver dispersed in the block MFC (Fig. 24e), and the surface functionalisation of the MFC with silica nanoparticles. Further investigation showed the movement of a single 50 μm sized particle in a custom microfluidic device, from a reservoir and into a 50 μm wide channel, illustrating the use of the MFC as a potential repositionable molecular gate (Fig. 24f and g).[147]

Silvestre and co-workers[218] were the first to apply an innovative pathway for achieving controlled MOF thickness around

a magnetic core, using the LbL approach. In their investigation, commercially available magnetic iron oxide–silica core–shell nanoparticles were initially functionalised with carboxylic groups through an APTES–glutaraldehyde–KMnO$_4$ approach, and then alternatively poured into two reaction baths containing the metal ions and the ligands, respectively. Upon collection with a magnet after every cycle, the authors were able to obtain a (Fe$_3$O$_4$@SiO$_2$)@HKUST-1 nanocomposite (Fig. 23j) and to relate the surface area of the resulting MFC with the number of cycles. This technique appears to be relatively time-consuming, as the cycle number was generally high to achieve an appreciable thickness (i.e. 40 cycles for 20–25 nm). As a proof-of-concept, the obtained MFC was used in the stationary phase for the chromatographic separation of three representative chemicals (pyridine, xylene, and toluene).[218]

A significant advancement in device fabrication for practical applications is the Fe$_3$O$_4$@ZIF-8 MFC designed by Zhang,[216] which was produced using the encapsulation technique based on PSS coating of Fe$_3$O$_4$ particles. The MFC was successfully positioned and anchored in a tubular microreactor using a magnet, and was used as a catalyst in the flow reactor (Fig. 25a). The system including the MFC was used to perform the Knoevenagel condensation[228] between benzaldehyde and ethyl cyanoacetate,

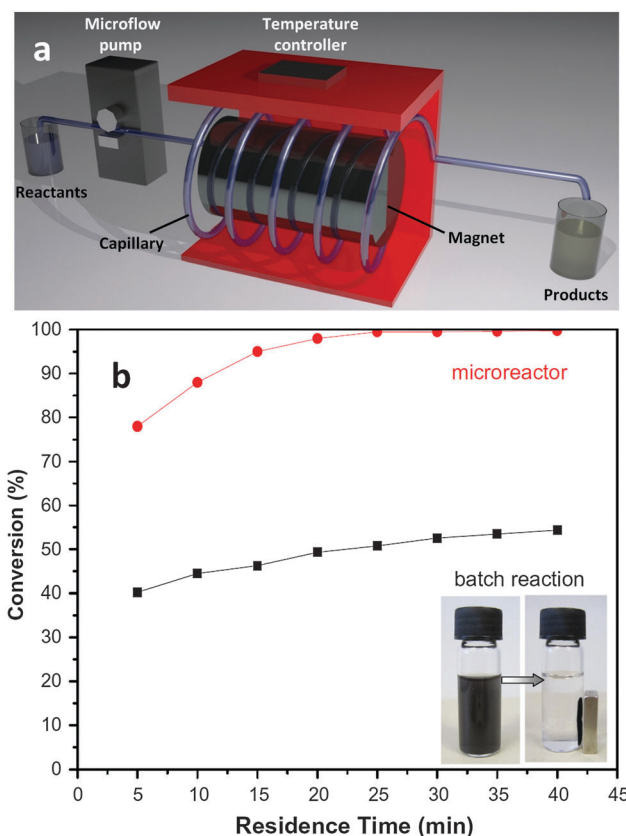Fig. 25 (a) Schematic of the reactor used for the condensation reaction between benzaldehyde and ethyl cyanoacetate using Fe$_3$O$_4$@ZIF-8 MFC immobilized along the tube with a magnet; (b) results of the catalytic conversion. The inset shows the fast collection of the composite with an external magnet. From Zhang et al.[216]
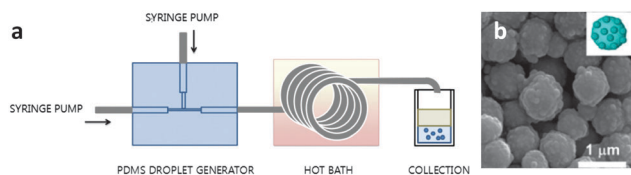
5538 | Chem. Soc. Rev., 2014, 43, 5513–5560

This journal is © The Royal Society of Chemistry 2014

Fig. 26 Microfluidic production and immobilization of Fe_3O_4@ZIF-8. (a) Schematic of the device used; (b) SEM images of magnetic iron oxide nanoparticles successfully coated with ZIF-8 MOF. From Faustini et al.[150]

illustrating the catalytic capability of ZIF-8 (HmIm ligand acted as an efficient base catalyst). The performance of this MFC was tested both in batch and in flow reactors, where 50% conversion and 100% were measured respectively after 25 minutes (Fig. 25b). Moreover, the magnetic field could be turned off in order to flush away the catalyst for subsequent washing and reactivation.

The first comprehensive study for an ultrafast, versatile and continuous synthesis method for producing MOFs and composites was recently reported by Faustini and coworkers.[150] This method for obtaining a number of different MOFs, as well as MOF@MOF core–shell systems and MFCs, takes advantage of a customized microfluidic device. The reaction was performed using microdroplets as reactors (Fig. 26a) providing significantly enhanced reaction rates. In the case of magnetic composites, a two-step protocol was adopted for the full synthesis of the porous magnetic material. Initially, Fe_3O_4 nanoparticles were prepared from an iron(III) chloride precursor, using an oil–water bubble sequence. The outcome of this step was transported downstream in a second T-junction reactor containing the ZIF-8 precursor solution along with PSS surfactant, a polymer shown effective for MOF grafting on magnetic particles. Overall, the process took 2 minutes at 80 °C for the iron oxide preparation, and an additional 5 minutes at 50 °C to obtain the final MFC (Fig. 26b). Moreover, the microfluidic device was used to perform a condensation reaction, by positioning the MFC at stages along the tube using an external magnetic field. The Knoevenagel model reaction between benzaldehyde and ethyl cyanoacetate was executed at 80 °C, obtaining a total conversion to product in less than 35 minutes of residence time. The novelty of this work is that functionalised ultraporous crystals were entirely synthesized and used in the miniaturised device, without the need for a conventional reactor and achieving appreciable yields. For example, in the case of HKUST-1, up to 100 mg per day were produced under controlled flow parameters.

3.3 Advantages and limitations

These examples of dynamic localisation of MFCs illustrate the ability to combine a highly versatile positioning tool (magnetism) with the functional porous characteristics of MOFs (adsorption, selectivity, catalysis, sensing, delivery). MFCs can be prepared using reaction conditions that differ significantly from the desired operating conditions, without the requirement of designing new frameworks. Thanks to their ability to be collected and positioned under the influence of an external magnetic field, they can potentially be recycled and reactivated if their performance degrades during utilization. Moreover, under an

electromagnetic field, they can be used for local heating or for temperature triggered release of absorbed species, and hence hold much promise for biomedical applications and pollutant sequestration. However, current limitations of MFCs include a lack of control over the orientation of crystals during magnetic positioning, reduced volume within the MOF crystals due to the magnetic particles, production rate is quite slow relative to other processes, and the biocompatibility of both MOFs and magnetic nanoparticles is yet to be proven.

4. Positioning functional materials within MOFs

Significant effort has been directed towards positioning functional materials within MOF crystals. Controlling the properties and the position of functional materials inside MOF crystals allows for the fabrication of a novel class of host–guest materials, which can take mutual advantage to elicit certain properties that are difficult to achieve using the guest functional materials or the host framework alone.

Compared with other porous materials, the exploitation of MOFs as a host for functional guest materials offers several benefits.[53] Structurally diverse MOFs with various pore sizes can be prepared from a wide choice of metal ions and organic linkers,[9,58] and thus an appropriate MOF can be easily selected as a host matrix. The three-dimensional porosity of MOFs, the presence of organic linkers that can stabilize guest materials, the sufficient structural properties and thermal stability makes MOFs suitable for use as host materials.

Traditionally, methods for positioning functional materials within MOFs have involved the direct doping of functional metal precursors, ligands, or functional particles during synthesis or through post functionalisation. Although this strategy has proven to be effective, engineering functional materials in precise locations within MOF crystals is a current area of research. Recently, new strategies have been proposed to precisely control the position of functional materials within a MOF crystal. These more sophisticated engineering methods for achieving control over the position of functional materials within MOF crystals opens a new research direction towards novel highly ordered hierarchical structures (Fig. 27).

This section will highlight several pioneering works for doping materials into MOFs, which have paved the road toward the
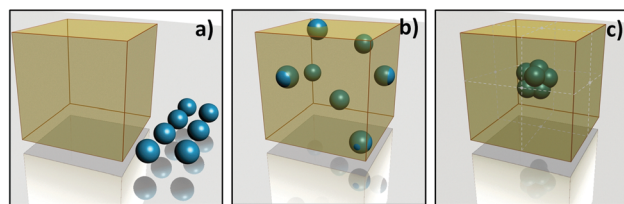
Fig. 27 Materials that need to be combined such as MOF crystal (yellow cube) and functional nanoparticles (blue spheres) (a). Once the two different materials are combined, the position of the particles within the crystal is often randomly distributed (b). However, improved control over the location of the functional particles (c) would allow MOF-based composites to be fabricated with improved or diverse functional properties.

This journal is © The Royal Society of Chemistry 2014

Chem. Soc. Rev., 2014, **43**, 5513–5560 | 5539

control of materials at a specific location with the ultraporous crystals. Novel methods for precisely controlling the position of functional materials within MOF crystals will be subsequently proposed.

4.1 Toward the design of functional materials within MOF crystals

Direct addition of dopants is a straightforward approach for synthesizing functional materials hosted by MOF crystals. The dopant is added directly with the metal precursor and ligand in the MOF growing solution. However, because the framework construction relies on the self-assembly process from a solution, any additional component often perturbs the delicate coordination equilibrium, preventing the formation of the desired porous crystals. Although dedicated reviews detailing the investigation of functionalised MOFs are available,[53,229–231] a general overview of the original methods used to achieve spatial control over functional materials within MOFs is presented here, in order to provide the background for subsequent sections.

Several remarkable examples have been reported that successfully doped functional metal elements into MOFs. Lin and co-workers incorporated catalytic metal ions of Ir, Re, and Ru into the UiO-67 $(Zr_6O_4(OH)_4(bpdc)_6)$.[232] The doping metals were complexed with their matching ligands initially, and then the metal-ligand complexes were doped into the original UiO-67 framework. This strategy allowed for the loading of a sterically demanding bridging ligand into the parent UiO-67 framework, as well as preservation of the parent framework porosity. In a later study, Chen et al. successfully doped a source of Eu^{3+} into a Tb-dmBDC [H_2dmBDC = 2,5-dimethoxy-1,4-benzenedicarboxylic acid] framework to form mixed-lanthanide frameworks.[233] Because the single-lanthanide Tb-dmBDC and Eu-dmBDC frameworks are isostructural with 3D rod-packing structures, mixed-lanthanide frameworks could be readily formed by mixing both metal precursors with the ligand. Remarkably, the Eu-doped framework demonstrated a temperature-dependent luminescent property; a two-colour emission spectra was observed based on temperature variations. In addition, Nenoff et al.[234] demonstrated that Eu^{3+} ions could be doped into In-btb [H_3btb = 1,3,5-tris(4-carboxyphenyl)benzene] frameworks. Eu^{3+} was successfully added at three concentrations into the framework by the addition of a Eu metal source as a starting reagent with $In(NO_3) \cdot H_2O$, H_3btb and oxalic acid. With a 9% Eu^{3+} doping, the MOFs showed remarkable white light emission of chromaticity coordinates (0.33, 0.33) very close to the standard target (0.3127, 0.3290) in the chromaticity diagram given by the Commission Internationale de l'Eclairage (CIE).[234,235]

Rather than doping functional metal ions, functional ligands could also be utilized to substitute the original organic linkers in MOFs, inducing new functionalities. Yaghi and co-workers showed that MOF-5 type structures could incorporate a range of functional derivatives of H_2BDC in a way that mixed with the BDC linker, rather than forming separate domains.[236] The synthesized multivariate MOF-5 type structures could incorporate up to 8 functional ligands ($-NH_2$, $-Br$, $-(Cl)_2$, $-NO_2$, $-(CH_3)_2$, $-C_4H_4$, $-(OC_3H_5)_2$, and $-(OC_7H_7)_2$), resulting in 18 variants containing two or more functional ligands of distinctive functional MOF-5 structures. Crystals of multivariate MOFs were obtained by adding $Zn(NO_3)_2 \cdot 4H_2O$ to a DMF solution mixture of the selected organic linkers. Exceptionally, the H_2 storage capacity of $-(OC_3H_5)_2$ and $-(OC_7H_7)_2$ functionalised BDC-doped MOF-5 was 84% greater than the original MOF-5 crystals, while $-NO_2$, $-(OC_3H_5)_2$ and $-(OC_7H_7)_2$ functionalised BDC-doped MOF-5 showed 400% better selectivity of CO_2 over CO compared with the original MOF-5 materials. Specific functionalities (e.g. $-NH_2$) can also be used for the uptake of metal ions.[147]

Bio-MOF-1 ($Zn_8(ad)_4(bpdc)_6O$, ad = adenine) formed by reactions between adenine and zinc acetate dihydrate in DMF, is occupied by dimethylammonium cations (the product of DMF decomposition) within the channels. This allows the introduction of cationic materials through an ion-exchange process.[237] Utilizing this property, Yu et al. loaded a cationic pyridinium hemicyanine dye into the framework.[238] As the amount of loaded dye increased, the luminescence of the framework gradually shifted from blue (from H_2bpdc linker) to red (dye) under UV irradiation. Importantly, the confinement of the dye within the pores of the framework restricted intramolecular torsional motion and π–π interactions between the dyes, overcoming the aggregation-caused quenching effect observed in both solution and powder form.

In 2012, Buso et al. adopted highly luminescent QDs as functional dopants within MOF-5 crystals.[239] In this work, the synthesis and functionalisation of the frameworks was achieved in a one-pot process. The surface of the QDs was decorated with 5-amino-1-pentanol, which enabled their dispersion in the typical solvents used in the synthesis of MOF-5. The doping of QDs in the MOF-5 precursor solution was shown to have no influence on the crystal-formation kinetics. Interestingly, by varying the growth media, the QDs displayed distinctive distribution patterns within MOF-5. QDs were aggregated in the frameworks when using DMF as a solvent, whereas they showed homogeneous distribution patterns within MOF-5 crystals when using DEF suspensions. The resulting QD@MOF-5 crystals demonstrated size-selective optical sensing ability, allowing a small molecular quencher to enter the pores and quench the QDs within the MOF, while large quenchers had no effect on the QD@MOF-5 because of the sieving properties provided by the MOF. Sada and co-workers embedded Au nanorods in MOF-5 crystals by functionalising the surface of the nanorods with carboxylate groups followed by seeded growth of MOF-5;[240] while Ke et al. prepared Au nanoparticles-loaded MIL-100(Fe) ($Fe_3O(OH)$-$(BTC)_2$) frameworks in a LbL fashion by consecutively dipping the Au nanoparticles between the metal precursor and the ligand.[241]

Recently, Lin et al. demonstrated photoactive MOFs that have the ability to generate metal nanoparticles upon visible light irradiation.[242] The MOFs were synthesized between Ir-chelated dicarboxylate-containing ligand and Zr^{4+}. The nanoparticle precursor K_2PtCl_4 was infiltrated into the framework in triethylamine (TEA)-containing solvents. The MOFs were then irradiated with visible light with a 420 nm cut-off filter. TEA reductively quenched the photo-excited Ir-containing ligand to

generate the radical, which reduces the metal precursor to form Pt nanoparticles within the host framework.

Microwave irradiation has also been explored for the formation of nanoparticles within MOF crystals.[243] Metal precursors were firstly diffused into the pores of MIL-101(Cr) where, upon microwave heating, activation of the pores and reduction of metal precursors occurred simultaneously in the presence of a reducing agent. This caused the formation of small Pd, Cu, and Pd–Cu nanoparticles within the pores and larger particles on the surface of the MOF crystals.

Utilizing the intrinsic redox-active properties of particular MOFs, functional nanoparticles can be formed inside the framework without the need of any capping or reducing agents. To this end, Suh's group synthesized various redox-active MOFs employing various Ni(II) square-planar macrocyclic complexes as metal building blocks as well as utilizing redox-active organic building blocks.[244–246] The inclusion of metal ion precursors into these frameworks resulted in the oxidation of incorporated Ni(II) species to Ni(III) and the simultaneous reduction of the metal ions, followed by the nucleation and growth of metal nanoparticles. Utilizing this strategy, this group has successfully formed Au, Ag, and Pb nanoparticles in the redox active frameworks.[244–246]

In a similar approach, Grzybowski and coworkers synthesized two cyclodextrin (CD)-based MOFs using RbOH and CsOH as the metal source.[247] The resulting MOFs contained one hydroxide counter ion per metal center, which can work either alone or cooperatively with the CD units as redox centers to reduce metal salt precursors into metal nanoparticles. It was demonstrated that the redox active MOFs could reduce Au and Ag ions to form nanoparticles when the metal precursors $HAuCl_4$ or $AgNO_3$ were infiltrated into the frameworks. Interestingly, the formation of Au nanoparticles occurred predominantly in the core of the crystal, while Ag nanoparticles were deposited throughout the entire MOF crystal.

By employing a reducing agent such as H_2 gas, metal precursors introduced into MOFs can be converted to nanoparticles within the framework. In one study, Latroche and co-workers immersed MIL-100(Al) $(Al_3O(OH)(BTC)_2)$ in Pb precursor solutions containing 10% (v/v) aqueous HCl solution of H_2PdCl_4. Up to 10 wt% Pd nanoparticles were formed within the frameworks using a flow of Ar–H_2.[248] Very recently, Xu and co-workers introduced a "double solvent" method for the formation of Pt nanoparticles inside MIL-101(Cr) frameworks.[249] The frameworks were immersed in a large amount of hydrophobic solvent (hexane), to which a hydrophilic solvent (water) containing the metal precursor H_2PtCl_6 was added, with an amount equal to or less than the total pore volume of the framework. Because the inner surface of the framework is much larger and more hydrophilic than the outer surface, the small amount of aqueous phase containing the metal precursor was readily incorporated into the pores by capillary forces, which minimizes the deposition of the precursor on the outer surface. After loading the precursor, a H_2–He stream was employed to produce the Pt nanoparticles within the framework.

Functional nanoparticles formed by chemical vapor deposition with MOFs involves the infiltration of volatile organometallic

precursors into the framework, followed by hydrogenolysis. MOF-5 has been shown to successfully host various organometallic precursors containing Pb, Cu, Au, and Ru in its pores. After the treatment with a H_2 stream at hydrogenolysis temperatures, metal nanoclusters were formed within MOF-5.[250,251] Recently, magnesium nanocrystal formation within the SNU-90 $(Zn_4O(atb)_2$, H_3atb = aniline-2,4,6-tribenzoic acid) framework was demonstrated.[252] The composite material was made by thermal decomposition of precursor vapor within the MOF crystals.

4.2 Positioning of functional materials within MOFs through self-assembly

Research directions for positioning functional materials within MOFs have shifted from doping towards a more precise engineering control of the location of functional materials within MOFs, producing a core–shell type of material with an active core and a MOF shell acting like a reservoir or a molecular sieve.

In 2011, Falcaro et al. pioneered this field of research by precisely positioning a multifunctional particle within MOF crystals.[125] They demonstrated how a multifunctional particle could be simultaneously employed as both a nucleating agent and a directing agent for MOF-5 crystal formation. They synthesized a novel class of α-hopeite microparticles (ceramic microspheres), which formed immediately within the starting MOF-5 precursor solution when Pluronic F-127 was introduced. As a result, the growth kinetics of MOF-5 in the presence of the α-hopeite microparticles is three times faster than the traditional solvothermal approach. The versatility of these ceramic microparticles was demonstrated by successful incorporation of catalytic metal nanoparticles (Pt and Pd), highly luminescent semiconductor QDs (CdSe–CdS–ZnS) or polymer nanoparticles (Teflon) in the core of MOF-5 crystals (Fig. 28a and b).

Furukawa and co-workers employed coordination replication techniques to position gold nanorods inside an Al(OH)(ndc) framework.[253] The surface of the gold nanorods were firstly coated with thiolated polyethylene glycol (SH-PEG). This provides surface properties which allowed a layer of amorphous alumina to be formed on its surface. The coordination replication process was carried out in the presence of H_2ndc in a microwave-assisted reaction to convert the out-of-equilibrium alumina coatings to more stable Al(OH)(ndc) frameworks. A model fluorescent molecule anthracene was loaded into the highly porous frameworks. Upon exposure to the near infrared (NIR) laser, the gold nanorods within the MOF crystals were rapidly heated, causing the release of the anthracene from the frameworks (Fig. 28c and d).

Lu et al. also demonstrated a versatile approach for positioning functional nanoparticles in ZIF-8 frameworks.[215] This strategy relies on coating various functional nanoparticles with PVP, followed by MOF crystal formation around PVP-coated nanoparticles. PVP served as both a "general" surfactant to stabilize various nanoparticles in polar solvents, and a capping agent to control the size and shape of nanoparticles. ZIF-8 crystals that contained Pt, CdTe, Fe_3O_4 and lanthanide-doped $NaYF_4$ nanoparticles/nanorods, Ag nanocubes, polystyrene (PS) spheres, β-FeOOH nanorods were prepared successfully using this approach. Nanoparticle-doped ZIF-8 exhibited molecular sieving and
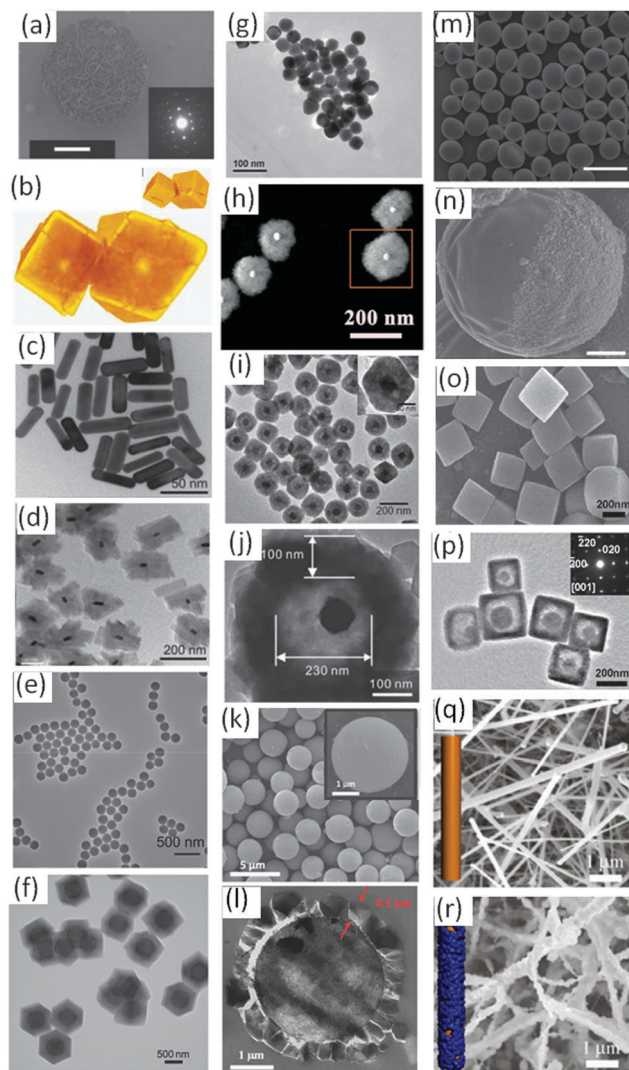
This journal is © The Royal Society of Chemistry 2014

Chem. Soc. Rev., 2014, 43, 5513–5560 | 5541

Fig. 28 (a) SEM image of a DRM. The inset of the figure shows the electron diffraction pattern of the DRMs, indexed as α-hopeite. (b) X-ray micro-tomography images of MOF-5 nucleated around two DRMs. The small images on the top-right are the measured tomography of the crystals' exterior surfaces.[125] TEM images of (c) Au nanorods, and (d) core–shell Au nanorod–MOF composites.[253] TEM image of (e) Au nanoparticles and (f) hybrid crystals obtained when Au nanoparticles were introduced 15 minutes after the initiation of the reaction.[215] (g) TEM image of bare Au nanoparticles. (h) HAADF-STEM image of core–shell Au@MOF-5 NPs.[254] (i) TEM image of the Pd@Cu2O core–shell nanoparticles. (j) Yolk–shell structures with ZIF-8 shell and Pd octahedra in the hollow space.[255] SEM image of (k) silica particles, and (l) ZIF-8 crystals around a silica particle.[256] SEM images of (m) Janus polymer microparticles, and (n) HKUST-1 nanocrystal-functionalised bicompartmental particles.[225] (o) SEM images of Prussian blue frameworks, and (p) TEM image of Prussian blue yolk–shell particles.[257] SEM image of (q) silicon nanowires, and (r) HKUST-1 on silicon nanowires.[258]

regioselective guest reactivity from the microporous nature of MOF as well as functional (catalytic, magnetic and optical) properties that derive from the incorporated nanoparticles (Fig. 28e and f).

He *et al.* reported a remarkable method of positioning individual Au nanoparticles within a single MOF-5 particle.[254] Different from the conventional two-step method to synthesize

nanoparticle–MOF composites by adding the pre-synthesized particles into the MOF precursors, they directly mixed both the Au and MOF precursors (HAuCl4, Zn(NO3)2·6H2O, and H2BDC) in the reaction solution containing DMF, PVP, and ethanol at 140 °C. DMF was expected to facilitate MOF-5 formation, while PVP was employed to stabilize the readily formed Au nano-particles,[219] and ethanol changed the coordination environment of metal ions such that MOF-5 grew preferentially around the Au nanoparticles instead of self-nucleating in solution. It was found that HAuCl4 was first reduced to Au nanoparticles by DMF within a very short time. Subsequently, MOF-5 was formed and spontaneously grew on the surface of the PVP-capped Au nanoparticles, so that uniform core–shell Au@MOF-5 crystals were produced (Fig. 28g and h).

Kuo *et al.* synthesized novel core–shell MOFs with Pd nano-particles as a core in a ZIF-8 shell.[255] Pd octahedral nanocrystals were firstly coated with Cu2O by the addition of CuCl2, NaOH, and NH2OH·HCl to form a Pd@Cu2O core–shell structure. After Cu2O coating, the Pd@Cu2O structures were mixed with the ZIF-8 precursors HmIm and zinc nitrate in methanol. Importantly, the addition of 2-meIm also caused the reduction of pH from 7 to 5, because of the deprotonation of HmIm, and the Cu2O was etched off simultaneously with the formation of ZIF-8 shell. Elemental analysis was used to confirm the complete removal of Cu2O within the core–shell structure (Fig. 28i and j). This novel structure provided excellent molecular-size selectivity. The results showed high activity for the ethylene and cyclohexene hydrogenations but not in the cyclooctene hydrogenation.

Sorribas *et al.* adopted 3 µm-diameter silica particles as a core to grow ZIF-8 crystals around the silica, forming core–shell structures.[256] This strategy involved *in situ* seeding and secondary crystal growth. Due to the abundant silanol groups on the silica surface, the interaction between silanol groups and metal pre-cursors Zn2+ promoted ZIF-8 nucleation on the spheres. After 5 min, this seeding process provided a uniform ZIF-8 seed layer around the silica spheres with an average crystal size of 180 nm, as confirmed by TEM. Thicker ZIF-8 layers were achieved simply by immersing the seeded silica particles in the ZIF-8 precursor solution once or twice, yielding ZIF-8 shell around silica parti-cles with a thickness of ∼410 nm and ∼550 nm, respectively (Fig. 28k and l).

Beyond the control of functional materials within MOFs, the architecture of the hybrid materials could also be controlled in a precise way. Very recently, Park and co-workers showed the spatio-selective growth of MOF nanocrystals on anisotropic poly-mer microparticles.[225] Janus particles were synthesized with an electrohydrodynamic co-jetting process. Carboxylic groups were functionalised only on one side of the particle surface. A spatially controlled layer-by-layer growth of HKUST-1 was therefore possi-ble only on the carboxylate-functionalised side. The inclusion of paramagnetic nanoparticles on the other side of the Janus particles allowed a new kind of hierarchically functionalised hybrid materials on which porous MOF nanocrystals could be magnetically manipulated (Fig. 28m and n). Hu *et al.* presented an elegant strategy to tailor the architecture of Prussian blue (PB) frameworks.[259] Hollow interiors within the frameworks

were created through controlled chemical etching in the presence of PVP. The hollow cavities and particle sizes could be tuned by changing the synthetic conditions, and the original PB crystallinity was preserved even after formation of interior hollows. They further developed this controlled hollowing process by step-by-step crystal growth and subsequent etching strategy. As a result, various types of crystals with shell-in-shell, yolk–shell, and yolk-double-shell hollow structures could be synthesized. The resultant hollow-based nanoarchitectures significantly increased gas adsorption and revealed interesting magnetic properties (Fig. 28o and p).[257] Cui and coworkers have selectively grown HKUST-1 crystals on silicon nanowires. The nanowires were firstly modified with carboxylates oxidizing a surface functionalisation initially involving (3-cyanopropyl)trichlorosilane. This allowed the preferential formation of MOF seeds on the nanowire surface. The MOF seed-coated nanowires were then immersed into MOF precursor solution in a step-by-step fashion (repeated LPE), yielding silicon nanowires coated with controlled thickness of MOF crystals (Fig. 28q and r).[258]

4.3 Positioning of functional materials within MOFs using an external control

De Vos's group exploited the photoactive nature of MOF-5 crystals and presented an elegant patterning strategy based on direct laser writing to fabricate patterns of metallic nanoparticles within a single MOF-5 crystal.[260] MOF-5 presents numerous advantages for light irradiation purposes; the crystal lattice can be considered as photoactive inorganic centers spaced by linkers acting as antennae; efficient energy transfer to the inorganic clusters, which contributes to the photoactivity; and the three-dimensional interconnected porosity allows for efficient diffusion of metal precursors for light-induced nanoparticle formation. MOF-5 crystals were firstly immersed in silver nitrate (AgNO$_3$) solution to allow the diffusion of silver precursors into the MOF-5 lattice. A femtosecond pulsed 780 nm laser generating UV irradiation was focused inside the MOF crystal, generating Ag nanoparticles at the focal point of the laser. Pattern generation was achieved by moving the sample using a computer controlled piezoelectric stage, thus positioning the laser focal point according to the pixel coordinates of a digitized image. Utilizing this technique, precise positioning of the metal nanoparticles within a single MOF crystal could be achieved. However, this technique seems to be limited to semiconductive MOFs which are able to effect the photo catalytic reduction of noble metal ions.

Han *et al.* developed a modified wet stamping technique that allowed for patterns of dyes and indicators to be imprinted into MOFs.[261] MOF-5 and CD-MOF-2 (CD = cyclodextrin) were selected for the proof of concept based on two reasons: the interconnected porosity of these frameworks allows the diffusion of the dyes and indicators through the framework, and the established method for preparing millimeter-scale frameworks makes it possible to use stamps with micron sized features. Stamps synthesized from agarose or furfurylamido-bisphenol A diglycidyl ether organogel were impregnated with a variety of dyes, the MOF crystal was then positioned on top of the stamp to allow the patterns to be transferred onto the MOF, and the
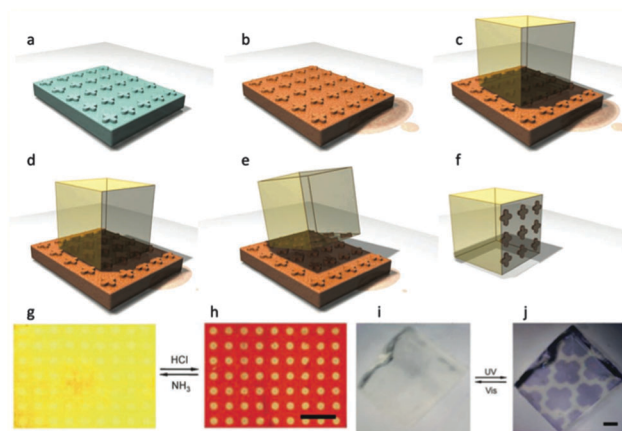

Fig. 29 (a–f) Schematic of wet printing technique to create micropatterns onto a single MOF. (a–b) A micropatterned stamp is impregnated with a dye (b). (c) The MOF crystal is then positioned on top of the stamp and (d and f) the pattern is transferred onto the MOF and the dye is adsorbed within the porous crystal. (g–j) Images of reversible and responsive micropatterns printed onto MOFs. (g and h) The pH indicator (methyl orange) printed frameworks switch between yellow and red upon exposure to ammonia gas and gaseous hydrochloric acid. (i and j) A photochromic dye (diaryl ethene) printed framework switches between transparent and blue when irradiated with UV and visible light repeatedly (scale bars 100 µs). Reproduced from Han *et al.*[261]

dyes were diffused within the porous crystal. Utilizing this technique, a pH indicator (methyl orange) and a photochromic dye (diarylethane) was patterned into the frameworks. The pH indicator-functionalised frameworks changed between yellow and red upon exposure to ammonia gas and gaseous hydrochloric acid, while the photochromic dye-functionalised MOFs changed between transparent and blue when irradiated with UV and visible light repeatedly (Fig. 29).[261]

Remarkable proof-of-concept applications have been provided. For example, the QD-loaded MOF-5 could be used as a molecular sieve sensor.[125] Using emission-quenching agents (thiols), it was shown that only thiols with a small enough molecular size could effectively diffuse through the framework and quench the emission of the functional QDs located in the crystals' cores. Similarly, the yolk–shell Pd@ZIF-8 crystals provided excellent molecular-size selectivity. Pd core showed high activity for the ethylene and cyclohexene hydrogenations but not in the cyclooctene hydrogenation due to the size exclusion of the ZIF-8 shell.[255] The Au nanorod-loaded Al(OH)(ndc) framework demonstrated photothermal properties, resulting in the implementation of unique motion-induced molecular release, triggered by the highly efficient conversion of optical energy into heat by Au.[253] This allowed temporal control of the release of a loaded drug, anthracene, from the framework for potential drug delivery applications. Moreover, Au nanoparticles inside MOF-5 crystal showed surface-enhanced Raman scattering (SERS) for highly sensitive detection of CO$_2$ by combining the advantage of the selective adsorption property of the MOF-5 shell and the optical enhancement of the Au nanoparticles.[254] in addition, the simple procedure to create patterns on a MOF by wet stamping and the precise control of Ag pattern in a MOF by direct laser

writing are expected to find applications in optic or micro-electronic device fabrications.[260,261]

4.4 Advantages and limitations

The ability to control the spatial location of functional materials within MOFs gives the advantage of confining specific material properties in precise locations. In this regard, the properties of MOFs (*e.g.* catalysis, adsorption, release, molecular sieve or dielectric features) can be combined with the intrinsic properties of a range of different molecules or nanomaterials (*e.g.* photochromics, energy conversion, catalysis, sensing, electrical conductivity) originating a new class of materials with unique synergic functionalities. The limitations of this approach are very similar to those related to heterogeneous seeding, namely decreased specific surface area, defects can be introduced into the lattice structure, and customised washing procedures may need to be applied. In addition, the functional material must be compatible with the synthesis methods used for the preparation of the MOFs.

5. MOF-based devices

Numerous devices have been proposed in the literature for a wide range of applications based on MOFs. To give a good appreciation of the potential of MOFs as functional materials, and to stimulate progress in the field of device fabrication, different applications are summarized and illustrated in the schematic of Fig. 30. We will focus on a few significant examples from the state of the art related to miniaturised MOF-based devices; an extended list is presented in Table 3.

5.1 Sensing

MOFs have been investigated for the fabrication of different sensors. HKUST-1 was used with a quartz crystal microbalance (QCM) for the detection of pyridine,[262] or methanol and hexane vapours,[263] due to the sorbent proprieties of this porous framework. The same MOF has been used with a piezoresistive microcantilever to sense water[264] as well as different Volatile Organic Compounds (VOCs),[184,265] and has been used for the fabrication of a capacitance film sensor[266] and surface acoustic wave (SAW) sensor.[267] HKUST-1 coated silver nanoparticles were also used as a CO$_2$ surface plasmon resonance (SPR) sensor device.[268] These examples show that HKUST-1 is versatile enough to be effectively combined with a variety of different detection systems *via* a number of different patterning protocols. Other types of sensors including optical, biological and electrochemical have been investigated and they are referred to in Table 3.

Allendorf *et al.* were the first to apply the LPE and LbL techniques to a sensor type device.[264] They formed a stress induced chemical detector consisting of an array of 10 Au-coated micro-cantilevers, with a thiol based SAM and then grew HKUST-1 MOF layers on top (Fig. 31a). As certain molecules were selectively absorbed into the highly porous MOF coating, the stress induced by the increased mass was detected on the micro-cantilever. The array was immersed in alternative ethanol

solutions of Cu(OAc)$_2$ and H$_3$BTC to build MOF films to a thickness of 100 nm. The resulting hydrated MOF sensors showed rapid and reversible responses to H$_2$O, MeOH and EtOH in the gas phase, and responded to CO$_2$ when the HKUST-1 MOF was used in its dehydrated state.[264] This study was further extended to detect VOCs. The piezoresistive microcantilevers responses allowed the detection of 12 different VOCs and were able to distinguish between them based on shape, response time and signal amplitude.[265]

MOFs have been grown on a QCM for the measurement and detection of small molecules within the highly porous films.[55,262,263,278,279] QCMs are highly sensitive mass sensors that measure the sorption properties of porous materials. The gold-coated piezo-active quartz crystals can be functionalised with a SAM for MOF growth. Bein *et al.* used a 11-mercapto-undecanol SAM layer for the direct growth of HKUST-1 and were able to show the water vapour sorption properties of the thin MOF films at various temperatures.[278] A hysteresis between the adsorption and desorption is seen at low temperatures but not at higher temperatures.[278] Wöll *et al.* measured the pyridine diffusion coefficient on a MOF-based QCM device by monitoring the time-dependence mass-uptake.[262] The thiolate-based SAM was coated on the quartz crystal to which HKUST-1 was grown using the LbL approach. Assuming Fickian diffusion and a hoping mechanism, the diffusion coefficient was in good agreement with the quantum mechanical calculations.[262]

Kitagawa's group have also demonstrated the use of HKUST-1 QCM devices (Fig. 31b) to measure the sorption of organic vapours (methanol and hexane)[263] and guest molecules of similar size but different chemistry (1-butanol, diethyl ether, and *n*-pentane).[55] They showed that strong intermolecular reactions can cause the guest molecules to cluster within the porous framework and temporarily slow desorption rates.[55] At low analyte concentration, the sensor response is dependent on the MOF crystal size, whereas at high analyte concentrations the sorption kinetics is more significant.[263] Recently Kitagawa's group extended the QCM study to heterogeneous MOF films where alternative layers of MOFs are epitaxially grown on the crystal surface.[279] Two MOFs of (type 1) [Cu$_2$(ndc)$_2$(dabco)]$_n$ and (type 2) [Cu$_2$(aBDC)$_2$(dabco)]$_n$; [Cu$_2$(HOOC-(CH$_2$)$_2$OCNH-bdc)(aBDC)(dabco)]$_n$, are grown in layers using the LbL approach.[279] The QCM results measuring VOCs of different size and polarity indicated that the sequence of the MOF coatings greatly affects the sensitivity. The QCM could selectively adsorb methanol from a methanol–hexane mixture if the type 2 MOF was grown on top of the type 1 MOF but the inverse structure did not show any selectivity.[279]

Liu *et al.* prepared a capacitive humidity sensor by the direct nucleation and growth of HKUST-1 MOFs on a copper substrate (Fig. 31c).[266] The uniform MOF film has two Al electrodes attached at each end and was connected to an electronic circuit and probed with an alternating current (AC). The capacitance response for the MOF sensor was linear at 1000 Hz frequency and showed good sensitivity and quick response to various relative humidities at different temperatures.[266] MOFs have also been used in impedimetric sensors for
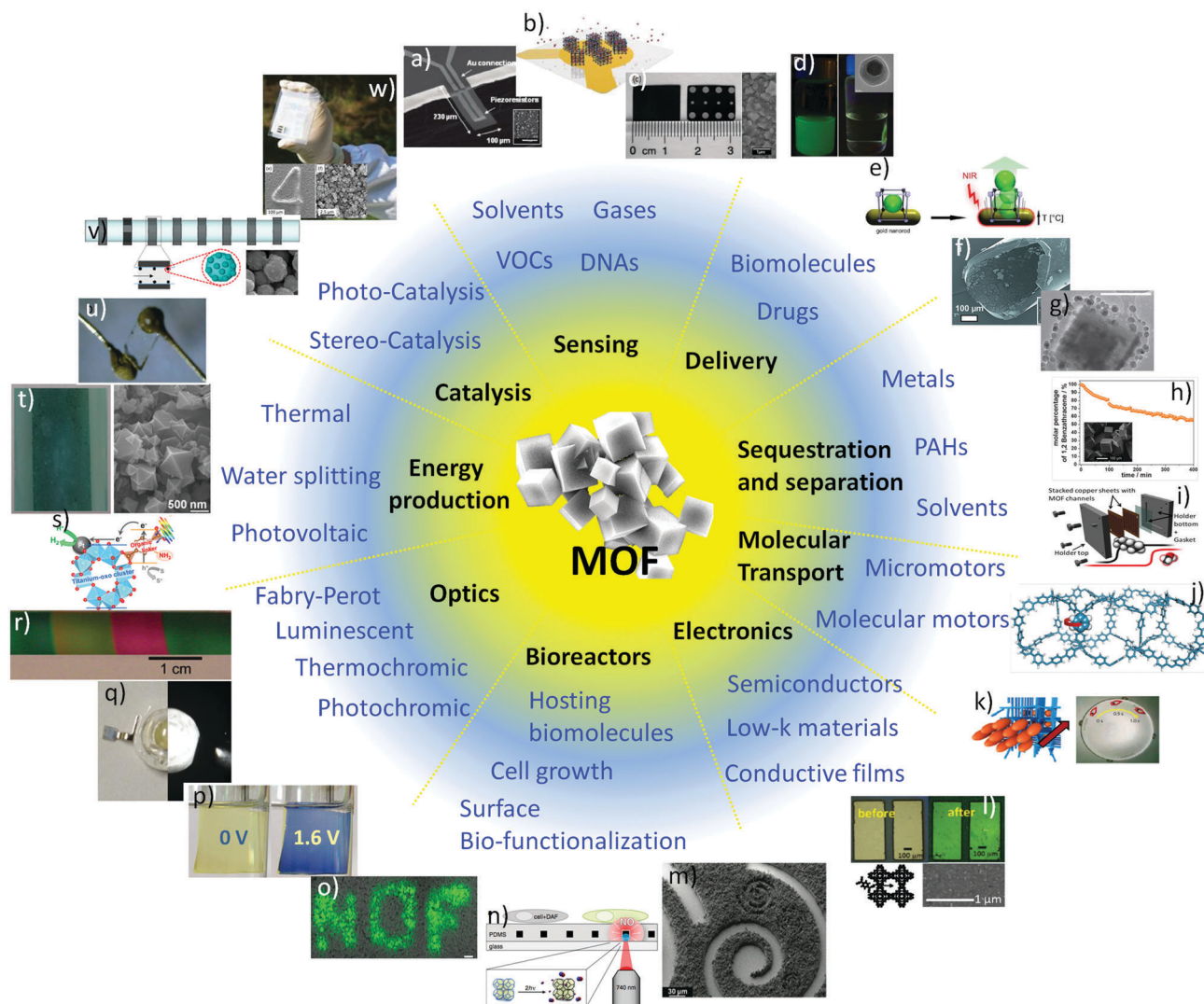
5544 | *Chem. Soc. Rev.*, 2014, **43**, 5513–5560

This journal is © The Royal Society of Chemistry 2014

Fig. 30 (a) MOF-based piezoresistive microcantilever;[264] (b) MOF-deposited gold QCM electrodes;[55] (c) HKUST-1 film on aluminium electrodes;[266] (d) magnetic manipulation of Fe_3O_4-loaded ZIF-8;[269] (e) near infrared-induced drug release from gold nanorod-loaded MOF;[253] (f) MOF-5-coated fused-silica capillary;[270] (g) HKUST-1-coated silica magnetic bead;[218] (h) MOF-5 magnetic framework composite and the uptake of benzanthracene;[271] (i) HKUST-1 incorporated micro-separator assembly;[100] (j) porous aromatic framework structure with a highlighted *p*-phenylene rotor;[22] (k) projection of a MOF–peptide 'boat' around the Petri-dish;[21] (l) TCNQ molecule entering a HKUST-1 film devices;[16] (m) MOF patterns created by UV lithography;[24] (n) photosensitive MOFs for cell activation;[57] (o) cell activation by irradiation-induced selective release of NO from MOF devices;[57] (p) MOF thin film-based reversible electrochromic device;[272] (q) MOF-based white emitting LED;[273] (r) ZIF-8-based Fabry–Perot interferometer;[274] (s) photoexcited organic linker induced electron transfer from the linker-to-cluster charge-transfer mechanism;[275] (t) MOF-coated doctor bladed TiO_2–MWCNTs composite;[276] (u) gold electrodes attached to a single MOF crystal;[277] (v) magnetic framework composite immobilized into a microfluidic catalytic system;[150] (w) HKUST-1 films on a photolithographed copper plate.[172]

the detection of hydrophilic molecules in the gas phase (*e.g.* water, alcohols).[280]

Allendorf *et al.* developed a MOF-based quartz SAW sensor for humidity detection.[267] The SAW sensor detects gases by measuring a frequency shift of acoustic waves parallel to the quartz substrate. The HKUST-1 MOF was prepared using an automated LbL technique directly on the quartz surface as the freshly cleaved quartz surface formed silanol groups from the hydrolysis of ambient water. The highly polar silanol groups coordinate with the water molecules in the $Cu_2(-CO_2)_4(H_2O)_2$-paddle-wheel building units during MOF formation.[267] The SAW sensor showed a 3-fold improvement in humidity response compared to the HKUST-1 QCM sensors.[15]

5.2 Drug delivery

Employing MOFs as carriers for drug delivery is an emerging field, largely owing to their unique advantages over other drug carriers. The tunable nature of the chemical composition, surface area, and pore sizes makes MOFs ideal candidates for loading a range of drugs and biomolecules. The need for controlling the loading and release of drugs from MOFs on demand is a prerequisite for designing the next generation of MOF-based delivery devices.

Furukawa and co-workers positioned Au nanorods inside aluminium-based MOFs to form a stimuli-responsive device
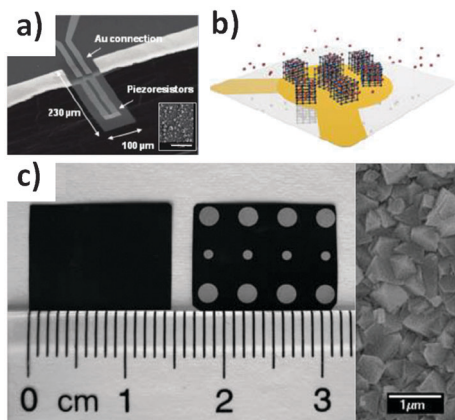
This journal is © The Royal Society of Chemistry 2014

Chem. Soc. Rev., 2014, **43**, 5513–5560 | **5545**

Fig. 31 (a) SEM of piezoresistive microcantilever and inset SEM of MOF deposition (scale bar 2 μm), from Allendorf et al.;[264] (b) schematic of the QCM platform (transparent plate) where MOFs are deposited on the gold electrodes (yellow), from Tsotsalas.;[55] (c) photograph of HKUST-1 MOF film (left) with Al electrodes attached (right) and SEM image of MOF film surface, from Liu et al.[266]
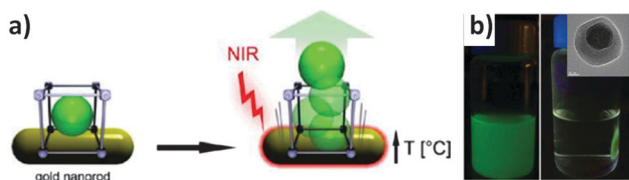

Fig. 32 (a) Concept of the light triggered release of a guest molecule from an aluminium based MOF containing Au nanorods, from Khaletskaya et al.;[253] (b) fluorescein doped magnetic ZIF-8 based nanoparticles collection and inset TEM of MOF composite, from Zhuang et al.[269]

(Fig. 32a).[253] This strategy relies on coordination replication techniques to convert the alumina-coatings on the Au nanorods to Al(OH)(ndc) frameworks.[170] A model drug, anthracene was loaded into the frameworks. The Au nanorods in the MOFs allowed the implementation of unique motion-induced molecular release of anthracene, triggered by the highly efficient conversion of optical energy into heat that occurs when the Au nanorods are irradiated into their plasmon band.[253]

ZIF-8 crystals have recently been optimised to serve as drug carriers (Fig. 32b).[269] Due to the pH-responsive nature of the imidazole ligand, the coordination between the zinc and imidazolate ions dissociates at acidic pH, which makes ZIF-8 ideal for targeting cancer cells where extracellular microenvironments (pH 5.7–7.8) are more acidic than healthy tissues. The encapsulation of magnetic nanoparticles in ZIF-8 spheres further enhanced their functionality, which offered a simple route for manipulating the location of the nanocrystals for potential target delivery applications.

HKUST-1 crystals were loaded with superparamagnetic magnetite particles, making a Magnetic Framework Composite (MFC)[32] called M-HKUST-1, providing an easy manipulation method for controlling the location of MOFs,[204] which could be beneficial for targeted drug delivery applications by applying a static magnetic field. Moreover, when exposed to an external

alternating magnetic field, M-HKUST-1 rapidly heated up, which could potentially trigger the release of loaded drugs.

5.3 Separation and sequestration

Due to their uniform pore sizes and high surface areas, MOFs are emerging as key materials for separation and storage applications for a range of molecules. Much work has been dedicated towards using MOFs for gas separation membranes and there are several reviews dedicated to the preparation and use of these materials.[281,282] Here we focus on the controlled growth of MOFs and applying them in various technologies using miniaturized devices.

The use of MOFs for gas separation is one of the most promising and developed applications. Recently MOF films and membranes have been prepared using the layer-by-layer growth techniques for these applications.[270,283,284] Münch et al. developed chromatographic capillaries coated with MOF-5 using the LbL approach with a carboxylic terminated SAM (Fig. 33a).[270] Controlled growth of MOF-5 was possible by pumping through the inorganic SBU and the organic linkers alternatively between washing steps. Although the technique produced thicker films than expected due to incomplete removal of the reactants between steps, the chromatography capillaries showed promising performance for more than 300 chromatographic separations.[270]

Fischer's group applied the liquid phase deposition technique to prepare CO_2 selective MOF membranes.[283] Pumping alternative metal precursor and organic linker reactants through the porous ceramic supports, two isoreticular MOF membranes were prepared; the non-polar $[Cu_2(ndc)_2(dabco)]_n$ and the polar $[Cu_2(BME-bdc)_2(dabco)]_n$. ($H_2BME-bdc$ = 2,5-bis(2-methoxyethoxy)-1,4-benzene dicarboxylic acid). The gas separation of equimolar CO_2–CH_4 mixtures indicated anti-Knudsen separation for the polar membrane and Knudsen separation from the non-polar membrane.[283] Lee et al. prepared Ni-MOF-74 membranes on
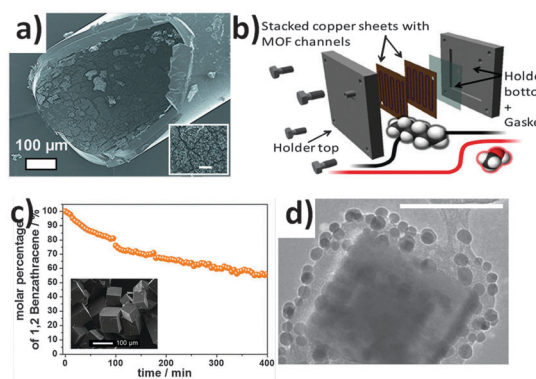
Fig. 33 (a) SEM image of a gas chromatography capillary coated with MOF-5 using the LbL technique and the inset shows a magnified view of the MOF coating (scale bar equals 10 μm), from Munch et al.;[270] (b) schematic of the micro-separator assembly which incorporates HKUST-1 into the micro-channels via electrochemical deposition, from Van Assche et al.;[100] (c) reduction of 1,2-benzanthracene from solution due to uptake from a MOF-5 magnetic framework composite (inset), from Doherty et al.;[23] (d) silica magnetic bead coated with HKUST-1 for sequestration of aromatic compounds (scale bar 100 nm), from Silvestre et al.[218]

alumina supports *via* a layer-by-layer seeding technique followed by secondary growth MOF formation.[284] The use of a SAM layer was not needed due to the covalent bonds between the carbonyl groups of the organic MOF linker and the surface hydroxide groups of the alumina supports. The resulting membranes showed Knudsen diffusion for H_2, N_2 and CH_4 and surface diffusion for CO_2.[284]

Van Assche *et al.* have recently developed a micro-separator integrating MOF micro channels *via* an electrochemical deposition technique.[96,100] The device comprised of HKUST-1 layers rapidly grown inside micro-channels machined into a copper sheet (Fig. 33b). The leak-free micro-separator device showed a promising ability for the separation of *n*-hexane and methanol vapours at faster adsorption rates than a conventional packed bed. The rapid mass and heat transfer make this suitable for catalysis and sensing type applications as the short adsorption–desorption cycles minimises the volume of MOF required.[100]

Sequestration of pollutants and contaminants is another promising field for MOF devices. Much work has focused on preparing magnetic framework composites (MFCs)[53] embedding magnetic particles so that the MOF crystals can be collected and the adsorbed molecules recovered/disposed.[23,25,218,285] Doherty *et al.* prepared MOF-5 MFCs for the sequestration of polycyclic aromatic hydrocarbons.[23] Using $NiFe_2O_4$ and $CoFe_2O_4$ fibres, they grew MOF-5 crystals which could be positioned in solution with the use of a commercial magnet. The MFCs successfully sequestered a four aromatic ring molecule, 1,2-benzanthracene, from solution with an uptake of 1.3 mmol g^{-1} over 400 minutes (Fig. 33c).[23]

Huo and Yan also demonstrated the sequestration of PAH from environmental water samples using MIL-101 MOF crystals decorated with magnetic nanoparticles.[25] Silvestre *et al.* used the LbL technique to coat HKUST-1 MOFs around COOH terminated silica magnetic beads (Fig. 33d).[218] They were then able to demonstrate the use of these MFCs[32] as chromatographic materials for toluene, *p*-xylene and pyridine. The results showed that pyridine had longer retention times within the porous MOF framework due to its ability to coordinate with the Cu(II) atoms. These appear to be promising materials for chromatography.[218]

The sequestration of heavy metal contaminants is another potential application for MFCs.[286,287] Bagheri *et al.* used magnetic FCs to uptake palladium from environmental samples. Pyridine-functionalised Fe_3O_4 nanoparticles were embedded into HKUST-1 MOFs and showed remarkable recovery of palladium from both real water samples and certified samples.[286]

5.4 Molecular transport

The use of MOFs for the molecular transport in terms of molecular rotors and motors are an emerging field of research. These devices have the potential to be incorporated into many applications including actuators, sensors, targeted drug injection and osmotic pumping devices.[21,22]

Ikezoe *et al.* demonstrated an autonomous biochemical motor through the integration of MOFs and self-assembling peptides.[21] The porous MOF framework ($[Cu_2(BDC)_2ted]_n$, ted = triethylendiamine) was initially loaded with diphenylalanine
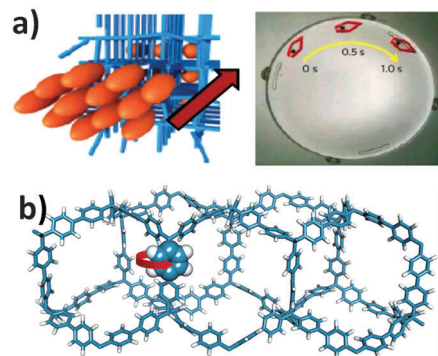

Fig. 34 (a) DPA peptides assembled within the porous MOF structure are released as the MOF decomposes and the resulting surface tension projects the MOF–peptide 'boat' around the Petri-dish, from Ikezoe *et al.*;[21] (b) schematic of the PAF structure (C-blue, H-white) with a highlighted *p*-phenylene rotor with van der Waals radii, from Gates *et al.*[2]

(DPA) peptides within its porous lattice (Fig. 34a) under incubation in 1,1,1,3,3,3-hexafluoro-2-propanol solvent. After the solvent was removed, the loaded MOFs were placed in a solution of water and sodium ethylenediaminetetraacetate (Na-EDTA). The EDTA allows the slow release of the DPA peptides due to the gradual decomposition of the MOF structure. Upon release from the MOF, the peptides re-align at the water/MOF interface which creates a large surface tension gradient around the MOF, hence propelling it through the solution (Fig. 34a).[21] These MOF–peptide composites offer the potential for using MOFs in biomimetic motors which can be studied to gain an understanding of energy transduction in biological systems.[21]

Comotti *et al.* recently reported on the potential of molecular rotors of porous aromatic frameworks (PAFs) by investigating the rotational motion of PAF's structural elements in response to guest molecules.[22] Fig. 34b shows a schematic of an ideal PAF where a *p*-phenylene rotor is represented with the van der Waals radii and the red arrow illustrates its rotary motion. This local rotational motion is detected with ^2H nuclear magnetic resonance (NMR) analysis and shows that dynamic motion is present even at low temperatures (200 K). Comotti *et al.* deduced that the rotors are each isolated within the PAF giving them freedom for fast rotation but this movement is dampened by the presence of guest molecules such as *n*-alkanes and iodine.[2] This sensitivity to guest molecules suggests that these porous materials would be ideal for sensing devices to detect the presence of pollutants or contaminants.[2] This work suggests that a similar concept might be applied into MOFs.

5.5 Electronics

The ability to prepare well defined, homogeneous MOF thin films *via* controlled methods such as LPE and LbL growth has opened up several avenues of research into electrical and electronic applications.[288–290] The ability to design MOF structures by selecting the ligands or the metal coordination complexes, means that the electronic properties of MOFs can often be tuned. This manipulation has given rise to much research into the modification of MOF band gaps[291–294] and new types of

semiconductors.[290,295] Here we focus on the use of patterned or controlled positioning of MOFs for device applications. Previous reviews have focused on the application of MOFs in electrochemical sensors[289] and investigating MOF properties as semiconductors.[290]

Dragässer et al. investigated the electrochemical properties of HKUST-1 films on Au substrates functionalised with a thiol SAM, by determining the charge transport across the insulating membrane using ferrocene as an immobilised redox mediator.[296] Tuning the electrical properties of SURMOFs using the controlled LPE technique makes them attractive materials as electrodes.[296] Huo et al. prepared ZIF-8 films on 3-aminopropyltriethoxysilane SAM coated indium tin oxide (ITO) electrodes using the LbL process, and investigated their potential use in photochemical applications.[297]

Allendorf and co-workers have recently reported the ability to tune the electrical conductivity in HKUST-1 MOF thin film devices.[16] Here, the pores within the MOFs are loaded with redox-active, conjugated guest molecules [7,7,8,8-tetracyanoquino-dodimethane (TCNQ)] (Fig. 35). The authors were able to tune the electrical conductivity over six orders of magnitude due to the TCNQ molecule providing a bridge between the dimeric Cu subunits, hence creating a conductive path through the MOF unit cell.[16]

As microelectronic chips are miniaturised, they also require insulating materials with low dielectric constants (κ) as well as relatively high elastic modulus (>3 GPa), minimal pore sizes (<5 nm) and hydrophobicity.[298,299] MOFs are emerging as possible candidates as potential low dielectric materials as the ability to control their localisation advances.[7] Eslava et al. have deposited ZIF-8 films on silicon wafers and measured the dielectric constant through impedance measurements at various temperatures and frequencies. The ZIF-8 films showed promising results with κ only 2.33 ± 0.05 at 100 kHz therefore indicating their potential for future microelectronic chips.[298]

Zhan et al. have developed MOF@semiconductor hetero-structures to demonstrate their selective photoelectrochemical response.[300] They prepared core–shell structures where ZIF-8 was grown onto ZnO nanorod arrays, which feature semi-conductive properties. The ZnO nanorods are the source of the Zn ions under hydrothermal conditions together with a solution of DMF and HmIm. The resulting metal oxide semiconducting@MOF

Fig. 35 Optical image of thin MOF film devices before and after TCNQ infiltration (above), schematic of TCNQ molecule entering a HKUST-1 MOF pore, and SEM of the MOF coating (below). Reproduced from Talin et al.[16]

core–shell heterostructures featured photochemical responses to hole scavengers small enough to enter the pores of the ZIF-8 shell. This was therefore an effective route to form a H_2O_2 sensor.[300]

5.6 Energy saving and production

Exploration of MOF properties is also occurring within the energy saving and energy production sectors. For energy saving, Janiak's group has been pioneering the fabrication of thermally driven adsorption chillers (TDCs) or adsorption heat pumps (AHPs).[26,27] These types of devices employ materials with sorbent properties (e.g. porous materials) combined with an evaporative refrigerant (e.g. water) for chilling purposes. An energy byproduct or renewable energy can potentially be used to regenerate the sorbent, in order to close the working cycle of the cooling device. These devices would be beneficial for a number of chilling applications (e.g. residential air-conditioning) which are responsible for a consistently increasing energy demand.[301] As reported by Janiak, MOFs are the most promising materials for these devices due to their superior water uptake capacity.[27,302] The ability to securely position MOFs would play a major role in the further development of this technology.

For energy production, there are different functionalities of MOFs that can be exploited for device fabrication, including hydrogen production, photovoltaics and fuel cells.[303] Gomes Silva and co-workers have been pioneering the field of hydro-gen production using UiO-66, NH_2-UiO-66, and Pt doped NH_2-UiO-66.[304] Under exposure to UV light, charge separation in the Zr–MOF systems was used for the production of hydrogen from a water–methanol mixture. A further extension to the visible light spectrum was proposed by Fateeva and co-workers using a post-functionalised Al–porphyrin MOF with Pt.[305] Horiuchi and co-workers used the linker-to-cluster charge-transfer (LCCT) mechanism for electron transfer from the photoexcited organic linker using a Pt–Ti-MOF-NH_2 system (Fig. 36a).[275] Although this research field is showing promising results, the ability to position MOFs with hydrogen production capability will help the fabrication, and potentially the commercialization of this type of green energy production device.

Another promising application in MOF technology is the fabrication of MOFs with the ability to harvest energy directly from light.[306] This is possible by tuning the energy gap of MOFs with their semiconductive properties.[292,293] Lee et al. reported the fabrication of HKUST-1 using the LbL technique, doped with iodine onto a doctor-bladed TiO_2 nanoparticle film.[307] The authors demonstrated that the electrical resistance behaviour of the system could be switched from an insulator to an electrical conductor. Remarkably, it was shown that the energy gap (HOMO–LUMO) and the positions of the iodine-doped Cu–MOFs are promising as a sensitizing layer in TiO_2-based liquid junction photovoltaic cells. In a subsequent report, Lee and co-workers demonstrated that the interfacial charge transfer resistance was significantly improved by adding multi wall carbon nanotubes (MWCNTs) into the TiO_2 particle film (Fig. 36b).[276] The improved electron transfer rate showed an enhanced photovoltaic performance.
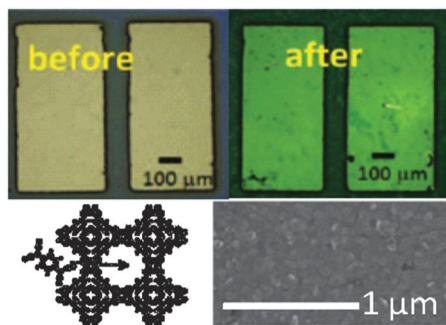
5548 | Chem. Soc. Rev., 2014, 43, 5513–5560

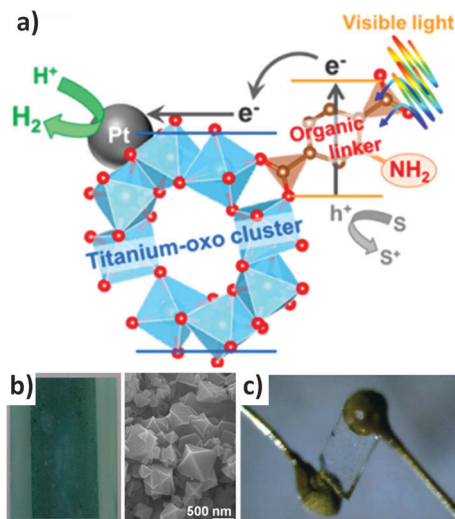This journal is © The Royal Society of Chemistry 2014

Fig. 36 (a) Schematic of the charge transfer mechanism in the photo-catalytic hydrogen production over titanium based MOF with Pt nano-particles, from Horiuchi et al.;[275] (b) composite film (left) of titania and multiwalled carbon nanotubes after sensitization with a Cu based MOF (left), from Lee et al.;[276] (c) a single crystal of a zinc based coordination framework attached to gold electrodes, from Umeyama et al.[277]

Fuel cells are an alternative technology for energy production with low carbon emissions. They are galvanic cells, in which the free energy of a chemical reaction is converted into electrical energy (*via* an electrical current).[308] Recently, MOFs have shown the capability to be used for proton conductivity,[309] which is an important functionality for fuel cell device fabrication.[277,310] MOFs can show proton conductive properties *via* the framework itself or by doping it with protonic charge carrier species (Fig. 36c). Reviews analysing in detail the different aspects related to this emerging technology have been recently published.[56,94,303,311] As highlighted by Horike et al.[56,277] MOF crystals can provide anisotropic ion conductivity (*e.g.* in a 2D layered MOF structure, the conductivity along the direction parallel to the 2-D layer is much higher than for the perpendicular direction). In this regard, mastering the crystal growth and position would help to engineer and optimise the conductive properties of MOFs.

5.7 Optics

Various engineered functional MOFs have been investigated with regards to their optical behaviour being tuned by different stimuli.[18–20,235,312] Europium and terbium based MOFs were found suitable due to the luminescent emitting properties of these two lanthanides. Indeed, mixed metal $Tb_xEu_{1−x}(BTC)(H_2O)$ frameworks exhibited tunable photoluminescence according to the different Eu doping,[313] while a thermochromic material prepared by doping a Tb based MOF with Eu was proposed as a luminescent thermometer in the range 50–200 K.[233] A thin film of an europium imidazolate framework was also prepared on sapphire to demonstrate its switchable and strong luminescence under visible and ultraviolet light exposure.[187] QDs were added into the MOFs to tune their optical response, such as in the case

of a CdSe–ZnS core shell QD combined with a Zn based MOF containing porphyrin ligands, that exploited energy transfer between QD and MOF for luminescence shift,[306] or a PEI coated carbon QD encapsulated into ZIF-8, capable of emitting blue light under UV irradiation.[314] A ZIF-8 interferometer was fabricated and used as a selective sensor for gases and vapours;[274] the relationship between the thickness of this MOF and its lumines-cent properties was subsequently proven by deposition onto an ITO substrate.[297] A white emitting LED was fabricated merging a blue emitting cadmium based MOF with a yellow emitting iridium complex,[273] and electrochromic films on FTO were prepared using Zn based MOFs with variously functionalised pyrazolate ligands, exhibiting colours from green to red to blue,[47] or with a Zr based MOF film showing a drastic and reversible blue shift.[272]

Lu and Hupp prepared a MOF-based Fabry–Perot inter-ferometer for selective gas sensing.[274] ZIF-8 was grown as thin films by cyclically immersing an etched silicon or glass slide in the precursor solutions containing zinc nitrate and HmIm, respectively (Fig. 37a). They were able to estimate the amount of deposited MOF using QCM measurements, relating the thickness with the repeated cycles. Moreover, different thick-nesses provided different colours due to the optical interference in the visible region. Thanks to the absorption feature provided by porous ZIF-8, and the resonating properties of this inter-ferometer, the authors obtained different transmission spectra upon exposing the film to various vapours. Therefore it was possible to correlate the peak shift to the concentration of various analytes, obtaining a mostly linear relationship in the case of propane, the possibility to distinguish between linear hexane and bulky cyclohexane, and eventually to detect the presence of ethanol in water as low as 0.3% v/v, corresponding to an ethanol concentration of 100 ppm.

Sun et al. built an efficient MOF-based white emitting LED with high quantum yield.[273] A cadmium based framework with a blue emitting hexadentate ligand [H_6TATPT = 2,4,6-tris-(2,5-dicarboxylphenylamino)-1,3,5-triazine] was produced on the

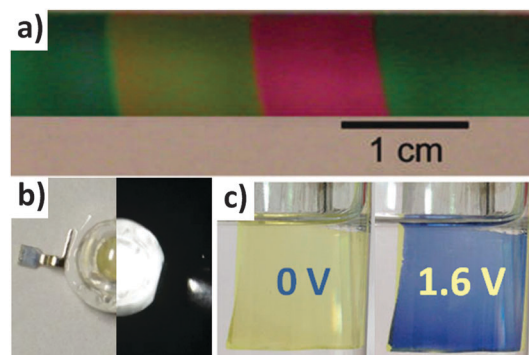**Fig. 37** (a) A series of ZIF-8 films of different thickness on a silicon substrate, from ref. 274; (b) photograph of a white LED fabricated using a cadmium based MOF loaded with an iridium base complex without (left) and with a 150 mA current applied (right), from ref. 273; (c) photos of the electrochromism of a zirconium based MOF thin film on FTO electrode before (left) and after (right) applying a 1.6 V potential, from ref. 272.

basis that d^{10} Cd^{II} metal centres exhibit highly photoactive capability when bound to functional ligands. In this case, the authors initially prepared the ligand reacting H_2aBDC and cyanuric chloride. Subsequently, a yellow emitting Ir^{III} complex was loaded into the cavities of the framework. With a loading of 3.5 wt% the resultant LED emitter generated bright white light upon excitation at 370 nm with a considerable quantum yield of 20.4% (Fig. 37b). This value was obtained because of the optimal separation provided by the MOF cavities of the encapsulated iridium complex, thus preventing its aggregation. Furthermore, exchange between dimethylammonium ions and Eu^{III} or Tb^{III} allowed a colour change emission from pink (due to europium) to green (due to terbium).

Kung et al. prepared an reversible electrochromic device based on a zirconium framework thin film.[272] Using FTO as the substrate, NU-901 ($Zr_6O_6(OH)_4(TBAPy)_3$) MOF was grown after a preliminary soaking in the tetradentate pyrene based ligand [H_4TBAPy = 1,3,6,8-tetrakis(4-carboxyphenyl)pyrene] and subsequent growth in a temperature gradient oven in the presence of more ligand and zirconium chloride. The transparent yellow coloured thin film with a uniform thickness of 1 μm was integrated in an electrochemical cell. Upon cyclic voltammetry analysis, a +1.6 V anodic peak was attributed to the redox response from the pyrene ligand, as the zirconium centres were found unresponsive. Under different applied potentials, UV-vis spectra showed a large absorbance increase centered at 587 nm, along with a decrease at 405 nm. This spectroscopic change was manifested with an evident colour switch from yellow to blue, that was also shown to be reversible during a 10-cycle test (Fig. 37c). The electrochromism was facilitated by the MOF porosity and its particular morphology, indeed Raman spectroscopy and electron paramagnetic resonance investigations demonstrated that a one-electron oxidation of the pyrene ligands was facilitated thanks to the spatial separation provided by the framework architecture, preventing the pyrene dimerization.

5.8 Bioreactors

Recently, the high-sensitivity of MOFs towards molecular sieving has been realized for biomedical applications. Proteins, enzymes, and DNA can be sensitive to their local environment and often resulting in the loss of their functionality. The utilization of MOFs for hosting biomolecules is promising because the porous crystal might offer protection and adds more functionalities towards the design of next generation bioreactor and biosensing devices.

Cell growth. Although rare, MOF-based devices have been employed for spatiotemporal cell stimulation and growth. Photoactive MOFs were synthesized using 2-nitroimidazole as ligands. The MOFs were embedded in a biocompatible matrix. Upon activation by a localised two-photon laser, the nitro-containing ligand within the MOFs underwent photo-induced nitro-to-nitrite rearrangement and subsequent bond cleavage to yield NO radicals. Through the movement of the focal point of the laser, precise control of the NO delivery was achieved. The biological relevance of the exogenous NO produced by this strategy is evident by an intracellular change in cellular
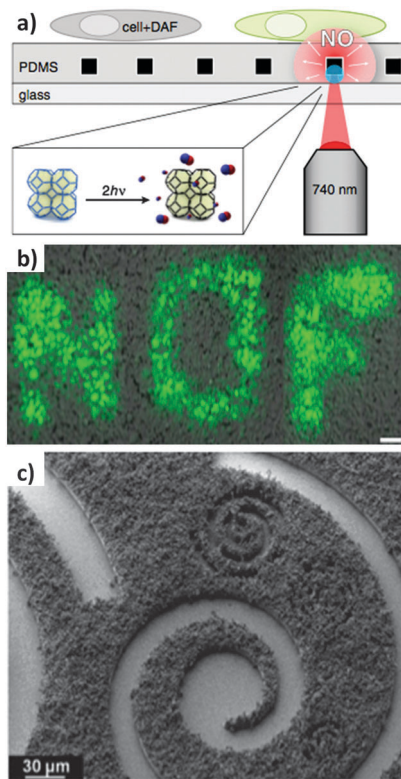

Fig. 38 (a) Schematic of the platform used for the localized cell stimulation mediated by the NO release from MOF, and the demonstration of spatial control, scale bar is 100 μm (b), from Diring et al.;[57] (c) aluminium based MOF patterned on SU-8 photoresist and grafted with an enzyme, from Doherty et al.[24]

calcium concentration, mediated by nitric oxide-responsive plasma membrane channel proteins (Fig. 38a and b).[57]

Hosting biomolecules. The employment of MOFs as a platform support for biomolecules has proven to be an effective strategy compared to their counterpart such as mesoporous silica.[315–317] Importantly, MOFs can serve not only as a support for biomolecules, but also as a functional component. Fluorescent dye-labelled hairpin-shaped oligonucleotides could be adsorbed on a 2D MOF support via interactions between DNA bases and the conjugated π-electron rich MOFs, leading to the quenching of the dye by MOFs. In the presence of the complementary DNA target, the dye-labelled oligonucleotides hybridize with the target DNA, causing the release from the MOF, leading to fluorescence recovery.[318] This DNA sensor has proved to be sensitive toward target DNA as low as in the sub-nM range. Although the synergy between MOFs and biomolecules have shown exciting advances, the potential is still largely unexplored.

Spatiotemporal control of MOF fabrication has been realized for designing advanced 3D MOF architectures such as hollow capsules that have found potential in bioreactors or loading of biomolecules.[152] Such capsules were synthesized by interfacial formation of a continuous MOF layer using a biphasic synthesis mixture consisting of an aqueous metal-ion-containing droplet in an organic ligand solution. Selective permeability of these capsules was directly related to the micropore size of the MOF

5550 | Chem. Soc. Rev., 2014, 43, 5513–5560

This journal is © The Royal Society of Chemistry 2014

crystallites forming the capsule walls. Moreover, with the ability to tune the structures and porosities of various MOFs, better interactions and higher drug loadings could be achieved. These devices are well suited for selectively hosting and release of biomolecules for biomedical applications.[319]

Surface bio-functionalisation. Using UV lithography, MOFs could be confined to precise locations for the fabrication of the next generation devices (Fig. 38c).[24] Biografting of biomolecules such as enzymes onto these patterns showed remarkable efficiency, which has moved a step towards the design of biomedical miniaturised devices.

5.9 Catalysis

Several applications have been proposed for MOF-based catalysis. A porphyrin based MOF with zinc metal centre was proposed as catalyst for the acyl transfer reaction.[320] HKUST-1 was embedded into silica monoliths for a continuous flow Friedländer reaction for the synthesis of substituted quinolines.[179] The same MOF was grown from a copper substrate and its performance was tested.[172] A $Zn_3(BTC)_2$ MOF thin film grown on zinc plate was evaluated for the photodegradation of a MB dye.[48] MFCs have been evaluated for condensation reactions using Fe_3O_4@DUT-4 in batch[204] or Fe_3O_4@ZIF-8 in a microfluidic device.[150] Copper based MOFs with dicarboxylic or bispyridyl ligands were similarly grown on carboxylic or amine terminated Fe_3O_4 particles and used as well for different oxidation or condensation reactions.[217,223] A complex MOF-based device on a UiO framework structure was prepared with Ir, Re and Ru complexes in the framework, and its versatility as a photocatalyst was pointed towards water oxidation, CO_2 reduction and organic reactions like aza-Henry, amine coupling, and thiol oxidation.[232] A similar MOF containing Ir based complexes as the ligand and Pt nanoparticles produced *in situ* under UV light, demonstrated the possibility to induce hydrogen evolution in photocatalytic conditions.[242] Asymmetric synthesis of enantiomerically enriched secondary alcohol was achieved using IRMOFs prepared with chiral ligands.[321]

Sachse *et al.*[179] were the first to prepare a MOF catalyst for a continuous flow reaction. Thanks to the coordinatively unsaturated copper metal centres, HKUST-1 was regarded as a suitable catalyst for the Lewis acid reaction. Firstly, they prepared a macro/mesoporous silica monolith by hydrolysis of tetraethyl orthosilicate (TEOS) in the presence of polyethyleneoxide polymer, growing the monolith onto a PVC tube. After drying and calcination, HKUST-1 was synthesized *in situ* by immersing the highly porous support in the HKUST-1 precursor solution, evaluating the catalyst content using a thermogravimetric approach and obtaining a 25% loading. The monolith was inserted into a heat-shrinkable tube and used for the continuous flow synthesis of a substituted quinoline *via* the Friedländer reaction, obtaining a steady 85% conversion after 4 h flow, a calculated yield of 826 g of product per g of catalyst per day, and demonstrating that the immobilized HKUST-1 was 2.5 times more productive than a commercial HKUST-1 powder, thanks to the higher efficiency of the nanosized MOF crystal in the monolith.

Okada *et al.*[271] produced patternable HKUST-1 films on a photolithographed copper plate. The HKUST-1 growth from the copper plate was achieved using a two-step protocol: at first, $Cu(OH)_2$ nanotubes were obtained on the copper substrate using a basic oxidation approach with ammonium persulphate,[175] they were then converted into HKUST-1 crystals adding an ethanolic aqueous solution of the tridentate ligand H_3BTC.[174] The HKUST-1 immobilized catalyst was proven mechanically resistant to sonication, and used for the Friedländer reaction obtaining an 80% conversion after 16 hours. Moreover, it was possible to grow this type of MOF on several substrates, flat plates, meshes, microsized grids, and PCB boards. Patterns were also prepared *via* a photolithographic approach using sunlight (Fig. 39a).

Faustini *et al.*[150] prepared a MFC and immobilized it into a flow reactor thanks to an external magnetic field. A two-step protocol was entirely performed using a microfluidic system generating confined microdroplet reactors using a water–oil fed T-junction, to obtain the core–shell Fe_3O_4@ZIF-8 composite. Initially iron oxide microspheres were prepared from iron chloride in ethylene glycol at 80 °C. The as-obtained magnetic particles were therefore injected into a second droplet generator, where a methanolic solution of zinc nitrate and HmIm in the presence of PSS was flowing. This polymer was found suitable for the efficient growth of MOF onto iron oxide nanoparticles because its anionic nature enhances the accumulation of zinc cations on the particles.[216] The magnetic ZIF composite was immobilized on the inside wall of a capillary microreactor by applying a magnetic field, and a Knoevenagel condensation between benzaldehyde and ethyl cyanoacetate was performed in continuous flow (Fig. 39b). Compared to the batch synthesis, the flow reaction efficiency was drastically improved from a 49% conversion after 50 minutes of reaction under mechanical stirring to a 99% conversion after 35 minutes of residence time in capillary, thanks to the fast mass transfer and efficient mixing between the heterogeneous catalyst and reagent in the microreactor.

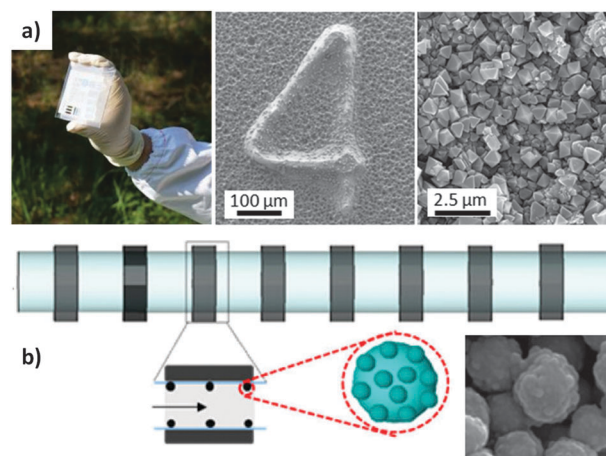Fig. 39 (a) Sunlight driven photolithography of a Cu plated plastic board for the subsequent HKUST-1 film growth (insets), from Okada *et al.*;[172] (b) schematic of the microfluidic device used for the flow reaction using Fe_3O_4@ZIF-8 magnetic framework composite (inset), from Faustini *et al.*[216]

This journal is © The Royal Society of Chemistry 2014

Chem. Soc. Rev., 2014, 43, 5513–5560 | 5551

6. Outlook and future requirements for MOF-based devices

From a thorough investigation of the various protocols reported in the literature, several aspects need to be improved in order to facilitate the fabrication and commercialization of effective MOF-based devices. In particular, we identified key aspects which represent technological gaps that should be filled. These are related to both fundamental and engineering challenges.

Crystal engineering

The ability to fully control MOF crystallisation processes is crucial to enable full access to their properties. In particular:

• Improved control over the location of crystal formation in order to have MOFs with functional properties only in selected regions resulting from bottom-up approaches.

• Mastering the crystal orientation (in plane and out of plane ordering and crystal density) is crucial to take full advantage of the anisotropic properties of the porous MOF crystals.

• Control over particle size distribution, particle morphology and form factor is important for achieving uniform and high resolution patterns, when pre-prepared MOFs are used for device fabrication. This is very important for top-down microfabrication techniques and dynamic localisation methods with MOFs.

• Optimization of the growing conditions of MOFs for hosting biomolecules. Although a few biomolecules such as anti-cancer drugs and sensing/fluorescent molecules have been successfully incorporated within MOFs, to encapsulate fragile biomolecules such as proteins and DNA that are sensitive to MOF growth conditions (e.g. organic solvent, high salt concentrations, low/high pH, high temperatures) still remains challenging.

• A deeper understanding of evaporative processes driving the self assembly of MOF-based materials should be sought. This would improve the versatility, crystal orientation, homogeneity and crystal density of MOFs for the fabrication of patterns where EISA is used. Important processes that would benefit from progress in this area include dip coating deposition, seeding, μCP, spray coating and ink-jet printing.

Micro-fabrication and control tools

Ready access to materials and tools suitable for device fabrication is a major requirement for the commercialisation of MOF-based devices.

• Access to new lithographic or positioning approaches for the fast, cheap and versatile micro-fabrication of MOFs is necessary for rapid progress in the field.

• Exploring continuous processes, rather than discontinuous ones, for industrial fabrication; the advantages of such protocols have been proposed, but further investigation is needed for a better understanding of the potential.

• MOFs that can be selectively etched would advance top-down fabrication methods. Different steps are involved in many lithographic protocols, and having access to MOFs capable of resisting certain type of solvents while dissolving in others would help photolithographic approaches. A key fabrication challenge is to logistically incorporate multiple MOF structures

of various chemistries and functionalities into one platform. This would expand the potential field of MOF-based applications.

• Using magnets with controllable features (e.g. miniaturised static or electro-magnets) would allow for precise and accurate positioning in the micrometer range for MFCs. Alternatively, incorporating them into microfluidic circuits would allow for MOF growth into integrated multifunctional platforms.

• Design of MOFs with specific stimuli-responsive properties for potential drug delivery applications. The utilization of either external triggers such as light, temperature and magnetic forces, or biological/cellular triggers such as pH, redox, and enzyme variations for MOF-based smart drug delivery devices should be achieved.

Compatibility, robustness, stability and aging

• Identification of robust MOF-based materials that can withstand a wide range of physical, chemical, and biological conditions (pH, aggressive treatments, antibodies, etc.).

• Investigation of the mechanical stability of patterned MOFs; ideally the pattern should be stable under mechanical stimuli and only a few reports have addressed this challenge in order to ensure that MOFs are firmly anchored on a substrate.

• Aging of MOFs should be optimised. Maintaining the integrity of MOFs, avoiding loss of functional properties and contamination due to decomposition of MOF components must be improved. This would allow for extended shelf-life of MOF-based devices.

• Two main aspects should be better investigated: the biocompatibility of framework based materials for in vivo applications, such as thermally triggered drug release possibly coupled with fluorescent labels; and the environmental compatibility, with regards to the synthetic techniques, which involves the elimination of hazardous solvents and ions, in order to fulfil green chemistry requirements.

Integrating MOFs with other functional materials

The integration of MOFs with other functional materials is an emerging research field. A better understanding of compatible processes using functionalised surfaces (e.g. SAMs) or the transformation from inorganic buffer layers (e.g. ceramics) would be of help for controlling the position of nanoparticles and making composites with new properties. Additionally, mixed membrane MOFs hold much promise and combining them with the ability to position the final composites would offer new improved functionalities for a number of important fields including separation and sequestration.

7. Conclusions

Over the last 15 years research on MOFs has demonstrated that these exceptional materials have great potential for different technological applications ranging from biomedics to opto-electronics. As with most functional materials, protocols for positioning them are a prerequisite for device fabrication. In particular the ability to integrate them with other functional

materials in a miniaturised fashion will help to make portable multifunctional platforms. In this review the protocols for MOF-based device production have been presented and their advantages and limitations are critically discussed. Examples of proof-of-concept devices have been highlighted as well as the gaps in MOF-based device miniaturisation. This on-going research requires joint effort from different areas of expertise, including chemistry, engineering, electronics, energy production, sensing and biology in order to successfully proceed on the path to the fabrication of commercially viable MOF-based devices.

Table 4 List of acronyms, minimum formulas and ligands abbreviations used in this article[a]

Abbreviation	Meaning
Acronyms used in the text	
μCP	Microcontact printing
CD	Cyclodextrin
DBT	Dibenzothiophene
DEF	Diethylformamide
DMF	Dimethylformamide
DMSO	Dimethylsulfoxide
DRM	Desert rose microparticle
EDTA	Ethylendiaminetetraacetic acid
EISA	Evaporation induced self assembly
FITC	Fluorescein isothiocyanate
FTO	Fluorine doped tin oxide
LB	Langmuir–Blodgett
LbL	Layer-by-layer
LPE	Liquid epitaxial growth
MFC	Magnetic framework composite
MIMIC	Micromolding in capillary
MOF	Metal organic framework
PAF	Porous aromatic framework
PAH	Polycyclic aromatic hydrocarbon
PCP	Porous coordination polymer
PDMS	Polydimethylsiloxane
PEEK	Polyether ether ketone
PEI	Polyethyleneimine
PhTES	Phenyl triethoxysilane
PSS	Polystyrene sulfonate
PVP	Polyvinylpyrrolidone
QCM	Quartz crystal microbalance
QD	Quantum dot
SAM	Self assembled monolayer
SBU	Secondary building unit
SPR	Surface plasmon resonance
SURMOF	SURface anchored metal organic framework
TCNQ	Tetracyanoquinodimethane
VOC	Volatile organic compound
ZIF	Zeolitic imidazolate framework
IRMOF	Isoreticular metal organic framework
Ligands names	
bix	1,4-Bis(1-imidazolyl)benzene
bpy	4,4′-Bispyridyl
dabco	1,4-Diazabicyclo[2.2.2]octane
H_2aBDC	2-Aminoterephthalic acid (2-amino-1,4-benzenedicarboxylic acid)
H_2ADA	4,4′-Azobenzenedicarboxylic acid
H_3atb	Aniline-2,4,6-tribenzoic acid
H_2BDC	Terephthalic acid (1,4-benzenedicarboxylic acid)
H_2bpdc	Biphenyl-4,4′-carboxylic acid
H_4bptc	1,1′-Biphenyl-2,2′,6,6′-tetracarboxylic acid
H_2bpydc	2,2′-Bipyridyl-5,5′-dicarboxylic acid
H_3btb	1,3,5-Tris(4-carboxyphenyl)benzene
H_3BTC	1,3,5-Benzenetricarboxylic acid
H_2dhBDC	2,5-Dihydroxy-1,4-benzenedicarboxylic acid
H_2dmBDC	2,5-Dimethoxy-1,4-benzenedicarboxylic acid

Table 4 (continued)

Abbreviation	Meaning
H_2ndc	1,4-Naphthalenedicarboxylic acid
H_2NDC	2,6-Naphthalenedicarboxylic acid
H_3ntb	4,4′,4″-Nitrilotrisbenzoic acid
H_6TATPT	2,4,6-Tris(2,5-dicarboxylphenylamino)-1,3,5-triazine
H_4TBAPy	1,3,6,8-Tetrakis(4-carboxyphenyl)pyrene
H_4TCPB	1,2,4,5-Tetrakis(4-carboxyphenyl)benzene
H_4TCPP	5,10,15,20-Tetrakis(4-carboxyphenyl)porphyrin
HIm	Imidazole
HmIm	2-Methylimidazole
HbIm	Benzimidazole
HnIm	2-Nitroimidazole
DUT-4	$Al(OH)(NDC)$
DUT-5	$Al(OH)(bpdc)$
HKUST-1	$Cu_3(BTC)_2$
IRMOF-3	$Zn_4O(aBDC)_3$
MIL-53(Al)	$Al(OH)(BDC)$
MIL-53(Fe)	$Fe(OH)(BDC)$
MIL-96(Al)	$Al_{12}O(OH)_{18}(Al_2(OH)_4)(BTC)_6$
MIL-100(Al)	$Al_3O(OH)(BTC)_2$
MIL-100(Cr)	$Cr_3OF(BTC)_2$
MIL-100(Fe)	$Fe_3O(OH)(BTC)_2$
MIL-101(Cr)	$Cr_3OF(BDC)_3$
NH_2-MIL-53(Al)	$Al(OH)(aBDC)$
NH_2-MIL-88B(Fe)	$Fe_3OCl(aBDC)_3$
NH_2-MIL-125(Ti)	$Ti_8O_8(OH)_4(aBDC)_6$
MOF-2	$Zn_2(bdc)_2$
MOF-5/IRMOF-1	$Zn_4O(BDC)_3$
MOF-74(Ni)	$Ni_3[O_3(BDC)_{1.5}]$
MOF-177	$Zn_4O(btb)_2$
MOF-508	$[Zn_2(BDC)_2(bpy)]$
NU-901	$Zr_6O_4(OH)_4(TBAPy)_3$
SNU-90	$[Zn_4O(atb)_2]$
UiO-66	$Zr_6O_4(OH)_4(BDC)_6$
UiO-67	$Zr_6O_4(OH)_4(bpdc)_6$
NH_2-UiO-66	$Zr_6O_4(OH)_4(aBDC)_6$
ZIF-7	$Zn(bIm)_2$
ZIF-8	$Zn(mIm)_2$
ZIF-9	$Co(bIm)_2$
ZIF-67	$Co(Im)_2$
ZIF-69	$Zn(nIm)_2$

[a] Framework sum formulas (water and solvent molecules omitted for simplicity).

Acknowledgements

References

1 T. Betancourt and L. Brannon-Peppas, *Int. J. Nanomed.*, 2006, **1**, 483–495.

2 B. D. Gates, Q. Xu, M. Stewart, D. Ryan, C. G. Willson and G. M. Whitesides, *Chem. Rev.*, 2005, **105**, 1171–1196.

3 D. Qin, Y. Xia, J. A. Rogers, R. J. Jackman, X.-M. Zhao and G. M. Whitesides, in *Microsystem Technology in Chemistry and Life Science*, ed. A. Manz and H. Becker, Springer, Berlin, Heidelberg, vol. 194, pp. 1–20.

4 S. Fransilla, *Introduction to Microfabrication*, John Wiley & Sons, Ltd, Chichester, UK, 2nd edn, 2010, pp. 1–13.

5 B. Ziaie, A. Baldi and M. Z. Atashbar, in *Springer Handbook of Nanotechnology*, ed. P. B. Bhushan, Springer, Berlin, Heidelberg, 2010, pp. 231–269.

6 M. E. Davis, *Nature*, 2002, **417**, 813–821.

7 P. Falcaro, D. Buso, A. J. Hill and C. M. Doherty, *Adv. Mater.*, 2012, **24**, 3153–3168.

8 S. L. James, *Chem. Soc. Rev.*, 2003, **32**, 276–288.

9 S.-I. Noro and S. Kitagawa, in *The Supramolecular Chemistry of Organic-Inorganic Hybrid Materials*, ed. K. Rurack and R. Martínez-Máñez, John Wiley & Sons, Inc., 2010, pp. 235–269.

10 H. Furukawa, K. E. Cordova, M. O'Keeffe and O. M. Yaghi, *Science*, 2013, **341**, 1230444.

11 K. Sumida, D. L. Rogow, J. A. Mason, T. M. McDonald, E. D. Bloch, Z. R. Herm, T.-H. Bae and J. R. Long, *Chem. Rev.*, 2012, **112**, 724–781.

12 M. P. Suh, H. J. Park, T. K. Prasad and D.-W. Lim, *Chem. Rev.*, 2012, **112**, 782–835.

13 J.-R. Li, J. Sculley and H.-C. Zhou, *Chem. Rev.*, 2012, **112**, 869–932.

14 M. Yoon, R. Srirambalaji and K. Kim, *Chem. Rev.*, 2012, **112**, 1196–1231.

15 L. E. Kreno, K. Leong, O. K. Farha, M. Allendorf, R. P. Van Duyne and J. T. Hupp, *Chem. Rev.*, 2012, **112**, 1105–1125.

16 A. A. Talin, A. Centrone, A. C. Ford, M. E. Foster, V. Stavila, P. Haney, R. A. Kinney, V. Szalai, F. E. Gabaly, H. P. Yoon, F. Léonard and M. D. Allendorf, *Science*, 2014, **343**, 66–69.

17 S. Bureekaew, S. Horike, M. Higuchi, M. Mizuno, T. Kawamura, D. Tanaka, N. Yanai and S. Kitagawa, *Nat. Mater.*, 2009, **8**, 831–836.

18 Y. Cui, Y. Yue, G. Qian and B. Chen, *Chem. Rev.*, 2012, **112**, 1126–1162.

19 Y. Cui, B. Chen and G. Qian, *Coord. Chem. Rev.*, 2013, DOI: 10.1016/j.ccr.2013.10.023.

20 Y. Cui, B. Chen and G. Qian, *Luminescent Properties and Applications of Metal-Organic Frameworks*, Springer, Berlin, Heidelberg, 2013, pp. 1–62.

21 Y. Ikezoe, G. Washino, T. Uemura, S. Kitagawa and H. Matsui, *Nat. Mater.*, 2012, **11**, 1081–1085.

22 A. Comotti, S. Bracco, T. Ben, S. Qiu and P. Sozzani, *Angew. Chem., Int. Ed.*, 2014, DOI: 10.1002/ange.20139362.

23 C. M. Doherty, E. Knystautas, D. Buso, L. Villanova, K. Konstas, A. J. Hill, M. Takahashi and P. Falcaro, *J. Mater. Chem.*, 2012, **22**, 11470–11474.

24 C. M. Doherty, G. Grenci, R. Riccò, J. I. Mardel, J. Reboul, S. Furukawa, S. Kitagawa, A. J. Hill and P. Falcaro, *Adv. Mater.*, 2013, **25**, 4701–4705.

25 S.-H. Huo and X.-P. Yan, *Analyst*, 2012, **137**, 3445–3451.

26 S. K. Henninger, F. Jeremias, H. Kummer and C. Janiak, *Eur. J. Inorg. Chem.*, 2012, 2625–2634.

27 C. Janiak and S. K. Henninger, *Chimia*, 2013, **67**, 419–424.

28 P. Horcajada, R. Gref, T. Baati, P. K. Allan, G. Maurin, P. Couvreur, G. Férey, R. E. Morris and C. Serre, *Chem. Rev.*, 2012, **112**, 1232–1268.

29 S. Keskin and S. Kızılel, *Ind. Eng. Chem. Res.*, 2011, **50**, 1799–1812.

30 J. Aizenberg, A. J. Black and G. M. Whitesides, *Nature*, 1999, **398**, 495–498.

31 D. Zacher, R. Schmid, C. Wöll and R. A. Fischer, *Angew. Chem., Int. Ed.*, 2011, **50**, 176–199.

32 R. Ricco, L. Malfatti, M. Takahashi, A. J. Hill and P. Falcaro, *J. Mater. Chem. A*, 2013, **1**, 13033–13045.

33 A. Carné, C. Carbonell, I. Imaz and D. Maspoch, *Chem. Soc. Rev.*, 2010, **40**, 291–305.

34 M. D. Allendorf, A. Schwartzberg, V. Stavila and A. A. Talin, *Chem. – Eur. J.*, 2011, **17**, 11372–11388.

35 ISI Web of Science, research performed during April 2014 using the following key words: Metal Organic Framework (orange), Metal Organic Framework AND (Device OR Pattern OR Positioning OR Fabrication) (blue).

36 S. Hermes, F. Schröder, R. Chelmowski, C. Wöll and R. A. Fischer, *J. Am. Chem. Soc.*, 2005, **127**, 13744–13745.

37 G. Lu, O. K. Farha, W. Zhang, F. Huo and J. T. Hupp, *Adv. Mater.*, 2012, **24**, 3970–3974.

38 A. Bétard and R. A. Fischer, *Chem. Rev.*, 2012, **112**, 1055–1083.

39 O. Shekhah, J. Liu, R. A. Fischer and C. Wöll, *Chem. Soc. Rev.*, 2011, **40**, 1081–1106.

40 O. Shekhah, H. Wang, S. Kowarik, F. Schreiber, M. Paulus, M. Tolan, C. Sternemann, F. Evers, D. Zacher, R. A. Fischer and C. Wöll, *J. Am. Chem. Soc.*, 2007, **129**, 15118–15119.

41 P. Horcajada, C. Serre, D. Grosso, C. Boissière, S. Perruchas, C. Sanchez and G. Férey, *Adv. Mater.*, 2009, **21**, 1931–1935.

42 R. Makiura, S. Motoyama, Y. Umemura, H. Yamanaka, O. Sakata and H. Kitagawa, *Nat. Mater.*, 2010, **9**, 565–571.

43 J. Gascon, S. Aguado and F. Kapteijn, *Microporous Mesoporous Mater.*, 2008, **113**, 132–138.

44 R. Ameloot, L. Stappers, J. Fransaer, L. Alaerts, B. F. Sels and D. E. De Vos, *Chem. Mater.*, 2009, **21**, 2580–2582.

45 M. Li and M. Dincă, *J. Am. Chem. Soc.*, 2011, **133**, 12926–12929.

46 M. Li and M. Dincă, *Chem. Sci.*, 2014, **5**, 107–111.

47 C. R. Wade, M. Li and M. Dincă, *Angew. Chem., Int. Ed.*, 2013, **52**, 13377–13381.

48 Z.-Q. Li, M. Zhang, B. Liu, C.-Y. Guo and M. Zhou, *Inorg. Chem. Commun.*, 2013, **36**, 241–244.

49 A. Schoedel, C. Scherb and T. Bein, *Angew. Chem., Int. Ed.*, 2010, **49**, 7225–7228.

50 M. C. So, S. Jin, H.-J. Son, G. P. Wiederrecht, O. K. Farha and J. T. Hupp, *J. Am. Chem. Soc.*, 2013, **135**, 15698–15701.

51 D. Zacher, O. Shekhah, C. Wöll and R. A. Fischer, *Chem. Soc. Rev.*, 2009, **38**, 1418–1429.

52 D. Zacher, A. Baunemann, S. Hermes and R. A. Fischer, *J. Mater. Chem.*, 2007, **17**, 2785–2792.

53 C. M. Doherty, D. Buso, A. J. Hill, S. Furukawa, S. Kitagawa and P. Falcaro, *Acc. Chem. Res.*, 2014, **47**, 396–405.

54 S. S. Nagarkar, B. Joarder, A. K. Chaudhari, S. Mukherjee and S. K. Ghosh, *Angew. Chem., Int. Ed.*, 2013, **52**, 2881–2885.

5554 | *Chem. Soc. Rev.*, 2014, **43**, 5513–5560

This journal is © The Royal Society of Chemistry 2014

55 M. Tsotsalas, P. Hejcik, K. Sumida, Z. Kalay, S. Furukawa and S. Kitagawa, *J. Am. Chem. Soc.*, 2013, **135**, 4608–4611.

56 S. Horike, D. Umeyama and S. Kitagawa, *Acc. Chem. Res.*, 2013, **46**, 2376–2384.

57 S. Diring, D. O. Wang, C. Kim, M. Kondo, Y. Chen, S. Kitagawa, K. Kamei and S. Furukawa, *Nat. Commun.*, 2013, **4**, 2684.

58 S. K. Ghosh and S. Kitagawa, in *Metal-Organic Frameworks*, ed. L. R. Mac Gillivray, John Wiley & Sons, Inc., 2010, pp. 165–192.

59 P. Innocenzi, L. Malfatti and P. Falcaro, *Water droplets to nanotechnology: a journey through self-assembly*, Royal Society of Chemistry, Cambridge, 2013.

60 B. A. Grzybowski, C. E. Wilmer, J. Kim, K. P. Browne and K. J. M. Bishop, *Soft Matter*, 2009, **5**, 1110–1128.

61 S. Zhang, *Nat. Biotechnol.*, 2003, **21**, 1171–1178.

62 M. Boncheva and G. M. Whitesides, *MRS Bull.*, 2005, **30**, 736–742.

63 S. Hermes, D. Zacher, A. Baunemann, C. Wöll and R. A. Fischer, *Chem. Mater.*, 2007, **19**, 2168–2173.

64 K. Szelagowska-Kunstman, P. Cyganik, M. Goryl, D. Zacher, Z. Puterova, R. A. Fischer and M. Szymonski, *J. Am. Chem. Soc.*, 2008, **130**, 14446–14447.

65 E. Biemmi, C. Scherb and T. Bein, *J. Am. Chem. Soc.*, 2007, **129**, 8054–8055.

66 C. Scherb, A. Schödel and T. Bein, *Angew. Chem., Int. Ed.*, 2008, **47**, 5777–5779.

67 F. Hinterholzinger, C. Scherb, T. Ahnfeldt, N. Stock and T. Bein, *Phys. Chem. Chem. Phys.*, 2010, **12**, 4515–4520.

68 S. Cobo, G. Molnár, J. A. Real and A. Bousseksou, *Angew. Chem., Int. Ed.*, 2006, **45**, 5786–5789.

69 G. Molnár, S. Cobo, J. A. Real, F. Carcenac, E. Daran, C. Vieu and A. Bousseksou, *Adv. Mater.*, 2007, **19**, 2163–2167.

70 O. Shekhah, H. Wang, T. Strunskus, P. Cyganik, D. Zacher, R. Fischer and C. Wöll, *Langmuir*, 2007, **23**, 7440–7442.

71 D. Zacher, K. Yusenko, A. Bétard, S. Henke, M. Molon, T. Ladnorg, O. Shekhah, B. Schüpbach, T. de los Arcos, M. Krasnopolski, M. Meilikhov, J. Winter, A. Terfort, C. Wöll and R. A. Fischer, *Chem. – Eur. J.*, 2011, **17**, 1448–1455.

72 O. Shekhah, H. Wang, M. Paradinas, C. Ocal, B. Schüpbach, A. Terfort, D. Zacher, R. A. Fischer and C. Wöll, *Nat. Mater.*, 2009, **8**, 481–484.

73 O. Shekhah, H. Wang, D. Zacher, R. A. Fischer and C. Wöll, *Angew. Chem., Int. Ed.*, 2009, **48**, 5038–5041.

74 C. Munuera, O. Shekhah, H. Wang, C. Wöll and C. Ocal, *Phys. Chem. Chem. Phys.*, 2008, **10**, 7257.

75 J.-L. Zhuang, D. Ceglarek, S. Pethuraj and A. Terfort, *Adv. Funct. Mater.*, 2011, **21**, 1442–1447.

76 J.-L. Zhuang, K. Lommel, D. Ceglarek, I. Andrusenko, U. Kolb, S. Maracke, U. Sazama, M. Fröba and A. Terfort, *Chem. Mater.*, 2011, **23**, 5366–5374.

77 S. Li, W. Shi, G. Lu, S. Li, S. C. J. Loo and F. Huo, *Adv. Mater.*, 2012, **24**, 5954–5958.

78 T. Ladnorg, A. Welle, S. Heißler, C. Wöll and H. Gliemann, *Beilstein J. Nanotechnol.*, 2013, **4**, 638–648.

79 C. Dimitrakakis, C. D. Easton, B. W. Muir, B. P. Ladewig and M. R. Hill, *Cryst. Growth Des.*, 2013, **13**, 4411–4417.

80 K. Kida, K. Fujita, T. Shimada, S. Tanaka and Y. Miyake, *Dalton Trans.*, 2013, **42**, 11128–11135.

81 O. Shekhah, *Materials*, 2010, **3**, 1302–1315.

82 J. Liu, B. Lukose, O. Shekhah, H. K. Arslan, P. Weidler, H. Gliemann, S. Bräse, S. Grosjean, A. Godt, X. Feng, K. Müllen, I.-B. Magdau, T. Heine and C. Wöll, *Sci. Rep.*, 2012, **2**, 921.

83 H. K. Arslan, O. Shekhah, D. C. F. Wieland, M. Paulus, C. Sternemann, M. A. Schroer, S. Tiemeyer, M. Tolan, R. A. Fischer and C. Wöll, *J. Am. Chem. Soc.*, 2011, **133**, 8158–8161.

84 B. Liu, M. Ma, D. Zacher, A. Bétard, K. Yusenko, N. Metzler-Nolte, C. Wöll and R. A. Fischer, *J. Am. Chem. Soc.*, 2011, **133**, 1734–1737.

85 C. Scherb, J. J. Williams, F. Hinterholzinger, S. Bauer, N. Stock and T. Bein, *J. Mater. Chem.*, 2011, **21**, 14849–14856.

86 O. Shekhah, H. K. Arslan, K. Chen, M. Schmittel, R. Maul, W. Wenzel and C. Wöll, *Chem. Commun.*, 2011, **47**, 11210–11212.

87 K. Yusenko, M. Meilikhov, D. Zacher, F. Wieland, C. Sternemann, X. Stammer, T. Ladnorg, C. Wöll and R. A. Fischer, *CrystEngComm*, 2010, **12**, 2086–2090.

88 R. Makiura and O. Konovalov, *Dalton Trans.*, 2013, **42**, 15931–15936.

89 S. Motoyama, R. Makiura, O. Sakata and H. Kitagawa, *J. Am. Chem. Soc.*, 2011, **133**, 5640–5643.

90 M. Tsotsalas, A. Umemura, F. Kim, Y. Sakata, J. Reboul, S. Kitagawa and S. Furukawa, *J. Mater. Chem.*, 2012, **22**, 10159–10165.

91 T. Lee, Z. X. Liu and H. L. Lee, *Cryst. Growth Des.*, 2011, **11**, 4146–4154.

92 J. Gascon and F. Kapteijn, *Angew. Chem., Int. Ed.*, 2010, **49**, 1530–1532.

93 S. S.-Y. Chui, S. M.-F. Lo, J. P. H. Charmant, A. G. Orpen and I. D. Williams, *Science*, 1999, **283**, 1148–1150.

94 U. Mueller, M. Schubert, F. Teich, H. Puetter, K. Schierle-Arndt and J. Pastré, *J. Mater. Chem.*, 2006, **16**, 626–636.

95 A. M. Joaristi, J. Juan-Alcañiz, P. Serra-Crespo, F. Kapteijn and J. Gascon, *Cryst. Growth Des.*, 2012, **12**, 3489–3498.

96 T. R. C. Van Assche, G. Desmet, R. Ameloot, D. E. De Vos, H. Terryn and J. F. M. Denayer, *Microporous Mesoporous Mater.*, 2012, **158**, 209–213.

97 B. Van de Voorde, R. Ameloot, I. Stassen, M. Everaert, D. D. Vos and J.-C. Tan, *J. Mater. Chem. C*, 2013, **1**, 7716–7724.

98 H. Li, M. Eddaoudi, M. O'Keeffe and O. M. Yaghi, *Nature*, 1999, **402**, 276–279.

99 A. D. Burrows, *CrystEngComm*, 2011, **13**, 3623–3642.

100 T. R. C. Van Assche and J. F. M. Denayer, *Chem. Eng. Sci.*, 2013, **95**, 65–72.

101 R. Ameloot, L. Pandey, M. V. der Auweraer, L. Alaerts, B. F. Sels and D. E. D. Vos, *Chem. Commun.*, 2010, **46**, 3735–3737.

This journal is © The Royal Society of Chemistry 2014

Chem. Soc. Rev., 2014, **43**, 5513–5560 | 5555

102 R. Ameloot, E. Gobechiya, H. Uji-i, J. A. Martens, J. Hofkens, L. Alaerts, B. F. Sels and D. E. De Vos, *Adv. Mater.*, 2010, **22**, 2685–2688.

103 R. Ranjan and M. Tsapatsis, *Chem. Mater.*, 2009, **21**, 4920–4924.

104 M. Arnold, P. Kortunov, D. J. Jones, Y. Nedellec, J. Kärger and J. Caro, *Eur. J. Inorg. Chem.*, 2007, 60–64.

105 Y.-S. Li, H. Bux, A. Feldhoff, G.-L. Li, W.-S. Yang and J. Caro, *Adv. Mater.*, 2010, **22**, 3322–3326.

106 Y.-S. Li, F.-Y. Liang, H. Bux, A. Feldhoff, W.-S. Yang and J. Caro, *Angew. Chem., Int. Ed.*, 2010, **49**, 548–551.

107 Y. Li, F. Liang, H. Bux, W. Yang and J. Caro, *J. Membr. Sci.*, 2010, **354**, 48–54.

108 H. Bux, A. Feldhoff, J. Cravillon, M. Wiebcke, Y.-S. Li and J. Caro, *Chem. Mater.*, 2011, **23**, 2262–2269.

109 S. R. Venna and M. A. Carreon, *J. Am. Chem. Soc.*, 2010, **132**, 76–78.

110 Y. Pan and Z. Lai, *Chem. Commun.*, 2011, **47**, 10275–10277.

111 V. V. Guerrero, Y. Yoo, M. C. McCarthy and H.-K. Jeong, *J. Mater. Chem.*, 2010, **20**, 3938–3943.

112 Y. Liu, G. Zeng, Y. Pan and Z. Lai, *J. Membr. Sci.*, 2011, **379**, 46–51.

113 Z. Zhao, X. Ma, Z. Li and Y. S. Lin, *J. Membr. Sci.*, 2011, **382**, 82–90.

114 D. Jiang, A. D. Burrows, R. Jaber and K. J. Edler, *Chem. Commun.*, 2012, **48**, 4965–4967.

115 Y. Hu, X. Dong, J. Nan, W. Jin, X. Ren, N. Xu and Y. M. Lee, *Chem. Commun.*, 2010, **46**, 737–739.

116 J. Nan, X. Dong, W. Wang and W. Jin, *Microporous Mesoporous Mater.*, 2012, **155**, 90–98.

117 F. Zhang, X. Zou, X. Gao, S. Fan, F. Sun, H. Ren and G. Zhu, *Adv. Funct. Mater.*, 2012, **22**, 3583–3590.

118 J. Nan, X. Dong, W. Wang, W. Jin and N. Xu, *Langmuir*, 2011, **27**, 4309–4312.

119 Y. Mao, W. Cao, J. Li, L. Sun and X. Peng, *Chem. – Eur. J.*, 2013, **19**, 11883–11886.

120 Z. Xie, J. Yang, J. Wang, J. Bai, H. Yin, B. Yuan, J. Lu, Y. Zhang, L. Zhou and C. Duan, *Chem. Commun.*, 2012, **48**, 5977–5979.

121 Y. Yoo and H.-K. Jeong, *Chem. Commun.*, 2008, 2441–2443.

122 Y. Yoo, Z. Lai and H.-K. Jeong, *Microporous Mesoporous Mater.*, 2009, **123**, 100–106.

123 Y. Yoo and H.-K. Jeong, *Cryst. Growth Des.*, 2010, **10**, 1283–1288.

124 K. Koh, A. G. Wong-Foy and A. J. Matzger, *Chem. Commun.*, 2009, 6162–6164.

125 P. Falcaro, A. J. Hill, K. M. Nairn, J. Jasieniak, J. I. Mardel, T. J. Bastow, S. C. Mayo, M. Gimona, D. Gomez, H. J. Whitfield, R. Riccò, A. Patelli, B. Marmiroli, H. Amenitsch, T. Colson, L. Villanova and D. Buso, *Nat. Commun.*, 2011, **2**, 237.

126 D. Buso, K. M. Nairn, M. Gimona, A. J. Hill and P. Falcaro, *Chem. Mater.*, 2011, **23**, 929–934.

127 D. Buso, A. J. Hill, T. Colson, H. J. Whitfield, A. Patelli, P. Scopece, C. M. Doherty and P. Falcaro, *Cryst. Growth Des.*, 2011, **11**, 5268–5274.

128 S. Liu, Y. Zhang, Y. Meng, F. Gao, S. Jiao and Y. Ke, *Cryst. Growth Des.*, 2013, **13**, 2697–2702.

129 M. Eddaoudi, J. Kim, N. Rosi, D. Vodak, J. Wachter, M. O'Keeffe and O. M. Yaghi, *Science*, 2002, **295**, 469–472.

130 J. Cravillon, S. Münzer, S.-J. Lohmeier, A. Feldhoff, K. Huber and M. Wiebcke, *Chem. Mater.*, 2009, **21**, 1410–1412.

131 C. J. Brinker, Y. Lu, A. Sellinger and H. Fan, *Adv. Mater.*, 1999, **11**, 579–585.

132 A. Kumar and G. M. Whitesides, *Appl. Phys. Lett.*, 1993, **63**, 2002–2004.

133 M. Mrksich and G. M. Whitesides, *Trends Biotechnol.*, 1995, **13**, 228–235.

134 J. L. Wilbur, A. Kumar, H. A. Biebuyck, E. Kim and G. M. Whitesides, *Nanotechnology*, 1996, **7**, 452.

135 M. Cavallini and F. Biscarini, *Nano Lett.*, 2003, **3**, 1269–1271.

136 Y. You, H. Yang, J. W. Chung, J. H. Kim, Y. Jung and S. Y. Park, *Angew. Chem., Int. Ed.*, 2010, **49**, 3757–3761.

137 C. Carbonell, I. Imaz and D. Maspoch, *J. Am. Chem. Soc.*, 2011, **133**, 2144–2147.

138 Y. Xia and G. M. Whitesides, *Annu. Rev. Mater. Sci.*, 1998, **28**, 153–184.

139 E. Bellido, S. Cardona-Serra, E. Coronado and D. Ruiz-Molina, *Chem. Commun.*, 2011, **47**, 5175–5177.

140 C. Carbonell, K. C. Stylianou, J. Hernando, E. Evangelio, S. A. Barnett, S. Nettikadan, I. Imaz and D. Maspoch, *Nat. Commun.*, 2013, **4**, 2173.

141 J. J. Gassensmith, P. M. Erne, W. F. Paxton, C. Valente and J. F. Stoddart, *Langmuir*, 2011, **27**, 1341–1345.

142 V. V. Rostovtsev, L. G. Green, V. V. Fokin and K. B. Sharpless, *Angew. Chem., Int. Ed.*, 2002, **41**, 2596–2599.

143 J. Puigmartí-Luis, *Chem. Soc. Rev.*, 2014, **43**, 2253–2271.

144 D. Witters, N. Vergauwe, R. Ameloot, S. Vermeir, D. De Vos, R. Puers, B. Sels and J. Lammertyn, *Adv. Mater.*, 2012, **24**, 1316–1320.

145 D. Witters, S. Vermeir, R. Puers, B. F. Sels, D. E. De Vos, J. Lammertyn and R. Ameloot, *Chem. Mater.*, 2013, **25**, 1021–1023.

146 D. Witters, K. Knez, F. Ceyssens, R. Puers and J. Lammertyn, *Lab Chip*, 2013, **13**, 2047–2054.

147 P. Falcaro, F. Lapierre, B. Marmiroli, M. Styles, Y. Zhu, M. Takahashi, A. J. Hill and C. M. Doherty, *J. Mater. Chem. C*, 2012, **1**, 42–45.

148 J. Puigmartí-Luis, M. Rubio-Martínez, I. Imaz, B. Z. Cvetković, L. Abad, A. Pérez del Pino, D. Maspoch and D. B. Amabilino, *ACS Nano*, 2014, **8**, 818–826.

149 B. Z. Cvetković, J. Puigmartí-Luis, D. Schaffhauser, T. Ryll, S. Schmid and P. S. Dittrich, *ACS Nano*, 2013, **7**, 183–190.

150 M. Faustini, J. Kim, G.-Y. Jeong, J. Y. Kim, H. R. Moon, W.-S. Ahn and D.-P. Kim, *J. Am. Chem. Soc.*, 2013, **135**, 14619–14626.

151 L. Paseta, B. Seoane, D. Julve, V. Sebastián, C. Téllez and J. Coronas, *ACS Appl. Mater. Interfaces*, 2013, **5**, 9405–9410.

152 R. Ameloot, F. Vermoortele, W. Vanhove, M. B. J. Roeffaers, B. F. Sels and D. E. De Vos, *Nat. Chem.*, 2011, **3**, 382–387.

5556 | *Chem. Soc. Rev.*, 2014, **43**, 5513–5560

This journal is © The Royal Society of Chemistry 2014

153 J. Puigmartí-Luis, M. Rubio-Martínez, U. Hartfelder, I. Imaz, D. Maspoch and P. S. Dittrich, *J. Am. Chem. Soc.*, 2011, **133**, 4216–4219.

154 E. A. Fluegel, A. Ranft, F. Haase and B. V. Lotsch, *J. Mater. Chem.*, 2012, **22**, 10119–10133.

155 P. Falcaro, L. Malfatti, L. Vaccari, H. Amenitsch, B. Marmiroli, G. Grenci and P. Innocenzi, *Adv. Mater.*, 2009, **21**, 4932–4936.

156 E. Zanchetta, G. D. Giustina, G. Grenci, A. Pozzato, M. Tormen and G. Brusatin, *Adv. Mater.*, 2013, **25**, 6261–6265.

157 U. Schulz, B. Saruhan, K. Fritscher and C. Leyens, *Int. J. Appl. Ceram. Technol.*, 2004, **1**, 302–315.

158 D. A. Streitwieser, N. Popovska, H. Gerhard and G. Emig, *J. Eur. Ceram. Soc.*, 2005, **25**, 817–828.

159 G. Xomeritakis and Y. S. Lin, *J. Membr. Sci.*, 1996, **120**, 261–272.

160 J.-J. Wu and S.-C. Liu, *Adv. Mater.*, 2002, **14**, 215–218.

161 M. Nanu, J. Schoonman and A. Goossens, *Nano Lett.*, 2005, **5**, 1716–1719.

162 G. L. Messing, S.-C. Zhang and G. V. Jayanthi, *J. Am. Ceram. Soc.*, 1993, **76**, 2707–2726.

163 R. McPherson, *Surf. Coat. Technol.*, 1989, **39–40**(Part 1), 173–181.

164 L. Sun, C. C. Berndt, K. A. Gross and A. Kucuk, *J. Biomed. Mater. Res.*, 2001, **58**, 570–592.

165 N. P. Padture, M. Gell and E. H. Jordan, *Science*, 2002, **296**, 280–284.

166 A. R. Studart, U. T. Gonzenbach, E. Tervoort and L. J. Gauckler, *J. Am. Ceram. Soc.*, 2006, **89**, 1771–1789.

167 L. Besra and M. Liu, *Prog. Mater. Sci.*, 2007, **52**, 1–61.

168 A. R. Boccaccini and I. Zhitomirsky, *Curr. Opin. Solid State Mater. Sci.*, 2002, **6**, 251–260.

169 X. Zou, G. Zhu, I. J. Hewitt, F. Sun and S. Qiu, *Dalton Trans.*, 2009, 3009–3013.

170 J. Reboul, S. Furukawa, N. Horike, M. Tsotsalas, K. Hirai, H. Uehara, M. Kondo, N. Louvain, O. Sakata and S. Kitagawa, *Nat. Mater.*, 2012, **11**, 717–723.

171 B. T. Holland, C. F. Blanford and A. Stein, *Science*, 1998, **281**, 538–540.

172 K. Okada, R. Ricco, Y. Tokudome, M. J. Styles, A. J. Hill, M. Takahashi and P. Falcaro, *Adv. Funct. Mater.*, 2014, **24**, 1969–1977.

173 I. Stassen, N. Campagnol, J. Fransaer, P. Vereecken, D. D. Vos and R. Ameloot, *CrystEngComm*, 2013, **15**, 9308–9311.

174 G. Majano and J. Pérez-Ramírez, *Adv. Mater.*, 2013, **25**, 1052–1057.

175 W. Zhang, X. Wen, S. Yang, Y. Berta and Z. l. Wang, *Adv. Mater.*, 2003, **15**, 822–825.

176 H. Guo, G. Zhu, I. J. Hewitt and S. Qiu, *J. Am. Chem. Soc.*, 2009, **131**, 1646–1647.

177 E. Pérez-Mayoral and J. Čejka, *ChemCatChem*, 2011, **3**, 157–159.

178 E. Pérez-Mayoral, Z. Musilová, B. Gil, B. Marszalek, M. Položij, P. Nachtigall and J. Čejka, *Dalton Trans.*, 2012, **41**, 4036–4044.

179 A. Sachse, R. Ameloot, B. Coq, F. Fajula, B. Coasne, D. D. Vos and A. Galarneau, *Chem. Commun.*, 2012, **48**, 4749–4751.

180 G. Majano, O. Ingold, M. Yulikov, G. Jeschke and J. Pérez-Ramírez, *CrystEngComm*, 2013, **15**, 9885–9892.

181 C. Mottillo, Y. Lu, M.-H. Pham, M. J. Cliffe, T.-O. Do and T. Friščić, *Green Chem.*, 2013, **15**, 2121–2131.

182 P. Calvert, *Chem. Mater.*, 2001, **13**, 3299–3305.

183 B.-J. de Gans, P. C. Duineveld and U. S. Schubert, *Adv. Mater.*, 2004, **16**, 203–213.

184 J.-L. Zhuang, D. Ar, X.-J. Yu, J.-X. Liu and A. Terfort, *Adv. Mater.*, 2013, **25**, 4631–4635.

185 H. K. Arslan, O. Shekhah, J. Wohlgemuth, M. Franzreb, R. A. Fischer and C. Wöll, *Adv. Funct. Mater.*, 2011, **21**, 4228–4231.

186 M. Hanke, H. K. Arslan, S. Bauer, O. Zybaylo, C. Christophis, H. Gliemann, A. Rosenhahn and C. Wöll, *Langmuir*, 2012, **28**, 6877–6884.

187 D. Fischer, L. V. Meyer, M. Jansen and K. Müller-Buschbaum, *Angew. Chem., Int. Ed.*, 2014, **53**, 706–710.

188 A. Zurawski, M. Mai, D. Baumann, C. Feldmann and K. Müller-Buschbaum, *Chem. Commun.*, 2010, **46**, 496–498.

189 C. Dimitrakakis, B. Marmiroli, H. Amenitsch, L. Malfatti, P. Innocenzi, G. Grenci, L. Vaccari, A. J. Hill, B. P. Ladewig, M. R. Hill and P. Falcaro, *Chem. Commun.*, 2012, **48**, 7483–7485.

190 P. Innocenzi, L. Malfatti and P. Falcaro, *Soft Matter*, 2012, **8**, 3722–3729.

191 P. Falcaro, S. Costacurta, L. Malfatti, D. Buso, A. Patelli, P. Schiavuta, M. Piccinini, G. Grenci, B. Marmiroli, H. Amenitsch and P. Innocenzi, *ACS Appl. Mater. Interfaces*, 2011, **3**, 245–251.

192 P. Falcaro, L. Malfatti, T. Kidchob, G. Giannini, A. Falqui, M. F. Casula, H. Amenitsch, B. Marmiroli, G. Grenci and P. Innocenzi, *Chem. Mater.*, 2009, **21**, 2055–2061.

193 P. Falcaro, S. Costacurta, L. Malfatti, M. Takahashi, T. Kidchob, M. F. Casula, M. Piccinini, A. Marcelli, B. Marmiroli, H. Amenitsch, P. Schiavuta and P. Innocenzi, *Adv. Mater.*, 2008, **20**, 1864–1869.

194 L. Malfatti, T. Kidchob, S. Costacurta, P. Falcaro, P. Schiavuta, H. Amenitsch and P. Innocenzi, *Chem. Mater.*, 2006, **18**, 4553–4560.

195 S. H. Han, C. M. Doherty, B. Marmiroli, H. J. Jo, D. Buso, A. Patelli, P. Schiavuta, P. Innocenzi, Y. M. Lee, A. W. Thornton, A. J. Hill and P. Falcaro, *Small*, 2013, **9**, 2277–2282.

196 K. S. Park, Z. Ni, A. P. Côté, J. Y. Choi, R. Huang, F. J. Uribe-Romo, H. K. Chae, M. O'Keeffe and O. M. Yaghi, *Proc. Natl. Acad. Sci. U. S. A.*, 2006, **103**, 10186–10191.

197 Y. Shirai, A. J. Osgood, Y. Zhao, K. F. Kelly and J. M. Tour, *Nano Lett.*, 2005, **5**, 2330–2334.

198 V. Serreli, C.-F. Lee, E. R. Kay and D. A. Leigh, *Nature*, 2007, **445**, 523–527.

199 T. Kudernac, N. Ruangsupapichat, M. Parschau, B. Maciá, N. Katsonis, S. R. Harutyunyan, K.-H. Ernst and B. L. Feringa, *Nature*, 2011, **479**, 208–211.

This journal is © The Royal Society of Chemistry 2014

Chem. Soc. Rev., 2014, **43**, 5513–5560 | 5557

200 L. Grill, K.-H. Rieder, F. Moresco, G. Rapenne, S. Stojkovic, X. Bouju and C. Joachim, *Nat. Nanotechnol.*, 2007, **2**, 95–98.

201 J. Godoy, G. Vives and J. M. Tour, *ACS Nano*, 2011, **5**, 85–90.

202 H. Xia, J. Wang, Y. Tian, Q.-D. Chen, X.-B. Du, Y.-L. Zhang, Y. He and H.-B. Sun, *Adv. Mater.*, 2010, **22**, 3204–3207.

203 P. Falcaro, F. Normandin, M. Takahashi, P. Scopece, H. Amenitsch, S. Costacurta, C. M. Doherty, J. S. Laird, M. D. H. Lay, F. Lisi, A. J. Hill and D. Buso, *Adv. Mater.*, 2011, **23**, 3901–3906.

204 M. R. Lohe, K. Gedrich, T. Freudenberg, E. Kockrick, T. Dellmann and S. Kaskel, *Chem. Commun.*, 2011, **47**, 3075–3077.

205 C. Dey, T. Kundu, B. P. Biswal, A. Mallick and R. Banerjee, *Acta Crystallogr., Sect. B: Struct. Sci., Cryst. Eng. Mater.*, 2013, **70**, 3–10.

206 S. Laurent, D. Forge, M. Port, A. Roch, C. Robic, L. Vander Elst and R. N. Muller, *Chem. Rev.*, 2008, **108**, 2064–2110.

207 Y. Lee, J. Lee, C. J. Bae, J.-G. Park, H.-J. Noh, J.-H. Park and T. Hyeon, *Adv. Funct. Mater.*, 2005, **15**, 503–509.

208 E. Coronado and G. M. Espallargas, *Chem. Soc. Rev.*, 2013, **42**, 1525–1539.

209 J. Della Rocca, D. Liu and W. Lin, *Acc. Chem. Res.*, 2011, **44**, 957–968.

210 F. Ke, Y.-P. Yuan, L.-G. Qiu, Y.-H. Shen, A.-J. Xie, J.-F. Zhu, X.-Y. Tian and L.-D. Zhang, *J. Mater. Chem.*, 2011, **21**, 3843–3848.

211 A. Carné-Sanchez, I. Imaz, M. Cano-Sarabia and D. Maspoch, *Nat. Chem.*, 2013, **5**, 203–211.

212 A. G. Marquez, P. Horcajada, D. Grosso, G. Ferey, C. Serre, C. Sanchez and C. Boissiere, *Chem. Commun.*, 2013, **49**, 3848–3850.

213 Y.-R. Lee, J. Kim and W.-S. Ahn, *Korean J. Chem. Eng.*, 2013, **30**, 1667–1680.

214 I. Imaz, J. Hernando, D. Ruiz-Molina and D. Maspoch, *Angew. Chem., Int. Ed.*, 2009, **48**, 2325–2329.

215 G. Lu, S. Li, Z. Guo, O. K. Farha, B. G. Hauser, X. Qi, Y. Wang, X. Wang, S. Han, X. Liu, J. S. DuChene, H. Zhang, Q. Zhang, X. Chen, J. Ma, S. C. J. Loo, W. D. Wei, Y. Yang, J. T. Hupp and F. Huo, *Nat. Chem.*, 2012, **4**, 310–316.

216 T. Zhang, X. Zhang, X. Yan, L. Kong, G. Zhang, H. Liu, J. Qiu and K. L. Yeung, *Chem. Eng. J.*, 2013, **228**, 398–404.

217 T. Arai, T. Sato, H. Kanoh, K. Kaneko, K. Oguma and A. Yanagisawa, *Chem. – Eur. J.*, 2008, **14**, 882–885.

218 M. E. Silvestre, M. Franzreb, P. G. Weidler, O. Shekhah and C. Wöll, *Adv. Funct. Mater.*, 2013, **23**, 1210–1213.

219 Z. Li and Y. Zhang, *Angew. Chem., Int. Ed.*, 2006, **45**, 7732–7735.

220 S. J. Yang, J. Y. Choi, H. K. Chae, J. H. Cho, K. S. Nahm and C. R. Park, *Chem. Mater.*, 2009, **21**, 1893–1897.

221 C. Petit and T. J. Bandosz, *Adv. Funct. Mater.*, 2010, **20**, 111–118.

222 M. Jahan, Q. Bao, J.-X. Yang and K. P. Loh, *J. Am. Chem. Soc.*, 2010, **132**, 14487–14495.

223 T. Arai, N. Kawasaki and H. Kanoh, *Synlett*, 2012, 1549–1553.

224 S. Couck, J. F. M. Denayer, G. V. Baron, T. Remy, J. Gascon and F. Kapteijn, *J. Am. Chem. Soc.*, 2009, **131**, 6326–6327.

225 T.-H. Park, K. J. Lee, S. Hwang, J. Yoon, C. Woell and J. Lahann, *Adv. Mater.*, 2014, DOI: 10.1002/adma.201305461.

226 G. Taylor, *Proc. R. Soc. London, Ser. A*, 1964, **280**, 383–397.

227 P.-G. de Gennes, *Angew. Chem., Int. Ed. Engl.*, 1992, **31**, 842–845.

228 E. Knoevenagel, *Ber. Dtsch. Chem. Ges.*, 1898, **31**, 2596–2619.

229 S. M. Cohen, *Chem. Rev.*, 2012, **112**, 970–1000.

230 H. R. Moon, D.-W. Lim and M. P. Suh, *Chem. Soc. Rev.*, 2013, **42**, 1807–1824.

231 A. Dhakshinamoorthy and H. Garcia, *Chem. Soc. Rev.*, 2012, **41**, 5262–5284.

232 C. Wang, Z. Xie, K. E. deKrafft and W. Lin, *J. Am. Chem. Soc.*, 2011, **133**, 13445–13454.

233 Y. Cui, H. Xu, Y. Yue, Z. Guo, J. Yu, Z. Chen, J. Gao, Y. Yang, G. Qian and B. Chen, *J. Am. Chem. Soc.*, 2012, **134**, 3979–3982.

234 D. F. Sava, L. E. S. Rohwer, M. A. Rodriguez and T. M. Nenoff, *J. Am. Chem. Soc.*, 2012, **134**, 3983–3986.

235 P. Falcaro and S. Furukawa, *Angew. Chem., Int. Ed.*, 2012, **51**, 8431–8433.

236 H. Deng, C. J. Doonan, H. Furukawa, R. B. Ferreira, J. Towne, C. B. Knobler, B. Wang and O. M. Yaghi, *Science*, 2010, **327**, 846–850.

237 J. An, S. J. Geib and N. L. Rosi, *J. Am. Chem. Soc.*, 2009, **131**, 8376–8377.

238 J. Yu, Y. Cui, H. Xu, Y. Yang, Z. Wang, B. Chen and G. Qian, *Nat. Commun.*, 2013, **4**, 2719.

239 D. Buso, J. Jasieniak, M. D. H. Lay, P. Schiavuta, P. Scopece, J. Laird, H. Amenitsch, A. J. Hill and P. Falcaro, *Small*, 2012, **8**, 80–88.

240 K. Sugikawa, S. Nagata, Y. Furukawa, K. Kokado and K. Sada, *Chem. Mater.*, 2013, **25**, 2565–2570.

241 F. Ke, J. Zhu, L.-G. Qiu and X. Jiang, *Chem. Commun.*, 2013, **49**, 1267–1269.

242 C. Wang, K. E. deKrafft and W. Lin, *J. Am. Chem. Soc.*, 2012, **134**, 7211–7214.

243 M. S. El-Shall, V. Abdelsayed, A. E. R. S. Khder, H. M. A. Hassan, H. M. El-Kaderi and T. E. Reich, *J. Mater. Chem.*, 2009, **19**, 7625–7631.

244 H. R. Moon, J. H. Kim and M. P. Suh, *Angew. Chem., Int. Ed.*, 2005, **44**, 1261–1265.

245 M. P. Suh, H. R. Moon, E. Y. Lee and S. Y. Jang, *J. Am. Chem. Soc.*, 2006, **128**, 4710–4718.

246 Y. E. Cheon and M. P. Suh, *Angew. Chem., Int. Ed.*, 2009, **48**, 2899–2903.

247 Y. Wei, S. Han, D. A. Walker, P. E. Fuller and B. A. Grzybowski, *Angew. Chem., Int. Ed.*, 2012, **51**, 7435–7439.

248 C. Zlotea, R. Campesi, F. Cuevas, E. Leroy, P. Dibandjo, C. Volkringer, T. Loiseau, G. Férey and M. Latroche, *J. Am. Chem. Soc.*, 2010, **132**, 2991–2997.

249 A. Aijaz, A. Karkamkar, Y. J. Choi, N. Tsumori, E. Rönnebro, T. Autrey, H. Shioyama and Q. Xu, *J. Am. Chem. Soc.*, 2012, **134**, 13926–13929.

250 S. Hermes, M.-K. Schröter, R. Schmid, L. Khodeir, M. Muhler, A. Tissler, R. W. Fischer and R. A. Fischer, *Angew. Chem., Int. Ed.*, 2005, **44**, 6237–6241.

251 F. Schröder, D. Esken, M. Cokoja, M. W. E. van den Berg, O. I. Lebedev, G. Van Tendeloo, B. Walaszek, G. Buntkowsky,

5558 | *Chem. Soc. Rev.*, 2014, **43**, 5513–5560

This journal is © The Royal Society of Chemistry 2014

H.-H. Limbach, B. Chaudret and R. A. Fischer, *J. Am. Chem. Soc.*, 2008, **130**, 6119–6130.

252 D.-W. Lim, J. W. Yoon, K. Y. Ryu and M. P. Suh, *Angew. Chem., Int. Ed.*, 2012, **51**, 9814–9817.

253 K. Khaletskaya, J. Reboul, M. Meilikhov, M. Nakahama, S. Diring, M. Tsujimoto, S. Isoda, F. Kim, K. Kamei, R. A. Fischer, S. Kitagawa and S. Furukawa, *J. Am. Chem. Soc.*, 2013, **135**, 10998–11005.

254 L. He, Y. Liu, J. Liu, Y. Xiong, J. Zheng, Y. Liu and Z. Tang, *Angew. Chem., Int. Ed.*, 2013, **52**, 3741–3745.

255 C.-H. Kuo, Y. Tang, L.-Y. Chou, B. T. Sneed, C. N. Brodsky, Z. Zhao and C.-K. Tsung, *J. Am. Chem. Soc.*, 2012, **134**, 14345–14348.

256 S. Sorribas, B. Zornoza, C. Téllez and J. Coronas, *Chem. Commun.*, 2012, **48**, 9388–9390.

257 M. Hu, A. A. Belik, M. Imura and Y. Yamauchi, *J. Am. Chem. Soc.*, 2013, **135**, 384–391.

258 N. Liu, Y. Yao, J. J. Cha, M. T. McDowell, Y. Han and Y. Cui, *Nano Res.*, 2012, **5**, 109–116.

259 M. Hu, S. Furukawa, R. Ohtani, H. Sukegawa, Y. Nemoto, J. Reboul, S. Kitagawa and Y. Yamauchi, *Angew. Chem., Int. Ed.*, 2012, **51**, 984–988.

260 R. Ameloot, M. B. J. Roeffaers, G. De Cremer, F. Vermoortele, J. Hofkens, B. F. Sels and D. E. De Vos, *Adv. Mater.*, 2011, **23**, 1788–1791.

261 S. Han, Y. Wei, C. Valente, R. S. Forgan, J. J. Gassensmith, R. A. Smaldone, H. Nakanishi, A. Coskun, J. F. Stoddart and B. A. Grzybowski, *Angew. Chem., Int. Ed.*, 2011, **50**, 276–279.

262 O. Zybaylo, O. Shekhah, H. Wang, M. Tafipolsky, R. Schmid, D. Johannsmann and C. Wöll, *Phys. Chem. Chem. Phys.*, 2010, **12**, 8093–8098.

263 H. Uehara, S. Diring, S. Furukawa, Z. Kalay, M. Tsotsalas, M. Nakahama, K. Hirai, M. Kondo, O. Sakata and S. Kitagawa, *J. Am. Chem. Soc.*, 2011, **133**, 11932–11935.

264 M. D. Allendorf, R. J. T. Houk, L. Andruszkiewicz, A. A. Talin, J. Pikarsky, A. Choudhury, K. A. Gall and P. J. Hesketh, *J. Am. Chem. Soc.*, 2008, **130**, 14404–14405.

265 I. Ellern, A. Venkatasubramanian, J.-H. Lee, P. Hesketh, V. Stavila, A. Robinson and M. Allendorf, *Micro Nano Lett.*, 2013, **8**, 766–769.

266 J. Liu, F. Sun, F. Zhang, Z. Wang, R. Zhang, C. Wang and S. Qiu, *J. Mater. Chem.*, 2011, **21**, 3775–3778.

267 A. L. Robinson, V. Stavila, T. R. Zeitler, M. I. White, S. M. Thornberg, J. A. Greathouse and M. D. Allendorf, *Anal. Chem.*, 2012, **84**, 7043–7051.

268 L. E. Kreno, J. T. Hupp and R. P. Van Duyne, *Anal. Chem.*, 2010, **82**, 8042–8046.

269 J. Zhuang, C.-H. Kuo, L.-Y. Chou, D.-Y. Liu, E. Weerapana and C.-K. Tsung, *ACS Nano*, 2014, **8**, 2812–2819.

270 A. S. Münch, J. Seidel, A. Obst, E. Weber and F. O. R. L. Mertens, *Chem. – Eur. J.*, 2011, **17**, 10958–10964.

271 C. M. Doherty, Y. Gao, B. Marmiroli, H. Amenitsch, F. Lisi, L. Malfatti, K. Okada, M. Takahashi, A. J. Hill, P. Innocenzi and P. Falcaro, *J. Mater. Chem.*, 2012, **22**, 16191–16195.

272 C.-W. Kung, T. C. Wang, J. E. Mondloch, D. Fairen-Jimenez, D. M. Gardner, W. Bury, J. M. Klingsporn, J. C. Barnes, R. Van Duyne, J. F. Stoddart, M. R. Wasielewski, O. K. Farha and J. T. Hupp, *Chem. Mater.*, 2013, **25**, 5012–5017.

273 C.-Y. Sun, X.-L. Wang, X. Zhang, C. Qin, P. Li, Z.-M. Su, D.-X. Zhu, G.-G. Shan, K.-Z. Shao, H. Wu and J. Li, *Nat. Commun.*, 2013, **4**, 2717.

274 G. Lu and J. T. Hupp, *J. Am. Chem. Soc.*, 2010, **132**, 7832–7833.

275 Y. Horiuchi, T. Toyao, M. Saito, K. Mochizuki, M. Iwata, H. Higashimura, M. Anpo and M. Matsuoka, *J. Phys. Chem. C*, 2012, **116**, 20848–20853.

276 D. Y. Lee, C. Y. Shin, S. J. Yoon, H. Y. Lee, W. Lee, N. K. Shrestha, J. K. Lee and S.-H. Han, *Sci. Rep.*, 2014, **4**, 3930.

277 D. Umeyama, S. Horike, M. Inukai, T. Itakura and S. Kitagawa, *J. Am. Chem. Soc.*, 2012, **134**, 12780–12785.

278 E. Biemmi, A. Darga, N. Stock and T. Bein, *Microporous Mesoporous Mater.*, 2008, **114**, 380–386.

279 M. Meilikhov, S. Furukawa, K. Hirai, R. A. Fischer and S. Kitagawa, *Angew. Chem., Int. Ed.*, 2013, **52**, 341–345.

280 S. Achmann, G. Hagen, J. Kita, I. M. Malkowsky, C. Kiener and R. Moos, *Sensors*, 2009, **9**, 1574–1589.

281 I. Erucar, G. Yilmaz and S. Keskin, *Chem. – Asian J.*, 2013, **8**, 1692–1704.

282 J. Gascon, F. Kapteijn, B. Zornoza, V. Sebastián, C. Casado and J. Coronas, *Chem. Mater.*, 2012, **24**, 2829–2844.

283 A. Bétard, H. Bux, S. Henke, D. Zacher, J. Caro and R. A. Fischer, *Microporous Mesoporous Mater.*, 2012, **150**, 76–82.

284 D.-J. Lee, Q. Li, H. Kim and K. Lee, *Microporous Mesoporous Mater.*, 2012, **163**, 169–177.

285 W. Zhang, F. Liang, C. Li, L.-G. Qiu, Y.-P. Yuan, F.-M. Peng, X. Jiang, A.-J. Xie, Y.-H. Shen and J.-F. Zhu, *J. Hazard. Mater.*, 2011, **186**, 984–990.

286 A. Bagheri, M. Taghizadeh, M. Behbahani, A. Akbar Asgharinezhad, M. Salarian, A. Dehghani, H. Ebrahimzadeh and M. M. Amini, *Talanta*, 2012, **99**, 132–139.

287 F. Zou, R. Yu, R. Li and W. Li, *ChemPhysChem*, 2013, **14**, 2825–2832.

288 H. Miyasaka, *Acc. Chem. Res.*, 2013, **46**, 248–257.

289 A. Morozan and F. Jaouen, *Energy Environ. Sci.*, 2012, **5**, 9269–9290.

290 C. G. Silva, A. Corma and H. García, *J. Mater. Chem.*, 2010, **20**, 3141–3156.

291 Y. Kobayashi, B. Jacobs, M. D. Allendorf and J. R. Long, *Chem. Mater.*, 2010, **22**, 4120–4122.

292 C.-K. Lin, D. Zhao, W.-Y. Gao, Z. Yang, J. Ye, T. Xu, Q. Ge, S. Ma and D.-J. Liu, *Inorg. Chem.*, 2012, **51**, 9039–9044.

293 C. H. Hendon, D. Tiana, M. Fontecave, C. Sanchez, L. D'arras, C. Sassoye, L. Rozes, C. Mellot-Draznieks and A. Walsh, *J. Am. Chem. Soc.*, 2013, **135**, 10942–10945.

294 E. Flage-Larsen, A. Røyset, J. H. Cavka and K. Thorshaug, *J. Phys. Chem. C*, 2013, **117**, 20610–20616.

295 A. Kuc, A. Enyashin and G. Seifert, *J. Phys. Chem. B*, 2007, **111**, 8179–8186.

This journal is © The Royal Society of Chemistry 2014

Chem. Soc. Rev., 2014, **43**, 5513–5560 | 5559

296 A. Dragässer, O. Shekhah, O. Zybaylo, C. Shen, M. Buck, C. Wöll and D. Schlettwein, *Chem. Commun.*, 2011, **47**, 663–665.

297 C. Hou, Q. Xu, J. Peng, Z. Ji and X. Hu, *ChemPhysChem*, 2013, **14**, 140–144.

298 S. Eslava, L. Zhang, S. Esconjauregui, J. Yang, K. Vanstreels, M. R. Baklanov and E. Saiz, *Chem. Mater.*, 2013, **25**, 27–33.

299 E. Redel, Z. Wang, S. Walheim, J. Liu, H. Gliemann and C. Wöll, *Appl. Phys. Lett.*, 2013, **103**, 091903.

300 W. Zhan, Q. Kuang, J. Zhou, X. Kong, Z. Xie and L. Zheng, *J. Am. Chem. Soc.*, 2013, **135**, 1926–1933.

301 M. Isaac and D. P. van Vuuren, *Energy Policy*, 2009, **37**, 507–521.

302 F. Jeremias, V. Lozan, S. K. Henninger and C. Janiak, *Dalton Trans.*, 2013, **42**, 15967–15973.

303 S.-L. Li and Q. Xu, *Energy Environ. Sci.*, 2013, **6**, 1656–1683.

304 C. Gomes Silva, I. Luz, F. X. Llabrés i Xamena, A. Corma and H. García, *Chem. – Eur. J.*, 2010, **16**, 11133–11138.

305 A. Fateeva, P. A. Chater, C. P. Ireland, A. A. Tahir, Y. Z. Khimyak, P. V. Wiper, J. R. Darwent and M. J. Rosseinsky, *Angew. Chem., Int. Ed.*, 2012, **51**, 7440–7444.

306 S. Jin, H.-J. Son, O. K. Farha, G. P. Wiederrecht and J. T. Hupp, *J. Am. Chem. Soc.*, 2013, **135**, 955–958.

307 D. Y. Lee, D. V. Shinde, S. J. Yoon, K. N. Cho, W. Lee, N. K. Shrestha and S.-H. Han, *J. Phys. Chem. C*, 2013, DOI: 10.1021/jp4079663.

308 L. Carrette, K. A. Friedrich and U. Stimming, *Fuel Cells*, 2001, **1**, 5–39.

309 J. A. Hurd, R. Vaidhyanathan, V. Thangadurai, C. I. Ratcliffe, I. L. Moudrakovski and G. K. H. Shimizu, *Nat. Chem.*, 2009, **1**, 705–710.

310 M. Sadakiyo, T. Yamada and H. Kitagawa, *J. Am. Chem. Soc.*, 2009, **131**, 9906–9907.

311 Y. Ren, G. H. Chia and Z. Gao, *Nano Today*, 2013, **8**, 577–597.

312 K. Hirai, P. Falcaro, S. Kitagawa and S. Furukawa, *Host–Guest Metal–Organic Frameworks For Photonics*, Springer, Berlin, Heidelberg, 2013, pp. 1–20.

313 H. Guo, Y. Zhu, S. Qiu, J. A. Lercher and H. Zhang, *Adv. Mater.*, 2010, **22**, 4190–4192.

314 X. Lin, G. Gao, L. Zheng, Y. Chi and G. Chen, *Anal. Chem.*, 2014, **86**, 1223–1228.

315 V. Lykourinou, Y. Chen, X.-S. Wang, L. Meng, T. Hoang, L.-J. Ming, R. L. Musselman and S. Ma, *J. Am. Chem. Soc.*, 2011, **133**, 10382–10385.

316 Y. Chen, V. Lykourinou, C. Vetromile, T. Hoang, L.-J. Ming, R. W. Larsen and S. Ma, *J. Am. Chem. Soc.*, 2012, **134**, 13188–13191.

317 W.-L. Liu, S.-H. Lo, B. Singco, C.-C. Yang, H.-Y. Huang and C.-H. Lin, *J. Mater. Chem. B*, 2013, **1**, 928–932.

318 T. Ye, Y. Liu, M. Luo, X. Xiang, X. Ji, G. Zhou and Z. He, *Analyst*, 2014, **139**, 1721–1725.

319 P. Horcajada, T. Chalati, C. Serre, B. Gillet, C. Sebrie, T. Baati, J. F. Eubank, D. Heurtaux, P. Clayette, C. Kreuz, J.-S. Chang, Y. K. Hwang, V. Marsaud, P.-N. Bories, L. Cynober, S. Gil, G. Férey, P. Couvreur and R. Gref, *Nat. Mater.*, 2010, **9**, 172–178.

320 A. M. Shultz, O. K. Farha, J. T. Hupp and S. T. Nguyen, *J. Am. Chem. Soc.*, 2009, **131**, 4204–4205.

321 L. Ma, J. M. Falkowski, C. Abney and W. Lin, *Nat. Chem.*, 2010, **2**, 838–846.

322 G. Xu, K. Otsubo, T. Yamada, S. Sakaida and H. Kitagawa, *J. Am. Chem. Soc.*, 2013, **135**, 7438–7441.

323 J. I. Feldblyum, E. A. Keenan, A. J. Matzger and S. Maldonado, *J. Phys. Chem. C*, 2012, **116**, 3112–3121.

5560 | *Chem. Soc. Rev.*, 2014, **43**, 5513–5560

This journal is © The Royal Society of Chemistry 2014